TRANSPIRATION AND FILM COOLING BOUNDARY LAYER COMPUTER PROGRAM

VOLUME I

Numerical Solution of the Turbulent Boundary Layer Equations with Equilibrium Chemistry

FINAL REPORT - CONTRACT NAS7-791

JUNE 1971

PREPARED BY JAY N. LEVINE

PREPARED FOR: NATIONAL AERONAUTICS AND SPACE ADMINISTRATION

DYNAMIC SCIENCE

A Division of Marshall Industries

2400 Michelson Drive, Irvine, California 92664 (714) 833-2670

SN-230

TRANSPIRATION AND FILM COOLING BOUNDARY LAYER COMPUTER PROGRAM

Volume I

Numerical Solutions of the Turbulent Boundary Layer Equations with Equilibrium Chemistry

Final Report - Contract NAS7-791

Prepared by: Jay N. Levine

Prepared for: National Aeronautics and Space Administration

June 1971

DYNAMIC SCIENCE
A Division of Marshall Industries
2400 Michelson Drive
Irvine, California 92664

FOREWORD

The present report is part of a two volume set which describes a turbulent boundary layer analysis and computer program that includes the effects of wall cooling and equilibrium chemistry. Volume I contains the analytical basis for the computer program and a discussion of the results obtained to date: Volume II of the set describes the computer program and serves as a user's manual.

This investigation is entitled TRANSPIRATION AND FILM COOLING BOUNDARY LAYER COMPUTER PROGRAM. The two volumes are additionally subtitled as follows:

Volume I - Numerical Solution of the Turbulent Boundary Layer Equations With Equilibrium Chemistry - by Jay N. Levine

Volume II - Computer Program and User's Manual - by Roger J. Gloss

Volumes I and II, and the computer program, have been distributed according to the attached distribution lists. Additional copies of the two volumes and the computer program (UNIVAC 1108 and IBM 360 versions) may be obtained from T. Reedy, CPIA, APL/JHU, 8621 Georgia Avenue, Silver Spring, Maryland 20910.

This investigation was conducted for the Jet Propulsion Laboratory, National Aeronautics and Space Administration under contract No. NAS7-791 with Walter B. Powell as technical monitor. Jay N. Levine of Dynamic Science was Program Manager.

TABLE OF CONTENTS

NOMENCLATURE

A	-	Van Driest damping constant in eddy viscosity formula
A_n, B_n, C_n	-	coefficients in the difference equations
b	-	value of $\tilde{y}_e$ at the initial station
C_p	-	specific heat
c_i	-	mass fraction of the ith species
C_f	-	local shear stress coefficient
D_n	-	right hand side of difference equations
D_T	-	eddy diffusivity
E	-	$\rho G' \zeta' \tilde{y} / \zeta$
F	-	$G' / \zeta^2 \, Re_r$, also thrust
G	-	function used to transform $\tilde{y}$
G', G''	-	1st and 2nd derivatives of the G function
H	-	total enthalpy, also shape factor = δ^* / θ
h	-	static enthalpy
j	-	equals 1 for axisymmetric flow, 0 for planar flow
K	-	acceleration parameter
k	-	thermal conductivity, also common ratio in geometric stepsize progressions
L	-	reference length
Le	-	molecular Lewis number
Le_T	-	turbulent Lewis number
ℓ	-	mixing length
M	-	molecular weight
$\dot{m}_w$	-	surface mass transfer rate = $\rho_w v_w$
m,n	-	mesh indicies
n	-	parameter in G function
P	-	pressure
P_{amb}	-	ambient pressure at nozzle exit
Pr	-	Prandtl number
Pr_T	-	turbulent Prandtl number
q_w	-	local heat transfer rate
r^*	-	nozzle throat radius
r_w	-	local radius of the wall

R	-	Universal gas constant
Re	-	Reynolds number
S	-	entropy
s	-	wetted length along wall
$St.$	-	Stanton number
T	-	temperature
u,v	-	velocity in s and y directions, respectively
u^+	-	dimensionless velocity ratio, $\bar{u} / u^*_w$
u^*_w	-	friction velocity, $(\tau_w / \bar{\rho}_w)^{1/2}$
v	-	velocity in y direction
v^+_w	-	dimensionless velocity ratio, $\bar{v}_w / u^*_w$
x	-	axial distance
y	-	normal coordinate
y^+	-	dimensionless normal coordinate, $\bar{y}\ u^*_w / \bar{\nu}$
$\tilde{y}$	-	nondimensional y coordinate = $\bar{y} / L\,\zeta$
α	-	constant in G function
α_i	-	mass fraction of the ith element
$\alpha_{i_{trans}}$	-	mass fraction of the ith element in the transpiration coolant
β	-	constant in G function
γ	-	ratio of specific heats
δ	-	boundary layer thickness
δ^*	-	displacement thickness
δ^*_{inc}	-	incompressible displacement thickness
ϵ	-	kinetmatic eddy viscosity
ζ	-	function used to scale $\bar{y}$
ζ'	-	$d\zeta / ds$
θ	-	momentum thickness
$\varkappa$	-	eddy conductivity

μ	-	molecular viscosity
ν	-	kinematic viscosity
ρ	-	density
$\sigma_1 \cdots \sigma_5$	-	used to represent various transport property terms
τ	-	shear stress

Subscripts

e	-	at the edge of the boundary layer
i	-	pertaining to the ith species
r	-	evaluated at reference conditions
w	-	at the wall
y	-	partial derivative with respect to y
yy	-	2nd partial derivative with respect to y

Superscripts

j	-	equals 1 for axisymmetric flow, 0 for two dimensional flow
'	-	denotes a fluctuating term
-	-	denotes a dimensional variable and/or a time averaged quantity

ABSTRACT

A finite difference turbulent boundary layer computer program has been developed. The program is primarily oriented towards the calculation of boundary layer performance losses in rocket engines, however, the solution is general, and has much broader applicability. The effects of transpiration and film cooling as well as the effect of equilibrium chemical reactions (currently restricted to the H_2-O_2 system) can be calculated.

The turbulent transport terms are evaluated using the phenomenological mixing length - eddy viscosity concept. The equations of motion are solved using the Crank-Nicolson implicit finite difference technique. The analysis and computer program have been checked out by solving a series of both laminar and turbulent test cases and comparing the results to data or other solutions. These comparisons have shown that the program is capable of producing very satisfactory results for a wide range of flows. Further refinements to the analysis and program, especially as applied to film cooling solutions, would be aided by the acquisition of a firm data base.

I. INTRODUCTION

This effort was carried out for the purpose of developing a practical, and immediately useful state-of-the-art engineering method for analytically predicting the boundary layer performance losses in liquid rocket engines, including the effects of transpiration and film cooling. The turbulent boundary layer analysis developed herein is, however, quite general and has much broader applicability.

The project also had as a primary short term goal the prediction of boundary layer/coolant performance losses for the space shuttle engine configurations currently under consideration by NASA. Therefore, the analysis and resulting computer program have been oriented towards the analysis of high pressure hydrogen-oxygen engines and the current version of the computer program is restricted to H_2-O_2 systems*. The analysis and program use equilibrium chemistry since the flow in the high pressure H_2-O_2 engines will most certainly be very close to equilibrium. The inclusion of finite rate kinetics to broaden the applicability of the program, would have jeopardized the chances of the program's working for the shuttle engines, since notorious numerical difficulties are encountered in finite rate kinetic boundary layer solutions at near equilibrium conditions.

In the past several years, the use of finite difference techniques, coupled with the mixing length-eddy viscosity concept, has enabled several investigators (e.g., Refs. 1-6) to obtain boundary layer solutions which compare quite favorably to experimental data for a broad range of flow conditions. Incompressible and compressible flows with and without wall heat and mass transfer have already been treated for a range of geometrical shapes; and for the most part, excellent results have been achieved. Reacting turbulent boundary layer flows have also been treated, although to a much lesser extent. In addition, the scarcity of

*The H_2-O_2 chemical system is the only reacting system that can be currently treated. Nonreacting perfect gas solutions can, however, be found for all values of γ and M.

good experimental data for reacting boundary layer flows has precluded a full evaluation of the applicability and accuracy of the latest theoretical techniques. It was felt, however, that the excellent results achieved to date with the finite difference-eddy viscosity technique justify its use even for reacting flows, until such time as more exact and computationally feasible turbulence models can be developed.

As is usual when turbulence models are being utilized, the current analysis and computer program are flexible enough to allow for the incorporation of widely varying eddy viscosity models; even though for development purposes only one such model has been treated.

To allow for greater generality, and a wider variety of applications for the program, provision has been made for the following options: equilibrium H_2-O_2 or arbitrary ideal gas solutions; laminar or turbulent flow; compressible or incompressible flow; and 2-D planar or axisymmetric geometry.

The numerical method chosen for the solution of the boundary layer equations is a Crank-Nicolson implicit finite difference technique. In applying this finite difference technique the difference analogs of the equations of motion are linearized and uncoupled and solved using a tridiagonal matrix inversion algorithm.

The final report for this effort is presented in two volumes. Volume I contains a description of the theoretical foundations and numerical methods employed in the solution, as well as a discussion of many of the solutions obtained to date. Volume II is a users manual for the computer program and contains detailed subroutine descriptions, input and output descriptions, and sample cases.

II. METHOD OF SOLUTION

A. BOUNDARY LAYER EQUATIONS

The boundary layer equations for compressible turbulent flow can be derived from the time dependent Navier-Stokes equations using the Reynolds time-averaging procedure and the usual boundary layer order of magnitude assumptions. There is no need to add the N + 1 st derivation to the literature so the final equations are presented below. Equations (1-4) are written in a curvilinear coordinate system in which s is the wetted length along the wall and y is measured normal to it (x is axial distance measured along the centerline). A bar over a quantity denotes the fact that it is a time averaged and/or a dimensional quantity. It has been assumed that the lateral and transverse curvature terms can be neglected (curvature effects can be relatively easily incorporated if desired). The conservation equations are:

Continuity

$$\frac{\partial}{\partial \bar{s}} \left(\bar{\rho}\, \bar{u}\, \bar{r}_w^j \right) + \frac{\partial}{\partial \bar{y}} \left[\left(\bar{\rho}\, \bar{v} + \overline{\rho' v'} \right) \bar{r}_w^j \right] = 0 \tag{1}$$

Momentum

$$\bar{\rho}\, \bar{u}\, \frac{\partial \bar{u}}{\partial \bar{s}} + \left(\bar{\rho}\, \bar{v} + \overline{\rho' v'} \right) \frac{\partial \bar{u}}{\partial \bar{y}} = - \frac{d\bar{P}_e}{d\bar{s}} + \frac{\partial}{\partial \bar{y}} \left[\left(\bar{\mu} + \bar{\rho}\, \bar{\epsilon} \right) \frac{\partial \bar{u}}{\partial \bar{y}} \right] \tag{2}$$

Energy

$$\bar{\rho}\, \bar{u}\, \frac{\partial \bar{H}}{\partial \bar{s}} + \left(\bar{\rho}\, \bar{v} + \overline{\rho' v'} \right) \frac{\partial \bar{H}}{\partial \bar{y}} = \frac{\partial}{\partial \bar{y}} \left\{ \left(\frac{\bar{\mu}}{Pr} + \frac{\bar{\rho}\, \bar{\epsilon}}{Pr_T} \right) \frac{\partial \bar{H}}{\partial \bar{y}} \right. \tag{3}$$

$$+ \left[\bar{\mu} \left(1 - \frac{1}{Pr} \right) + \bar{\rho}\, \bar{\epsilon} \left(1 - \frac{1}{Pr_T} \right) \right] \bar{u}\, \frac{\partial \bar{u}}{\partial \bar{y}}$$

$$\left. + \sum_i \left[\frac{\bar{\mu}}{Pr} \left(Le - 1 \right) + \frac{\bar{\rho}\, \bar{\epsilon}}{Pr_T} \left(Le_T - 1 \right) \right] \bar{h}_i \frac{\partial \bar{c}_i}{\partial \bar{y}} \right\}$$

Element Conservation

$$\bar{\rho}\,\bar{u}\,\frac{\partial \bar{\alpha}_i}{\partial \bar{s}} + \left(\bar{\rho}\,\bar{v} + \overline{\rho' v'}\right)\frac{\partial \bar{\alpha}_i}{\partial \bar{y}} = \frac{\partial}{\partial \bar{y}}\left[\left(\frac{\bar{\mu}\,Le}{Pr} + \bar{\rho}\,\bar{\epsilon}\,\frac{Le_T}{Pr_T}\right)\frac{\partial \bar{\alpha}_i}{\partial \bar{y}}\right] \qquad (4)$$

where $j = 0$ for 2-D planar flow, $j = 1$ for axisymmetric flow, μ, Le, Pr, are the usual molecular viscosity, Lewis number, and Prandtl number, respectively, and ϵ, Le_T, Pr_T are their turbulent counterparts.

The boundary conditions at the edge of the boundary layer, $y = \delta$, are set by the inviscid flow and are:

Edge: $y = \delta$

$$\bar{u} = \bar{u}_e \qquad (5)$$
$$\bar{H} = \bar{H}_e$$
$$\bar{\alpha} = \bar{\alpha}_{i_e}$$

In practice, many times the pressure distribution, rather than the edge velocity, is specified. In such cases the velocity distribution is found from the given pressure field using Bernoulli's equation.

At the wall, $y = 0$, the boundary conditions are:

Wall: $y = 0$

$$\bar{u} = 0 \qquad (6)$$
$$\bar{\rho}\,\bar{v} + \overline{\rho' v'} = \bar{\rho}_w \bar{v}_w = \bar{\dot{m}}_w, \text{ given mass transfer distribution}$$
$$\bar{T} = \bar{T}_w, \text{ specified wall temperature distribution}$$
$$\frac{\partial \bar{\alpha}_i}{\partial \bar{y}}\Big|_w = \bar{\rho}_w \bar{v}_w \left(\bar{\alpha}_{i_w} - \bar{\alpha}_{i_{Trans}}\right)\frac{Pr_w}{\bar{\mu}_w Le_w}$$

where the α_{i_w} boundary condition is determined by the condition that the net elemental mass flux at the wall (i.e., the sum of the convective and diffusive fluxes) must equal the elemental mass injection rate.

B. TURBULENT TRANSPORT PROPERTIES

In formulating the turbulent equations of motion (1-4) it was assumed that the turbulent flux terms $\bar{\rho}\,\overline{u'v'}$, $\bar{\rho}\,\overline{v'h'}$ and $\bar{\rho}\,\overline{v'c_i'}$ could be related to mean, time averaged quantities, through the use of the phenomenological mixing length-eddy viscosity concept. Accordingly, the eddy viscosity, ϵ, eddy conductivity κ, eddy diffusivity, D_T, turbulent Lewis number, Le_T, and turbulent Prandtl number, Pr_T, have been defined as follows:

$$\epsilon = -\frac{\overline{u'v'}}{\partial \bar{u}/\partial y} \qquad \kappa = -\frac{C_P\,\overline{v'h'}}{\partial \bar{h}/\partial y} \tag{7}$$

$$Le_T = \frac{\bar{\rho}\,C_P D_T}{\kappa} \qquad D_T = -\frac{\overline{v'c_i'}}{\partial \bar{c}_i/\partial y}$$

$$Pr_T = \frac{\epsilon\,C_P}{\kappa}$$

The eddy conductivity as defined in equation (7) and used, via the turbulent Prandtl and Lewis numbers, in equations (3 and 4), is based on static enthalpy fluctuations. Other investigators (e.g., Refs. 1 and 5) have at times defined the eddy conductivity and turbulent Prandtl number on a total enthalpy basis. Bushnell and Beckwith[7] derived the following relation between the turbulent Prandtl number based on total enthalpy, Pr_T' and Pr_T, which is based on static enthalpy. The relation is

$$Pr_T' = Pr_T \left\{ 1 + \frac{u_e^2}{2H_e}\left(Pr_T - 1\right) \frac{\partial (u/u_e)/\partial y}{\partial (H/H_e)/\partial y} \right\}^{-1} \tag{8}$$

From equation (8) it can be seen that the difference between the two Prandtl numbers will be small when either $Pr_T \approx 1$, or viscous dissipation is negligible ($u_e^2/2H_e \leq 1$).

As pointed out in the Introduction, the computer program is designed to allow flexibility in the choice of a turbulence model. Also pointed out, was the fact that for developmental purposes only a single model was pursued. In evaluating the literature, it was felt that the model developed, and then extended, by Cebeci, et al[1,8] was the most thoroughly tested over a wide range of applications, hence, it was selected as the model to be used herein. As more is learned about turbulent flows and reacting turbulent flows, in particular, more refined models will be developed. Hopefully, these advances will be incorporated into the present analysis as they become available.

The details of Cebeci's extended eddy viscosity model may be found in Reference 8, so they will not be reiterated here. The final results are, however, given for the sake of completeness. The model uses a two-layer representation of the eddy viscosity. In the inner region, closer to the wall, the eddy viscosity is based on Prandtl's mixing length theory, as modified by Van Driest to account for the damping effect of the wall, and as extended by Cebeci to include wall mass transfer, compressibility and pressure gradient effects. Thus, the eddy viscosity in the inner region is given by

$$\epsilon_i = \ell^2 \left| \frac{\partial \bar{u}}{\partial \bar{y}} \right| \tag{9}$$

where the mixing length, ℓ, is

$$\ell = .4\,\bar{y}\,[1 - \exp(-\bar{y}/A)] \tag{10}$$

the Van Driest "damping factor," A, is defined as

$$A = \frac{26\bar{\mu}}{(\tau_w \bar{\rho})^{\frac{1}{2}} N} \tag{11}$$

and the factor, N, which accounts for pressure gradient and mass transfer effects is given by

$$N^2 = -\frac{d\bar{P}}{d\bar{x}} \frac{\bar{\mu}}{(\overline{\rho v})_w} \frac{1}{\tau_w} \left[1 - \exp \frac{11.8(\overline{\rho v})_w \bar{\mu}_w}{(\bar{\rho}_w \tau_w)^{\frac{1}{2}} \bar{\mu}} \right] + \exp \frac{11.8(\overline{\rho v})_w \bar{\mu}_w}{(\bar{\rho}_w \tau_w)^{\frac{1}{2}} \bar{\mu}} \tag{12}$$

If $(\overline{\rho v})_w$ equals zero equation (12) becomes a degenerate form and N must be calculated as

$$N^2 = 1 + 11.8 \frac{d\bar{P}}{d\bar{x}} \left(\bar{\rho}_w \bar{\mu}_w \frac{\partial \bar{u}}{\partial \bar{y}} \Big|_w^3 \right)^{-\frac{1}{2}} \tag{13}$$

in the outer, wake-like, portion of the boundary layer, Clauser's form of the eddy viscosity, modified to include an intermittency factor, is used. The outer eddy viscosity is given by

$$\epsilon_o = 0.0168 \, \bar{u}_e \, \delta^*_{inc} \left[1 + 5.5 \left(\frac{\bar{y}}{\delta} \right)^6 \right]^{-1} \tag{14}$$

where the term in brackets is an approximation to Klebanoff's error function intermittency relationship and δ^*_{inc} is the incompressible displacement thickness defined as

$$\delta^*_{inc} = \int_0^\infty \left(1 - \frac{u}{u_e} \right) dy \tag{15}$$

The eddy viscosity for the inner region is used from the wall outward until the height at which $\epsilon_o = \epsilon_i$ is reached. From that point, to the boundary layer edge, the outer expression for eddy viscosity is utilized.

The experimental data of Simpson, et al[9] and others have shown that the turbulent Prandtl number varies considerably across the boundary layer. The calculations of Thielbahr, et al[10] show that for many flows the variation in turbulent Prandtl number must be properly accounted for. The current analysis uses the turbulent Prandtl number formulation developed in Reference 8, thus Pr_T is taken to be

$$Pr_T = \frac{k_m}{k_h} \frac{\left[1 - \exp\left(-y^+/A^+\right) \right]}{\left[1 - \exp\left(-y^+ Pr^{\frac{1}{2}}/B^+\right) \right]} \tag{16}$$

where $k_m = .4$, $k_h = .44$ are the momentum and enthalpy Prandtl mixing length constants, respectively, and

$$y^+ = y u_w^* / \nu_w$$

$$A^+ = 26 \left(\frac{\bar{\rho}_w}{\bar{\rho}} \right)^{\frac{1}{2}} \left(\frac{\bar{\mu}}{\bar{\mu}_w} \right)^{\frac{1}{N}} \tag{17}$$

$$B^+ = 34 \left(\frac{\bar{\rho}_w}{\bar{\rho}} \right)^{\frac{1}{2}} \left(\frac{\bar{\mu}}{\bar{\mu}_w} \right)^{\frac{1}{N}}$$

$$u_w^* = \left(\tau_w / \rho_w \right)^{\frac{1}{2}}$$

at the wall, $y = 0$, equation (16) reduces to

$$Pr_T = \frac{k_m}{k_h} \frac{B^+}{A^+} Pr^{-\frac{1}{2}} \tag{18}$$

Figure 1, taken from Reference 8, contains a comparison of the present Pr_T model with the measurements of Simpson, et al[9] and Jenkins'[11] model.

Not too much is known about the turbulent Lewis number. The somewhat rough results of Reference 12 indicate that it is probably close to unity. In the current analysis the equations and computer program have been kept general, to allow for an arbitrary variation of Le_T. However, no attempt has been made to calculate or model Le_T, and it has been assumed to be equal to unity in all the calculations performed to date.

C. EQUATION OF STATE AND CHEMICAL SYSTEM

In all cases the equation of state may be written as

$$P = \frac{\rho R T}{M} \tag{19}$$

For perfect gas calculations arbitrary values of γ and M may be selected and the following relations are used:

$$C_P = \frac{\gamma (R/M)}{\gamma - 1} \tag{20}$$

$$h = C_P T \tag{21}$$

In its current form the program is only capable of treating a single component ideal gas, the modifications required to treat diffusion effects for a system of nonreacting ideal gases are straightforward and can be incorporated into the analysis in the future, if desired.

While in theory there are no restrictions on the chemical system for which equilibrium computations may be carried out, in practice, core storage limitations and economic constraints on computer execution time can restrict the class of chemical systems which can be treated. The computer program is currently set up and dimensioned to handle the hydrogen-oxygen system and considers two elements (H,O) and six species (H_2, H, OH, H_2O, O_2, O). Only slight modifications would be required to solve a slightly larger chemical system, but, a significantly larger chemical system would not fit in "core" on a standard Univac 1108 system (65K memory)*. Larger chemical systems could be accommodated on other computer systems, however.

The boundary layer equations (1-4) for equilibrium flow are written in terms of the total enthalpy, H, and elemental mass fractions, α_i, however, the species mass fractions, c_i, also appear in the energy equation if Le or Le_T is not equal to unity (in which case the species enthalpies, h_i, also are present). The equilibrium state calculations in the present analysis are performed by selected subroutines from the One-Dimensional Equilibrium (ODE) JANNAF Performance Program[13]. This program is a descendant of the NASA Lewis Equilibrium Program[14] and uses the JANNAF thermodynamic tables[15]. Given the element mass fractions and two thermodynamic state variables the program solves for the species mass fractions and all of the other thermodynamic state variables. At various times in the analysis the following three types of state calculations are performed:

Given	Calculated
α_i, h, P	c_i, T, ρ, S, h_i, etc.
α_i, T, P	c_i, h, ρ, S, h_i, etc.
α_i, S, P	c_i, h, T, ρ, h_i, etc.

*If the analysis is formally restricted to Le and Le_T equal to unity then the C_i and h_i need not be stored in memory and larger chemical systems can be accommodated.

The static enthalpy for a mixture of gases is given by

$$h = \sum_i c_i h_i \tag{22}$$

where, h_i, the enthalpy of each species is defined as

$$h_i = \int_{298}^{T} C_{P_i} dT + \Delta h_{f_{i_{298}}} = h_i(T) - h_i(298) + \Delta h_{f_{i_{298}}} \tag{23}$$

The enthalpies are based on the same reference state as the JANNAF Tables, i.e., the enthalpies of the elements are zero in their standard state at $T = 298^{\circ}K$. A more detailed description of the equilibrium analysis can be found in References 13 and 14.

D. LAMINAR TRANSPORT PROPERTIES

There are no theoretical restrictions on the transport property formulations which can be used and the subroutine structure of the computer program is designed to allow the method of calculating the transport properties to be easily modified. The present formulation requires only the viscosity, Prandtl number and Lewis number to be calculated. The methods used to calculate these quantities are presented below.

Since the ideal gas calculations performed to date were basically for program check-out purposes the transport property calculations for such flows did not receive a great deal of attention. The ideal gas option is restricted to a one component gas so the Lewis number is not required. The Prandtl number is assumed to be a constant. Its value can be selected to approximate the gas being considered. Most of the ideal gas calculations have been for air and currently the viscosity calculation is based on Sutherland's Law expressed as

$$\mu = \frac{2.27 \times 10^{-8} T^{\frac{1}{2}}}{(1 + 198.6/T)} \tag{24}$$

For gases other than air a different viscosity formulation should be used, however, at present no other options are provided for and equation (24) is used for all ideal gas calculations.

The calculation of the laminar transport properties for a mixture of gases (currently H_2-O_2 system) is based on the following. The viscosity of each specie, μ_i, was taken from Reference 16 and is stored as data in tabular form. The viscosity of the mixture is then calculated from Wilke's semi-empirical formula[17].

$$\mu = \sum_{i=1}^{n_s} \mu_i \left(1 + \sum_{\substack{j=1 \\ j\neq i}}^{n_s} \varphi_{ij} \frac{x_j}{x_i}\right)^{-1} \tag{25}$$

where n_s is the number of species, x_i is the mole fraction of species i, and φ_{ij} is

$$\varphi_{ij} = \frac{1}{2^{3/2}} \left(1 + \frac{M_i}{M_j}\right)^{-\frac{1}{2}} \left[1 + \left(\frac{\mu_i}{\mu_j}\right)^{\frac{1}{2}} \left(\frac{M_j}{M_i}\right)^{1/4}\right]^2 \tag{26}$$

Mason and Saxena[18] found the thermal conductivity of a mixture of polyatomic gas could be very satisfactorily approximated by slight modifications to Eucken's relation (which relates the conductivity of a species to its viscosity) and Wilke's formula. Their resulting expression is

$$k = \sum_{i=1}^{n_s} k_i \left(1 + 1.065 \sum_{\substack{j=1 \\ j\neq i}}^{n_s} \varphi_{ij} \frac{x_j}{x_i}\right)^{-1} \tag{27}$$

where k_i the conductivity of the i th species is given by

$$k_i = \frac{15}{4} \mu_i \left(.354\, C_{P_i} + .115\, R/M_i\right) \tag{28}$$

The specific heat of the mixture is*

$$C_P = \sum_{i=1}^{n_s} c_i C_{P_i} \tag{29}$$

and the Prandtl number can then be calculated as

$$Pr = \frac{\mu C_P}{k} \tag{30}$$

Table 1 contains the results of a limited comparison of the predictions for μ and Pr from the above, with the more accurate results of Svehla's calculations[19]. The comparison was made at a pressure of 1 atmosphere, hydrogen mass fractions of 11.19% and 17.5% and temperatures of 1000°K to 4000°K. The results show that the present much simpler and faster calculations are more than adequate and their use is recommended.

The diffusion coefficient and, hence, Lewis number also needs to be determined. In the present effort the effect of nonunity Lewis number was not studied and Le was assumed to be unity. The equations, however, are general (for binary diffusion) and if a method for calculating Le is developed it can easily be adopted. If desired, the effects of multicomponent diffusion, also ignored in the present study, can be considered with some modification to the analysis. The use of the bifurcation approximation[20] is recommended if the effects of multicomponent diffusion are to be considered.

E. NONDIMENSIONALIZED EQUATIONS

The numerical solution of equations (1-4) involves a matrix inversion procedure. In an effort to improve the accuracy and reduce the possibility of round-off error in the solution, the independent and dependent variables have been nondimensionalized and scaled, when necessary, so that the resulting normalized variables are much more uniform in magnitude. The independent and

*The specific heat as defined in equation (29) is sometimes referred to as the "frozen" specific heat.

TABLE 1

COMPARISON OF CURRENT TRANSPORT PROPERTY CALCULATIONS WITH THE RESULTS OF SVEHLA[19]

Pressure = 1 Atmosphere

$\%H_2$	$T^{\circ}K$	Viscosity (Poises)		Prandtl Number	
		Current	Svehla	Current	Svehla
11.19	1000	358.7×10^{-6}	356×10^{-6}	.7069	.7477
	2000	663.8×10^{-6}	660×10^{-6}	.7120	.7237
	3000	893.0×10^{-6}	895×10^{-6}	.6182	.6178
	4000	942.6×10^{-6}	974×10^{-6}	.4281	.4255
17.5	1000	344.2×10^{-6}	351×10^{-6}	.5297	.537
	2000	619.2×10^{-6}	614×10^{-6}	.5632	.5605
	3000	829.0×10^{-6}	820×10^{-6}	.5530	.5381
	4000	872.6×10^{-6}	878×10^{-6}	.4485	.4181

dependent variables have been normalized as follows:

$$s = \bar{s}/L \qquad y = G(\tilde{y}),\ \tilde{y} = \bar{y}/L\zeta(s)$$

$$u = \frac{\bar{u}}{u_r} \qquad \rho = \frac{\bar{\rho}}{\rho_r} \qquad \rho v = \frac{(\bar{\rho}\bar{v} + \bar{\rho}'\bar{v}')}{\rho_r u_r \zeta(s)} \tag{31}$$

$$p_e = \frac{\bar{p}_e}{\rho_r u_r^2} \qquad H = \frac{\bar{H}}{u_r^2} \qquad h_i = \frac{\bar{h}_i}{u_r^2}$$

$$\mu = \frac{\bar{\mu}}{\mu_r} \qquad \epsilon = \frac{\bar{\epsilon}}{\nu_r} \qquad r_w^j = \frac{\bar{r}_w^j}{L}$$

where r subscripted quantities are reference values and L is a reference length.

The function $\zeta(s)$ has been defined such that it is always almost equal to the boundary layer thickness

$$\zeta = (\bar{y}/L)_\zeta \quad \text{where } (\bar{y}/L)_\zeta \text{ is the value of } \bar{y}/L \text{ where } |1 - u/u_e| = .01^*$$

Using ζ to normalize $\bar{y}/L$ then yields $\tilde{y}$ values at the edge of the boundary layer of about unity for all s, and, hence, few, if any, mesh points have to be added as the finite difference calculations proceed downstream. In addition, the normal coordinate is also stretched by the function $G(\tilde{y})$ (see Section H). This function has been designed to stretch $\tilde{y}$ near the wall (in order to cope with the steep wall gradients in turbulent boundary layers), while allowing constant step size to be taken in the transformed coordinate, y. Constant step size in the normal direction is not mandatory, however, it does yield much simpler difference equations.

*This condition could possibly be satisfied at more than one location in the boundary layer, however, the program will always determine the largest value of $\bar{y}/L$ which meets the test.

The partial derivatives in the transformed coordinates are given by:

$$\frac{\partial}{\partial \bar{s}} = \frac{1}{L}\frac{\partial}{\partial s} - G'\frac{\zeta'}{\zeta}\frac{\tilde{y}}{L}\frac{\partial}{\partial y}$$

$$\frac{\partial}{\partial \bar{y}} = \frac{G'}{L\zeta}\frac{\partial}{\partial y} \qquad (32)$$

and the nondimensional equations become

Continuity

$$\frac{1}{r_w^j}\frac{\partial}{\partial s}(\rho u r_w^j) - \frac{G'\zeta'}{\zeta}\tilde{y}\frac{\partial}{\partial y}(\rho u) + G'\frac{\partial}{\partial y}(\rho v) = 0 \qquad (33a)$$

Momentum

$$\rho u\frac{\partial u}{\partial s} - \rho u\frac{G'\zeta'}{\zeta}\tilde{y}\frac{\partial u}{\partial y} + \rho v G'\frac{\partial u}{\partial y} = -\frac{dp_e}{ds} + \frac{G'}{\zeta^2}\frac{1}{Re_\infty}\frac{\partial}{\partial y}\left[G'(\mu + \rho\epsilon)\frac{\partial u}{\partial y}\right] \qquad (33b)$$

Energy

$$\rho u\frac{\partial H}{\partial s} - \rho u\frac{G'\zeta'}{\zeta}\tilde{y}\frac{\partial H}{\partial y} + \rho v G'\frac{\partial H}{\partial y} = \frac{G'}{\zeta^2}\frac{1}{Re_\infty}\frac{\partial}{\partial y}\left\{G'\left(\frac{\mu}{Pr} + \frac{\rho\epsilon}{Pr_T}\right)\frac{\partial H}{\partial y}\right.$$
$$\left. + G'\left[\mu\left(1-\frac{1}{Pr}\right) + \rho\epsilon\left(1-\frac{1}{Pr_T}\right)\right]u\frac{\partial u}{\partial y} + \sum_i G'\left[\frac{\mu}{Pr}(Le-1) + \rho\epsilon(Le_T-1)\right]h_i\frac{\partial c_i}{\partial y}\right\} \qquad (33c)$$

Element

$$\rho u\frac{\partial \alpha_i}{\partial s} - \rho u\frac{G'\zeta'}{\zeta}\tilde{y}\frac{\partial \alpha_i}{\partial y} + \rho v G'\frac{\partial \alpha_i}{\partial y} = \frac{G'}{\zeta^2}\frac{1}{Re_\infty}\frac{\partial}{\partial y}\left[G'\left(\frac{\mu Le}{Pr} + \rho\epsilon\frac{Le_T}{Pr_T}\right)\frac{\partial \alpha_i}{\partial y}\right] \qquad (33d)$$

The eddy viscosity formulas, equations (9-15) must be written in terms of nondimensionalized variables. With the exception of the equation for ϵ_i, the procedure is simple and straightforward. The nondimensional form for ϵ_i

is given below:

$$\epsilon_i = .16\, Re_r\, \zeta\, G'\, \tilde{y}^2 \left|\frac{\partial u}{\partial y}\right| \left\{1 - \exp\left[-\frac{Re_r\, \zeta\, \tilde{y}\, N}{26\mu}\left(\frac{\rho \mu_w}{Re_r\, \zeta}\, \frac{\partial u}{\partial \tilde{y}}\Big|_w\right)^{\frac{1}{2}}\right]\right\}^2 \quad (34)$$

where

$$N^2 = -\frac{dP_e}{ds}\, \frac{\mu}{(\rho v)_w \mu_w\, \partial u/\partial \tilde{y}|_w}\left[1 - \exp\left\{\frac{11.8\,(\rho v)_w}{\mu}\left[\frac{Re_r\, \zeta^3 \mu_w}{\rho_w\, \partial u/\partial \tilde{y}|_w}\right]^{\frac{1}{2}}\right\}\right] \quad (35)$$

$$+ \exp\left\{\frac{11.8(\rho v)_w}{\mu}\left[\frac{Re_r\, \zeta^3 \mu_w}{\rho_w\, \partial u/\partial \tilde{y}|_w}\right]^{\frac{1}{2}}\right\}$$

however, if $(\rho v)_w = 0$, then

$$N^2 = 1 + 11.8\, \frac{dP_e}{ds}\left[\frac{Re_r\, \zeta^3}{\rho_w \mu_w\, \partial u/\partial \tilde{y}\,|_w^3}\right]^{\frac{1}{2}} \quad (36)$$

F. FINITE DIFFERENCE EQUATIONS

Most of the more recent numerical boundary layer solutions[1-6] have utilized some sort of so-called "implicit" finite difference technique. The basic reason for the selection is the inherent numerical stability that implicit techniques offer. In the current analysis the finite difference technique used to solve the equations of motion is based upon the Crank-Nicolson[21] implicit method. In deriving the finite difference equations the following mesh notation was used:

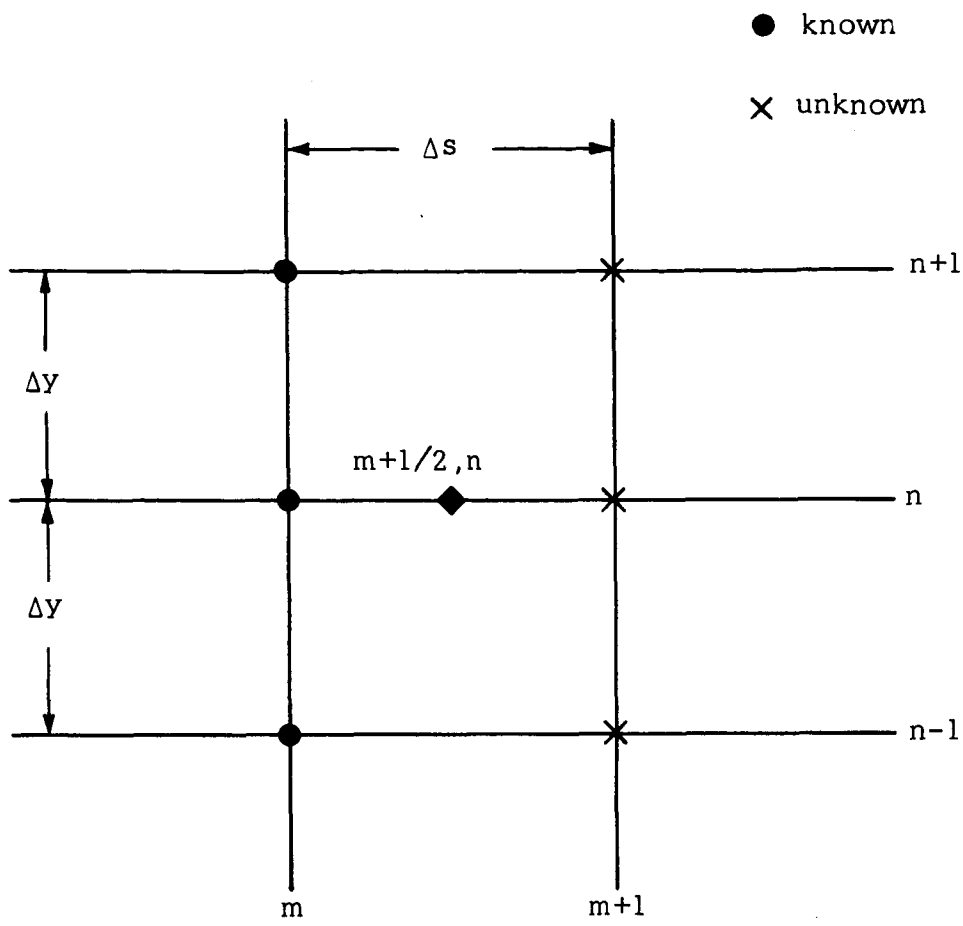

Finite Difference Mesh

The dependent variables are known at grid points (m) and are unknown at grid points (m + 1) a small distance, Δs, downstream. In the Crank-Nicolson finite difference scheme the unknowns at (m + 1) are found by replacing the partial derivatives with linear difference quotients and evaluating the partial differential equations at m + 1/2, n.

If V and W are used to denote the unknown dependent variables, the difference quotients at (m + 1/2, n) can be written as:

$$\frac{\partial V}{\partial x} = (V_{m+1,n} - V_{m,n})/\Delta s \qquad (37)$$

$$\frac{\partial V}{\partial y} = \frac{1}{2} V_{y_{m,n}} + (V_{m+1,\,n+1} - V_{m+1,\,n-1})/4\Delta y \tag{38}$$

$$\frac{\partial^2 V}{\partial y^2} = \frac{1}{2} V_{yy_{m,n}} + (V_{m+1,\,n+1} - 2\,V_{m+1,n} + V_{m+1,n-1})/2\Delta y^2 \tag{39}$$

$$\frac{\partial V}{\partial y}\frac{\partial W}{\partial y} = \left[V_{y_{m,n}}(W_{m+1,n+1} - W_{m+1,n-1}) + W_{y_{m,n}}(V_{m+1,n+1} - V_{m+1,n-1})\right]/4\Delta y \tag{40}$$

where:

$$V_{y_{m,n}} = (V_{m,n+1} - V_{m,n-1})/2\,\Delta y \tag{41}$$

$$V_{yy_{m,n}} = (V_{m,n+1} - 2\,V_{m,n} + V_{m,n-1})/\Delta y^2 \tag{42}$$

Nonlinear terms involving products of the dependent variables are written as

$$V^2 = V_{m,n}\,V_{m+1,n} \tag{43}$$

$$VW = \frac{1}{2}(V_{m,n}\,W_{m+1,n} + V_{m+1,n}\,W_{m,n}) \tag{44}$$

All of the previous approximations involve truncation errors on the order of $(\Delta s^2, \Delta y^2)$. To obtain truncation errors of similar magnitude for terms of the following type

$$V\frac{\partial W}{\partial s},\ \lambda\frac{\partial V}{\partial y},\ \lambda\frac{\partial V}{\partial s},\ \lambda V,\ \text{etc.}$$

the difference quotients would have to be written as

$$V_{m+1/2,n}(W_{m+1,n} - W_{m,n})/\Delta s$$

$$\lambda_{m+1/2,n}(V_{m+1,n} - V_{m,n})/\Delta s, \text{ etc.} \tag{45}$$

where λ represents any secondary dependent variable, i.e., ρ, μ, etc. Difference quotients like (45) lead to nonlinear difference equations and are unacceptable for present purposes. In order to surmount this difficulty the m + 1/2 unknowns in forms like (45) must be evaluated in a linearized manner. Presently, m + 1/2 variables are calculated as

$$\lambda^{(i)}_{m+1/2,n} = 1/2(\lambda_{m,n} + \lambda^{(i-1)}_{m+1,n}) \tag{46}$$

where superscript i refers to the number of iterations. Initially, $\lambda_{m+1/2,n} = \lambda_{m,n}$, and the truncation error is of order Δs. To reduce the truncation error one has the option of reducing the step size, or iterating the solution at each finite difference step. One iteration is sufficient to reduce the truncation error to order Δs^2 (22)

When the above difference approximations (37-46) are substituted into the nondimensionalized equations (33) a set of $(2 + n_e)N$ linear algebraic equations for u, H, $\alpha_i (i = 1, \ldots n_e)$ are generated. As a direct result of the linearization, the solution for (ρv) becomes uncoupled and it may be found by numerically integrating the continuity equation after u, H and the α_i have been calculated.

The equations for u, H and α_i may be solved as a coupled set (e.g., Refs. 22 and 23) or they may be uncoupled and solved successively. The latter, uncoupled, method of solution was selected since it requires less computer memory storage and is computationally faster (the more chemical elements considered the greater the advantage becomes).

The resulting finite difference equations for the momentum, energy and element continuity equations can all be written in the following form:

$$A_n W_{m+1,n+1} + B_n W_{m+1,n} + C_n W_{m+1,n-1} = D_n \quad n = 1 \ldots N-1 \tag{47}$$

where W stands for either u, H or α_i.

In deriving the A_n, B_n, C_n, D_n coefficients, equations (37-46) were used and the order of solution was chosen to be momentum first, followed in order by the energy and successive element continuity equations (for the H-O system there is only 1 element continuity equation). In addition, the final form of the coefficients, as presented below, makes use of the following definitions:

$$E = \frac{\rho G' \zeta' \tilde{y}}{\zeta} \qquad F = \frac{G'}{\zeta^2} \frac{1}{Re_r}$$

$$\begin{aligned}
\sigma_1 &= (\mu + \rho \epsilon) \\
\sigma_2 &= \left(\frac{\mu}{Pr} + \frac{\rho \epsilon}{Pr_T}\right) \\
\sigma_3 &= \mu \left(1 - \frac{1}{Pr}\right) + \rho \epsilon \left(1 - \frac{1}{Pr_T}\right) \\
\sigma_4 &= \frac{\mu}{Pr} (Le - 1) + \frac{\rho \epsilon}{Pr_T} (Le_T - 1) \\
\sigma_5 &= \frac{\mu Le}{Pr} + \frac{\rho \epsilon Le_T}{Pr_T}
\end{aligned} \tag{48}$$

For the sake of brevity, the quantities to be evaluated at $m + 1/2, n$ have been left unsubscripted. They are calculated in the manner prescribed by equation (46).

Momentum Coefficients

$$A_n = \frac{-Eu_{m,n}}{4\Delta y} + \frac{\rho v G'}{4\Delta y} - F\left[\left(\frac{G''}{G'}\sigma_1 + G'\sigma_{1y}\right)/4\Delta y + \frac{G'\sigma_1}{2\Delta y^2}\right]$$

$$B_n = \frac{\rho u}{\Delta s} - \frac{E}{2}u_{y_{m,n}} + \frac{FG'\sigma_1}{\Delta y^2}$$

$$C_n = \frac{E u_{m,n}}{4\Delta y} - \frac{\rho v G'}{4\Delta y} + F\left[\left(\frac{G''}{G'}\sigma_1 + G'\sigma_{1y}\right)/4\Delta y - \frac{G'\sigma_1}{2\Delta y^2}\right] \qquad (49)$$

$$D_n = \frac{\rho u u_{m,n}}{\Delta s} - \frac{dp_e}{ds} + \frac{FG'\sigma_1 u_{yy_{m,n}}}{2} - \frac{\rho v G' u_{y_{m,n}}}{2} + \frac{F}{2}\left[\frac{G''}{G'}\sigma_1 + G'\sigma_{1y}\right]u_{y_{m,n}}$$

Energy Coefficients

$$A_n = -\frac{Eu_{m,n}}{4\Delta y} + \frac{\rho v G'}{4\Delta y} - \frac{F}{4\Delta y}\left(\frac{G''}{G'}\sigma_2 + G'\sigma_{2y}\right) - \frac{G'\sigma_2 F}{2\Delta y^2}$$

$$B_n = \frac{\rho u}{\Delta s} + \frac{FG'\sigma_2}{\Delta y^2}$$

$$C_n = -A_n - \frac{FG'\sigma_2}{\Delta y^2}$$

$$D_n = \frac{\rho u H_{m,n}}{\Delta s} - \frac{\rho v G'}{2} H_{y_{m,n}} + \frac{F}{2}\left[\left(\frac{G''}{G'}\sigma_2 + G'\sigma_{2y}\right)H_{y_{m,n}} \right. \qquad (50)$$

$$\left. + G'\sigma_2 H_{yy_{m,n}}\right] + \frac{F}{2}\left(\frac{G''}{G'}\sigma_3 + G'\sigma_{3y}\right)\frac{u_{m,n}}{2\Delta y}\left(u_{m+1,n+1} - u_{m+1,n-1}\right)$$

$$+ \frac{FG'\sigma_3}{2\Delta y}\left(u_{y_{m,n}} + \frac{u_{m,n}}{\Delta y}\right)\left(u_{m+1,n+1} + u_{m+1,n-1}\right) - \frac{FG'\sigma_3}{\Delta y} u_{y_{m,n}} u_{m+1,n-1}$$

$$+\left[\frac{E}{2}H_{y_{m,n}} + \frac{F}{2}\left(\frac{G''}{G'}\sigma_3 + G'\sigma_{3y}\right)u_{y_{m,n}} + \frac{FG'\sigma_3}{2}\left(u_{yy_{m,n}} - \frac{2u_{m,n}}{\Delta y^2}\right)\right] u_{m+1,n}$$

$$+ F\sum_i\left[G'\sigma_4 h_i c_{i_y}\right]_y$$

Element Coefficients

$$A_n = \frac{-E\,u_{m,n}}{4\Delta y} + \frac{\rho v G'}{4\Delta y} - \frac{F}{2}\left[\left(\frac{G''}{G'}\sigma_5 + G'\sigma_{5y}\right)/2\Delta y + \frac{G'\sigma_5}{\Delta y^2}\right]$$

$$B_n = \frac{\rho u}{\Delta s} + \frac{FG'\sigma_5}{\Delta y^2} \qquad (51)$$

$$C_n = -A_n - \frac{FG'\sigma_5}{\Delta y^2}$$

$$D_n = \frac{\rho_u \alpha_{i_{m,n}}}{\Delta s} - \frac{\rho v G'}{2}\alpha_{i_{y_{m,n}}} + \frac{F}{2}\left[\left(\frac{G''}{G'}\sigma_5 + G'\sigma_{5y}\right)\alpha_{i_{y_{m,n}}} + G'\sigma_5\alpha_{i_{yy_{m,n}}}\right] + \frac{E}{2}\alpha_{i_{y_{m,n}}} u_{m+1,n}$$

G. SOLUTION OF THE DIFFERENCE EQUATIONS

The difference equations, in the form of equation (47), are tridiagonal in nature and a very efficient method of solution is available[24]. The method is based on Gaussian elimination, but it takes advantage of the highly structured form of a tridiagonal matrix. The tridiagonal system of equations for each of the equations of motion (Eq. (47)) can be rewritten in the following matrix form

$$AW = B \qquad (52)$$

If the mesh indexing is set up so that 1 corresponds to the wall and N to the last point at the edge of the boundary layer, then A is an (N - 2) x (N - 2) matrix of coefficients, W is an (N - 2) column vector of unknowns and B is also of dimension (N - 2) and contains all of the nonhomogeneous terms in the equations. For each variable (u, H, α_i) at each finite difference station there are actually (N) unknowns, represented by $W_{m+1,n}$ n = 1, 2, . . . , N. Two equations for the unknowns are supplied by the boundary conditions at the wall and at the boundary layer edge. The boundary conditions, depending

upon their nature, either specify a wall or edge value, or specify a condition which can be used to relate the value of the variable at the wall or edge to its value at one or several internal mesh points. Thus, there remains the set of (N - 2) equations for (N - 2) unknowns given by equation (52). The tridiagonal form of the coefficient matrix, A, is depicted below:

$$A = \begin{Vmatrix} a_{11} & a_{12} & & & & \\ a_{21} & a_{22} & a_{23} & & & \\ & a_{32} & a_{33} & a_{34} & & \\ & & \ddots & \ddots & \ddots & \\ & & & a_{N-2,N-3} & a_{N-2,N-2} \end{Vmatrix} \tag{53}$$

As its name infers all of the nonzero elements lie along the three main diagonals of the matrix. The solution of the equations given by (52) is simply effected using the following recursion relations, which correspond to forward (Gaussian) elimination and back substitution.

Forward Elimination

$$\lambda_1 = \frac{a_{12}}{a_{11}} \qquad \beta_1 = \frac{b_1}{a_{11}} \tag{54}$$

$$\lambda_i = \frac{a_{i,i+1}}{a_{i,i} - \lambda_{i-1}, a_{i,i-1}} \qquad \beta_i = \frac{b_i - \beta_{i-1}\, a_{i,i-1}}{a_{i,i} - \lambda_{i-1}\, a_{i,i-1}} \tag{55}$$

$$i = 2, 3, \ldots, N-2$$

Back Substitution

$$W_{N-1} = \beta_{N-1} \tag{56}$$

$$W_i = \beta_i - W_{i+1}\,\lambda_i \qquad i = N-2,\ N-3,\ \ldots,\ 2 \tag{57}$$

The values of the unknown W_i's at the wall, W_1, and edge, W_N, are then found from the boundary conditions. From equations (5) and (31) it follows that

$$u_N = \frac{\bar{u}_e}{u_r}$$

$$H_N = \frac{\bar{H}_e}{u_r^2} \tag{58}$$

$$\alpha_{i_N} = \alpha_{i_e}$$

and equations (6) and (31) yield

$$u_1 = 0$$

$$H_1 = \frac{\bar{H}_w}{u_r^2} = \frac{\bar{h}_w}{u_r^2}^{*} \tag{59}$$

$$\alpha_{i_1} = \frac{4\alpha_{i_2} - \alpha_{i_3} + 2\Delta y\, A_o \alpha_{i_{Trans}}}{2\Delta y A_o + 3}$$

*For a perfect gas specifying $\bar{T}_w$ is equivalent to specifying $\bar{h}_w$. For a real gas flow in chemical equilibrium $\bar{h}_w$ can also be immediately found from $\bar{T}_w$ when there is no mass transfer at the wall. With no mass transfer the α_i at the wall, and in fact throughout the boundary layer, remain constant and given $\bar{P}$, $\bar{T}_w$ and the α_i, $\bar{h}_w$ can be found from the known equilibrium state. With mass addition, however, the α_{i_w} at the next station (m + 1) are not known until the species continuity equation has been solved. In order to solve the equations, however, the boundary conditions must be specified in advance. In this case, in finding the $\bar{h}_w$ corresponding to the specified T_w the α_{i_w} must be approximated. Currently, in finding $\bar{h}_w$, $\alpha^{(j)}_{i_{w_{(m+1)}}}$ is set equal to $\alpha^{(j-1)}_{i_{w_{(m+1)}}}$, where superscript (j) refers to the number of iterations. On the first pass $\alpha^{(1)}_{i_{w_{(m+1)}}} = \alpha_{i_{w_{(m)}}}$.

where

$$A_o = \frac{Re_r \zeta^2 \dot{m}_w Pr_w}{G' \mu_w Le_w} \tag{60}$$

and $\alpha_{i_{Trans}}$ is the mass fraction of element i in the transpiration coolant. In deriving the equation for α_{i_1} in equation (59) the derivative $\partial\alpha_i/\partial y|_w$ was written in finite difference form using the 3 point numerical derivative given by

$$\frac{\partial \alpha_i}{\partial y}\Big|_w = \frac{1}{2\Delta y}(-3\alpha_1 + 4\alpha_2 - \alpha_3) \tag{61}$$

The edge boundary conditions, equation (5), are in theory only satisfied asymptotically in the limit as y approache infinity. It, therefore, follows that the boundary conditions imply that

$$\lim_{y\to\infty} \frac{\partial u}{\partial y} = \lim_{y\to\infty} \frac{\partial H}{\partial y} = \lim_{y\to\infty} \frac{\partial \alpha_i}{\partial y} = 0 \tag{62}$$

In practice, the boundary conditions must be applied at a finite value of y (unless a scale transformation which maps $y = 0 \to \infty$ into a finite domain is used) and the conditions expressed in equation (62) can only be satisfied to within a specified tolerance. The smaller the tolerance the greater the y value at the edge of the boundary layer. The actual solution is carried out assuming a value for the tolerance, ϵ, has been specified. Then, after the momentum equation has been solved, the solution is tested to see if the derivative at the edge of the boundary layer is sufficiently close to zero. The actual test is

$$\frac{1}{u_e} \frac{\partial u}{\partial y}\Big|_e \leq \epsilon \tag{63}$$

where $\frac{\partial u}{\partial y}\Big|_e$ is approximated as

$$\frac{\partial u}{\partial y}\Big|_e = \frac{1}{2\Delta y}\left(-3u_{m+1,N} + 4u_{m+1,N-1} - u_{m+1,N-2}\right) \tag{64}$$

If this test is not satisfied an extra mesh point is added and the solution is repeated. This procedure continues until equation (63) is satisfied. The use of the ζ function to normalize the boundary layer height keeps the number of points added to a minimum*.

Equivalent tests are carried out on the enthalpy and element mass fraction profiles after the energy and element equations have been solved.

After the momentum, energy and element equations have been solved at a particular station, and the corresponding fluid and transport properties have been evaluated, the continuity equation can be numerically integrated as follows. The derivatives and coefficients in the continuity equation are evaluated at $m + 1/2$, $n - 1/2$.

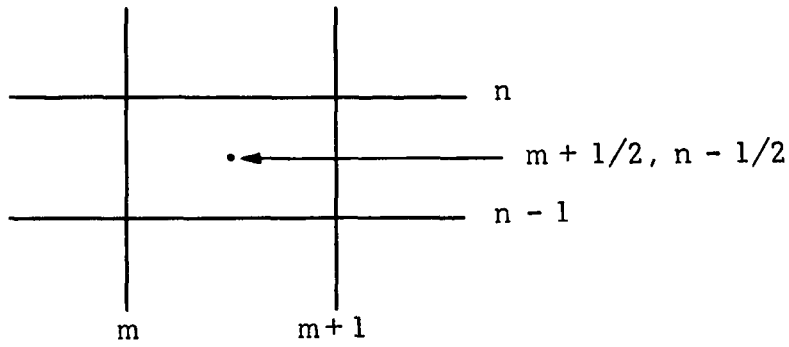

*In the program if equation (63) is not satisfied after five mesh points are added at a given station, the solution is terminated, since such a result is usually symptomatic of errors either in the input tables or the selection of step sizes.

using central difference quotients. This allows ρv to be calculated from the wall to the boundary layer edge as

$$\rho v_{m+\frac{1}{2},n} = \rho v_{m+\frac{1}{2},n-1} + \left\{ - \frac{1}{G'_{n-\frac{1}{2}}} \frac{\partial \rho u}{\partial s} - \frac{\rho u_{m+\frac{1}{2},n-\frac{1}{2}}}{G'_{n-\frac{1}{2}} r^j_{w_{m+\frac{1}{2}}}} \frac{dr^j_w}{ds} \Big|_{m+\frac{1}{2}} \right. \tag{65}$$

$$\left. + \left(\frac{\zeta' \tilde{y}}{\zeta} \right)_{m+\frac{1}{2},n-\frac{1}{2}} \frac{\partial \rho u}{\partial y} \right\} \Delta y$$

where

$$\begin{aligned}
\frac{\partial}{\partial s} \rho u &= \left(\rho u_{m+1,n} + \rho u_{m+1,n-1} - \rho u_{m,n} - \rho u_{m,n-1} \right) / 2\Delta s \\
\rho u_{m+\frac{1}{2},n-\frac{1}{2}} &= \frac{1}{4} \left(\rho u_{m+1,n} + \rho u_{m+1,n-1} + \rho u_{m,n} + \rho u_{m,n-1} \right) \\
\frac{\partial \rho u}{\partial y} &= \left(\rho u_{m+1,n} + \rho u_{m,n} - \rho u_{m+1,n-1} - \rho u_{m,n-1} \right) 2\Delta y \\
\frac{\partial \rho v}{\partial y} &= \left(\rho v_{m+\frac{1}{2},n} - \rho v_{m+\frac{1}{2},n-1} \right) / \Delta y
\end{aligned} \tag{66}$$

The value of ρv at the wall required to start the calculation is either zero or equal to $\dot{m}_w$, the local mass flux rate, depending on whether transpiration cooling is present.

After the continuity equation has been solved, the solution at that station is complete and the boundary layer profile parameters can be calculated. However, an option to iterate the solution until the change in skin friction is less than a specified percentage, or until a specified number of iterations have been performed, has also been included*. There is a trade-off between iterating and taking more steps in the s direction. In order to optimize the choice, more experience with the program will be required.

*In Reference 1 the eddy viscosity at each mesh point was averaged with its value at four surrounding points (two above and two below) in order to aid in convergence of the iteration procedure. This procedure was also adopted in the current analysis early in its development and it seemed to improve the results by preventing error growth by feedback between the velocity profile and eddy viscosity.

H. STRETCHING OF THE NORMAL COORDINATE - G FUNCTION

Turbulent boundary layers are much thicker than laminar ones and yet have much steeper gradients near the wall. In order to accurately compute turbulent boundary layers using finite difference techniques alone, thousands of steps would have to be taken if equal step sizes in physical coordinates were used. Other investigators (e.g., Refs. 1 and 4) have solved this problem by employing variable step sizes in the y direction. This, however, leads to a much more complicated set of difference equations than those presented herein (developed for constant step size). In the present analysis, the problem is solved by analytically mapping the physical normal coordinate $\tilde{y}$ into y such that constant step size in y yields very small $\tilde{y}$ steps near the wall and larger steps as one proceeds outward. In order to be applicable a function should possess, at a minimum, the following characteristics: its first and second derivatives should be continuous and monatonically decreasing. The function currently utilized is

$$\frac{y}{b} + \beta = \left\{ \ln \left[(e-1) \left(\frac{\tilde{y}}{b} + \alpha \right) + 1 \right] \right\}^{1/n} \tag{67}$$

which has the inverse

$$\tilde{y} = b \left[\frac{1}{e-1} \left(e^{(y/b + \beta)^n} - 1 \right) - \alpha \right] \tag{68}$$

The constants α and β are determined by the condition that $\frac{dy}{d\tilde{y}} \Big|_{\tilde{y}=0}$ equals a specified number. The constant, b, is equal to the value of $\tilde{y}$ at the edge of the boundary at the initial station. Figure 2 shows what this function looks like for several values of n, with α and $\beta = 0$ (α and $\beta = 0$ yield $dy/d\tilde{y} \Big|_{\tilde{y}=0} = \infty$). The amount of stretching is basically controlled by the parameter n. The first and second derivatives of the stretching function (equation (67)) are also required in the analysis and are:

$$\frac{dy}{d\tilde{y}} = G' = \frac{(e-1)}{nD} (\ln D)^{\left(\frac{1}{n} - 1\right)} \tag{69}$$

$$\frac{d^2y}{d\tilde{y}^2} = G'' = \frac{1}{nb}\left(\frac{e-1}{D}\right)^2\left[\left(\frac{1}{n}-1\right)\left(\ell n D\right)^{\left(\frac{1}{n}-2\right)} - \left(\ell n D\right)^{\left(\frac{1}{n}-1\right)}\right] \quad (70)$$

where,

$$D = \left(e-1\right)\left(\frac{\tilde{y}}{b}+\alpha\right)+1 \quad (71)$$

Another form for the G function which could be used is

$$y = \frac{\Delta y}{\ln K}\ln\left[1+\frac{(K-1)\tilde{y}}{\Delta\tilde{y}_o}\right] \quad (72)$$

which has the inverse

$$\tilde{y} = \Delta\tilde{y}_o\,\frac{K^{y/\Delta y}-1}{K-1} \quad (73)$$

In this latter formulation the initial step size from the wall in the physical plane $\Delta\tilde{y}_o$ is specified and each succeeding step is larger by the factor K (thus in the physical plane the step sizes are a geometric progression). The step size variation generated by this formula in the physical plane is identical to that used in the variable step size formulation of Reference 1. The latter G function was not tried during the current effort so it has not been conclusively established which is better. However, it does appear that the second form would require the use of considerably more mesh points since the step size does not increase as rapidly away from the wall as it does with equation (67). It is probable, however, that in return for the greater number of mesh points a somewhat higher accuracy is achieved.

A further discussion of the stretching function is given later on when the results of the test cases are presented.

I. THE SCALING FUNCTION, ζ

As defined and described in Section E, the purpose of the ζ function is to scale the normal coordinate $\bar{y}$ such that the normalized coordinate $\tilde{y}$ is about unity at the edge of the boundary layer. Therefore, ζ must be directly related to the thickness of the boundary layer.

The chief difficulty to be surmounted is the fact that the boundary layer thickness is not known until the solution has been obtained. In Reference 5 where a similar type of scaling function has been utilized, the problem was partially overcome by specifying the equivalent of ζ in advance, based on experience or the results of similarity solutions. This procedure, while better than no scaling at all, is limited in its ability to adequately scale general problems with arbitrary boundary conditions (including surface mass transfer) for which there is little or no foreknowledge. On the other hand, attempts to calculate a scaling function, like ζ, as one proceeds, by predictor-corrector or other methods can very often encounter numerical difficulties and become unstable.

In the present analysis the latter course was taken. Numerical difficulties were encountered in developing a procedure for calculating ζ, however, the method presented below has worked quite well for the solutions obtained to date.

Assuming the solution has been completed at station m and the solution at m + 1 is being sought, ζ is found as follows: ζ_m, ζ'_m and ζ_{m-1} are known, ζ_{m+1} is then predicted as

$$\zeta_{m+1} = \zeta_m + \zeta'_m \, \Delta s \tag{74}$$

the difference equations are then solved and a temporary corrected value of ζ_{m+1}, denoted ζ^*_{m+1}, is calculated from the velocity profile as the $\bar{y}/L$ value where $| 1 - u/u_e | = .01$. A value for ζ'_{m+1} is then calculated as

$$\zeta'_{m+1} = \frac{\zeta^*_{m+1} - \zeta_{m-1}}{\Delta s + \Delta s_{-1}} \tag{75}$$

where Δs_{-1} is the step size between stations m and m-1. A corrected value of ζ_{m+1} is then found as follows:

$$\zeta_{m+1} = \zeta_m + \zeta'_{m+1} \Delta s \tag{76}$$

If further iterations are carried out at station m+1 a new value of ζ^*_{m+1} and ζ_{m+1} is then obtained after each iteration. The initial values of ζ and ζ', unless otherwise specified (i.e., through the use of input profiles) are determined as follows. The value of ζ is assumed to be .833 δ, where δ is the initial boundary layer thickness. An initial estimate for ζ' is obtained by applying the results of flat plate incompressible similarity solutions (Ref. 27). First, a virtual origin, x_o, is located; x_o being the upstream length of a flat plate having boundary layer thickness δ. ζ' is then calculated as $.833\, d\delta/dx|x_o$.

For laminar flow

$$\begin{aligned} x_o &= Re_L \zeta^2/25 \\ \zeta' &= \frac{5}{2}\left(Re_L x_o\right)^{-1/2} \end{aligned} \tag{77}$$

while for turbulent flow

$$\begin{aligned} x_o &= \left(\frac{\delta}{.37}\right)^{5/4} Re_L^{1/4} \\ \zeta' &= .833(.37)(.8)(Re_L x_o)^{-1/5} \end{aligned} \tag{78}$$

where $Re_L = \bar{\rho}_e \bar{u}_e L/\bar{\mu}_e$.

In general, when started near the origin of the boundary layer, the solution does not appear to be very sensitive to the initial value of ζ' and, to date, the development of a more sophisticated starting procedure has not been warranted.

J. BOUNDARY LAYER EDGE CONDITIONS

For a so-called first order noninteracting boundary layer solution, the edge boundary conditions are given by the wall streamline results of an inviscid solution. On the inviscid wall streamline the entropy, total enthalpy and element mass fractions are all known and are constant along its whole length. Only one other thermodynamic state quantity can therefore be specified without overdetermining the boundary conditions. Currently this state quantity is assumed to be pressure, or, optionally, for perfect gas flows, velocity, from which pressure is found from Bernoulli's equation.

The initial thermodynamic state is determined from the given inviscid pressure and temperature at the initial station*. The conditions along the boundary layer edge are then found by isentropic expansion (or compression) to the local pressure. For a perfect gas

$$\frac{h_e}{h_{e_i}} = \left(\frac{P_e}{P_{e_i}}\right)^{\frac{\gamma-1}{\gamma}} \tag{79}$$

and

$$u_e = \left[2(H_e - h_e)\right]^{1/2} \tag{80}$$

If u_e is specified the procedure is reversed and h_e is determined from (80) and then P_e from (79).

*Stagnation values can be used if they do not differ too much from the values at the initial station.

For equilibrium cases, the required edge conditions are determined using the P, s option* of the One Dimensional Equilibrium (ODE) portion of the Two Dimensional Kinetics Program (TDK)[13].

The pressure gradient term in the boundary layer equations is also determined by the inviscid pressure distribution. The pressure distribution at the edge of the boundary layer will be known as the result of theoretical calculations or experimental results. In either case the pressure distribution will normally be given in either a graphical or tabular format. The gradient, dP/dx, must therefore be determined by numerical differentiation. The numerical problems inherent in trying to numerically differentiate a function which is not necessarily smooth and well behaved and has large variations in its derivative are well known. Under the above conditions the theoretically achievable accuracy of a given difference formula can rarely be obtained, and in many cases so-called higher order methods result in greater rather than smaller errors. In the present case it was found that standard three point parabolic differentiation or a more complicated scheme using averaged parabolic derivatives (subroutine XNTERP from Ref. 25) would, for most of the problems considered, give erroneous pressure derivatives (sometimes even of the wrong sign) in one or more regions of the flow. Linear derivatives which, in principle, for smooth well defined functions, are of lesser accuracy can be used to eliminate the problem of locally erroneous results, but have the drawback of being only piecewise continuous, i.e., the derivative at the junction of two linear segments takes a finite jump. A method has been developed which hopefully takes advantage of the best features of linear and parabolic differentiation without the drawbacks of either. This method uses averaged linear derivatives and its usage is described below for an arbitrary function $F(x)$. Figure 3 is included for illustrative purposes and shows a portion of a curve, $F(x)$, defined at four points,

*Several subroutines from ODE have been incorporated into the current program, with little or no modification, in order to do the required equilibrium state calculations.

$x_i \rightarrow x_{i+3}$. The linear derivative between each successive pair of points is calculated from

$$F'_i = \frac{F_{i+1} - F_i}{x_{i+1} - x_i} \tag{81}$$

The derivatives for each segment are then considered to represent the derivative at the midpoint of each segment, x_{m_i}, defined as

$$x_{m_i} = \frac{x_i + x_{i+1}}{2} \tag{82}$$

The derivative, $F'(x)$, at all other points* is then found by linear interpolation in a table of $F'_i(x)$ vs x_{m_i}, i.e.,

$$F'(x) = F'_i + \left(F'_{i+1} - F'_i\right) \frac{\left(x - x_{m_i}\right)}{\left(x_{m_{i+1}} - x_{m_i}\right)} \qquad x_{m_i} \le x \le x_{m_{i+1}} \tag{83}$$

The above procedure gives results quite similar to those obtained by 3 point parabolic differentiation for smooth well behaved functions. In fact, for equally spaced points the 3 point derivative at the midpoint (point 2) is equal to the derivative of the straight line connecting points 1 and 3. On the other hand, the current technique is much better behaved if the function is not smooth, like most experimental data.

In the computer program the previously described method of obtaining a numerical derivative was used to calculate a velocity rather than a pressure derivative, since the Bernoulli relation

$$\rho_e u_e \frac{du_e}{dx} = -\frac{dP_e}{dx} \tag{84}$$

*For x values less than the first midpoint and greater than the last, a constant uninterpolated linear derivative is used.

was utilized to eliminate dP_e/dx from the equations.

K. INITIAL PROFILES AND STEP SIZES

As a result of the parabolic nature of the boundary layer equations, initial profiles are required to begin the solution. For certain problems in which the calculations are to begin at a leading edge or stagnation point exact initial profiles can be obtained if similarity coordinates are employed. However, for a more general class of problems the initial profiles must be obtained by an alternative means, such as experimental data, or by approximation.

Currently, the computer program allows two alternative methods for specifying the initial profiles. If the velocity and other required profiles are known, either from experimental data or other calculations, they are input in tabular form. If, however, initial profile information is lacking, provision has been made to start the calculations from power law initial profiles. In either case accurate foreknowledge of the ρv profile is not necessary as errors in this quantity usually have little effect and are quickly damped out.

For an incompressible boundary layer solution only the velocity (u) profile has to be specified (the ρv profile has been arbitrarily made to linearly vary from $(\rho v)_w$ at y = 0 to $[(\rho v)_w + 1]$ at the edge of the boundary layer). For compressible perfect gas problems an initial enthalpy profile must also be specified. Equilibrium H_2-O_2 solutions additionally require an initial hydrogen mass fraction profile. If there is no wall coolant flow at the initial station and there has been none upstream either, then the mass fraction of hydrogen in the boundary layer will be constant and equal to its edge value*. If there is mass addition at the initial station, or there has been upstream, the initial hydrogen mass fraction will vary across the boundary layer, and the variation must either be known or approximated.

If the solution is initiated near the origin of the flow, where the boundary layer is very thin, it would be expected (corroborated by the results presented in Part III) that errors in the initial profiles would be quickly damped out. This welcome circumstance results from the fact that as the boundary layer initially undergoes rapid growth by entrainment the fraction of the total mass, momentum,

*Unless the initial hydrogen mass fraction profile was taken to be nonuniform for some other reason.

and energy flux attributable to the initial profile rapidly decreases. Thus, while the magnitude of the initial errors may not be reduced, percentage wise they asymptotically approach zero as the boundary layer continues to grow.

If, however, for some reason, one wishes to initiate a solution at a downstream location where the boundary layer already has grown to an appreciable fraction of its ultimate thickness, then relatively accurate initial u, h and α_i profiles should be used (an accurate ρv profile is not required), if possible, since further growth and adjustments cannot be counted on to reduce the initial errors to an insignificant level.

For linear systems of equations it can be shown that the Crank-Nicolson finite difference method is unconditionally stable. For nonlinear equations no such proof is possible, however, past experience with the method (e.g., Refs. 22,23) indicates that it is quite stable,at least for laminar boundary layer problems. Numerical problems were, however, encountered, at times, in the development and check out of the present method. While most of these problems were attributable to early, unsatisfactory, formulations for the ζ and G functions; it does appear that, at least with the current technique, step size selection is somewhat more important than it is for a laminar flow. Clausing's studies[26] also shed additional light on the stability of numerical boundary layer solutions and the reasons for, and possible ways of eliminating, oscillations in the solution.

Two methods of varying the longitudinal step size, Δx,* have been provided for. The two methods can be used separately, or together, to suit the requirements of a particular problem. The step size can either be increased or decreased discontinuously or through the use of geometric progressions. Sudden large changes in step size do not usually cause problems as long as they are not encountered too frequently. (Equilibrium solutions can be more sensitive to step size changes). A large step size change can cause a local perturbation in the solution which normally quickly damps out. If the step size is repeatedly changed by a significant factor, before the perturbations from the previous

*For the sake of convenience the axial distance increment, Δx, is specified and the actual computational step size, Δs, is then calculated as $\Delta s = \Delta x/\cos \theta_w$.

changes have disappeared, then erroneous results can be computed.

At times, a problem may require the step size to be changed by one, or several, orders of magnitude in a relatively short distance. Such step size variations can many times be efficiently handled by employing a geometric progression in which each step is a multiple (not too far from unity) of the previous one. If the last value of x computed is denoted by x_o, the latest step size by Δx_o and the common ratio of the progression by k, then the following formulas can be used to compute the step size and distance covered after n additional steps.

$$\Delta x_n = \Delta x_o \, k^n \tag{85}$$

$$x_n = x_o + \Delta x_o \, \frac{k^n - 1}{k - 1} \tag{86}$$

A large number of problems have not yet been solved with the present program and a serious effort to optimize step size selection was not possible. Therefore, the step sizes utilized in the successful solution of the problems considered to date should serve only as a guideline and not as an absolute limit on the step sizes which may be advantageously employed. The size of the x steps that can be used is affected, to a major extent, by the magnitude of the longitudinal gradients, e.g., dr_w/dx, dT_w/dx, dP_e/dx, $d\dot{m}_w/dx$, etc. The higher the gradients the smaller the step size required to maintain a given level of truncation error. Many times discontinuities in one, or several, of the boundary conditions are encountered. Although, theoretically, discontinuities violate the assumptions on which finite difference analyses are based, is it possible to still obtain adequate solutions if the difference method is stable. If the method of solution is stable, the large local truncation errors introduced by the discontinuity will normally damp out over a distance small in comparison with the total region of interest.

In regions where rapid gradients or discontinuities are not present, a step size on the order of 1/100 of the length to be computed has typically been used. Much smaller steps have been used without changing the results by more than 1 or 2%, however, the effect of larger steps has not been

adequately determined. In regions with sizeable gradients, smaller steps should be used. Experience will be the only guide as to how small a step one need take in order to achieve the desired accuracy.

The step size, or number of mesh points, in the y direction must also be selected. Since the use of the ζ function allows the solution to progress without the addition of a significant number of mesh points, the spacing on the initial line essentially determines the mesh size for the whole solution.

The initial number of mesh points for turbulent boundary layer flows has been varied from 80 to 160 in the solutions obtained to date. Most of the computations have been started out with 120 points. The exact number of mesh points to use is not critical since the computed results are usually fairly insensitive to the mesh spacing over a considerable range. The few laminar solutions which have been obtained used 40 to 60 mesh points and no stretching, i.e., $G = 1$, $G' = G'' = 0$. Again, the optimum number of mesh points should be selected on the basis of an accuracy-solution time trade-off.

The equilibrium state calculations are performed by subroutines taken from Reference 13 (based on the method of Reference 14). This method of solving for chemical equilibrium is quite general and is designed to accurately perform a limited number of calculations. For the H_2-O_2 chemical system currently being considered a less general, but more efficient, equilibrium solution could be achieved, however, the time to develop such a solution was not available.

Typical boundary layer solutions for problems of interest involve tens of thousands of mesh points. If an equilibrium state solution was obtained at each mesh point, computation times of one hour or more (Univac 1108) would be encountered. As a result, the feasibility of performing equilibrium state calculation at every "nth" mesh point was investigated. It has been found that solutions can be achieved with equilibrium properties calculated at only every 8th mesh point, without seriously affecting the accuracy of the results (errors are typically of the order of 1%). Currently, averaged parabolic interpolation is used to find the equilibrium properties at mesh points not directly calculated. Improved, accuracy, or a larger allowable spacing, might be achieved by using an interpolation procedure

based on cubic overlapping spline fits.

L. BOUNDARY LAYER PARAMETERS

Once the solution at station m + 1 has been obtained, all of the usual boundary layer profile parameters can be calculated. Currently, the following parameters are computed: displacement thickness, δ^*; momentum thickness, θ; local shear stress and shear stress coefficient, τ and C_f; local heat transfer rate and Stanton number, $-q_w$ and St. If desired, other parameters such as the local Reynolds number based on s and θ, the energy thickness, shape factor δ^*/θ, total mass in the boundary layer and total mass injected into the boundary layer can be easily computed. For rocket engine calculations, the thrust loss due to boundary layer effects and the nozzle wall shape corrected by the displacement thickness are also calculated.

The equations for the profile parameters currently computed are presented below, in both physical and nondimensional coordinates.

$$\delta^* = \int_0^{\bar{y}_e} \left(1 - \frac{\bar{\rho}\,\bar{u}}{\bar{\rho}_e \bar{u}_e}\right) d\bar{y} + \frac{1}{\bar{\rho}_e \bar{u}_e \bar{r}_w^j} \int_0^{\bar{s}} \dot{\bar{m}}_w \bar{r}_w^j \, d\bar{s}$$

$$= L\left\{\zeta \int_0^{y_e} \left(1 - \frac{\rho u}{\rho_e u_e}\right) \frac{dy}{G'} + \frac{1}{\rho_e u_e r_w^j} \int_0^{s} \dot{m}_w \zeta r_w^j \, ds\right\} \tag{87}$$

$$\theta = \int_0^{\bar{y}_e} \frac{\bar{\rho}\,\bar{u}}{\bar{\rho}_e \bar{u}_e} \left(1 - \frac{\bar{u}}{\bar{u}_e}\right) d\bar{y} = L\zeta \int_0^{y_e} \frac{\rho u}{\rho_e u_e} \left(1 - \frac{u}{u_e}\right) \frac{dy}{G'} \tag{88}$$

$$\tau_w = \bar{\mu}_w \left.\frac{\partial \bar{u}}{\partial \bar{y}}\right|_w = \mu_r u_r \frac{G'}{L\zeta} \mu_w \left.\frac{\partial u}{\partial y}\right|_w \tag{89}$$

$$C_f = \frac{\tau_w}{\frac{1}{2}\bar{\rho}_e \bar{u}_e^2} \tag{90}$$

$$-q_w = \frac{\bar{\mu}_w}{Pr_w}\left[\frac{\partial \bar{h}}{\partial \bar{y}}\Big|_w + (Le_w - 1)\sum_i \bar{h}_i \frac{\partial c_i}{\partial \bar{y}}\Big|_w\right] \tag{91}$$

$$= \mu_r' u_r^2 \frac{G'}{L\zeta}\frac{\mu_w}{Pr_w}\left[\frac{\partial h}{\partial y}\Big|_w + (Le_w - 1)\sum_i h_i \frac{\partial c_i}{\partial y}\Big|_w\right]$$

$$St. = \frac{-q_w}{\bar{\rho}_e \bar{u}_e (\bar{H}_e - \bar{H}_w)} \tag{92}$$

The second term of the displacement thickness equation (87) accounts for the effect of mass addition into the boundary. However, as currently defined, the mass addition rate must be a continuous (or piecewise continuous) function for equation (87) to be applicable. In order to treat the case of film cooling, when all of the mass addition occurs at one location, the integral must be replaced by a definite correction term proportional to the total amount of added mass, ΔM.*

The derivatives $\frac{\partial u}{\partial y}\Big|_w$ and $\frac{\partial h}{\partial y}\Big|_w$ in the definitions of τ_w and q_w have to be evaluated numerically. Currently, these derivatives are evaluated using the standard 3 point difference quotient (a parabola is fit through the first three mesh points). Under certain conditions this method of calculating the derivatives is not as accurate as is desirable, and as a result, the possibility of using an integral definition of τ_w and q_w was investigated. In this method the shear stress, for example, is evaluated by integrating the momentum equation across the boundary layer and is given by the following quadrature:

$$\tau_w = -\frac{L\zeta}{\mu_r u_r}\left\{\int_0^{y_e} \frac{1}{F}\left[\rho u \frac{\partial u}{\partial s} + (\rho v G' - EU)\frac{\partial u}{\partial y} + \frac{dP_e}{ds}\right] dy\right\} \tag{93}$$

*The correction term for film cooling is[40] $\Delta M/2\pi \bar{\rho}_e \bar{u}_e \bar{r}_w$

This definition of τ_w proved to be unsatisfactory. When the solution was smooth and had not been perturbed by large step size changes, very rapid boundary condition variation, etc., both (93) and (89) gave essentially equivalent results. However, when the solution was perturbed for some reason, the evaluation of τ_w using equation (93) was seriously affected, while equation (89) was not. This result appears to be due to the problem of accurately evaluating the $\partial u/\partial s$ derivative in equation (93). Reference 26 recommends the use of an averaged 3 and 4 point difference formulation for calculating the wall derivatives. This formula was not evaluated in the present effort, but could easily be tested in the future.

The definition of Stanton number, equation (92), is based on total enthalpy. At times, other definitions have been used so when current Stanton numbers are compared to other results, or data, one should first check if the definitions are the same.

The thrust loss due to boundary layer effects is also calculated for rocket engine flows. The formula used to compute the thrust loss comes from Reference 40, the JANNAF recommended procedure. The formula compares the thrust of an engine with mass flow M + ΔM and boundary layer losses (ΔM is the amount of coolant mass addition) to the thrust of an engine with mass flow M and no boundary layer losses. The thrust loss is given as

$$\Delta F = \left(2\pi \bar{r}_w \bar{\rho}_e \bar{u}_e^2 \cos\theta_w\right)\left(\theta - \frac{1}{\bar{\rho}_e \bar{u}_e \bar{r}_w} \int_0^s \bar{\dot{m}}_w \bar{r}_w \, d\bar{s}\right) - 2\pi \bar{r}_w \cos\theta_w \left(\bar{P}_e - \bar{P}_{amb}\right) \delta^* \tag{94}$$

Equation (94) has been written assuming the coolant mass flow is a continuous distribution (i.e., transpiration), for film cooling the term subtracted from θ would be changed to $\Delta M/2\pi \bar{\rho}_e \bar{u}_e \bar{r}_w$.

III. NUMERICAL RESULTS

In order to checkout both the analysis and the programming, a series of test cases have been solved, and the results compared to other theories and/or data, as the case may be. The checkout procedure is best performed in a logical step by step manner, starting with the simplest cases and progressing upwards in difficulty. The time constraints on the current project did not allow for as many test cases as would be desirable to be considered. Nor was there enough time to systematically vary all of the program operating parameters to try to optimize the accuracy-solution time trade-off. However, the comparisons carried out to date have, in general, validated the current approach.

The first problems to be considered were laminar flows, since the laminar equations can be solved as a purely mathematical problem. Thus, the accuracy of the numerical method and the programming of it can be verified without extraneous complicating factors. The solution of turbulent boundary layer flows, on the other hand, depends upon a certain degree of empiricism (in the modeling of the turbulent flux terms) and "exact" mathematical solutions cannot be achieved. For this reason, turbulent boundary layer solutions are best compared to experimental data.

A. LAMINAR INCOMPRESSIBLE FLOW

The first test case considered was the "old standby" laminar incompressible flat plate flow, for which the classical Blasius solution is exact. A linear initial profile was used for u, ρv was taken to be zero at the initial station, and the initial boundary layer thickness δ/L was set to $10^{-4}(L=1)$. Forty points were used in the y direction and the longitudinal step size Δx (s and x are the same for a flat plate) was 10^{-4} for the first 50 steps and was then increased to 10^{-2}. The criteria for adding points to the boundary layer, and the convergence criteria for iterating the solution were varied from 10^{-1} to 10^{-3} and resulted in no more than a 1% change in the results.

Figure 4 shows a comparison of the calculated results (at station 70) compared with the Blasius profile taken from Reference 27. To graphical

accuracy the current profile is identical to the Blasius solution, in reality the results are only accurate to within approximately 1/2 of 1%. The Blasius solution also gives the following equations for the profile parameters: $C_f(Re_x)^{\frac{1}{2}} = .664$; $\delta^*(Re_r/x)^{\frac{1}{2}} = 1.72$; $\theta\,(Re_r/x)^{\frac{1}{2}} = .664$. The present results yield $C_f(Re_x)^{\frac{1}{2}} = .666$, $\delta^*(Re_r/x)^{\frac{1}{2}} = 1.714$, and $\theta\,(Re_r/x)^{\frac{1}{2}} = .666$ after 70 stations and these values remain constant thereafter. Thus, the calculated profile parameters also agree to about 1/2 of 1% with the Blasius solution.

Figure 5 demonstrates the asymptotic way in which the solution approaches the correct answer when approximate initial profiles are used. As stated above, the initial profiles for this case were far from correct. Initially, then, the solution begins to rapidly adjust due to the combination of profile adustment (the linear initial profiles begin to adjust and take on a reasonable shape) and boundary layer growth (the initial mass and momentum flux, with its inherent error, begins to be a smaller and smaller percentage of the total). This initial rapid adjustment is best carried out with a small step size, both for numerical reasons and to confine the initial sizeable errors to as small a region as is feasible. Once the solution has settled down and the step size is increased the solution rapidly approaches the correct result.

A more difficult problem, the development of a laminar boundary layer in a linearly retarded velocity field given by

$$u_e = 100\,(1 - ax) \quad a = 0.125 \tag{95}$$

has also been computed. This flow was originally studied by Howarth[28] and its exact solution is known essentially all the way up to where the boundary layer separates ($ax \approx .120$). The local skin friction coefficient modified as $\frac{C_f}{2}\,\frac{\bar{u}_e^2}{\bar{u}^2}\left(\frac{Re_r}{.125}\right)^{\frac{1}{2}}$, has been plotted in Figure 6 where it is compared to the exact solution. Up until very near separation the current solution agrees to within one percent of the exact results. The present solution used linear initial profiles, 40 mesh points across the boundary layer and the following x step sizes: 30×10^{-4} steps, 30×10^{-3} steps, then a step size of .007 the rest of the way. In order to achieve an accurate solution closer to the separation

point more points and smaller steps (probably on the order of 0.0001 would have to be taken). All of the above results were calculated with $y = \tilde{y}$ (no stretching).

In preparation for the calculation of turbulent flows, the Howarth solution was repeated using the G function with n = 1.2. The results were essentially identical.

B. LAMINAR COMPRESSIBLE FLOW

The formulation and solution of the energy equation was checked by solving several compressible laminar boundary layer problems. The first compressible flows considered had zero pressure gradients and Pr and Le equal to unity. Under these conditions the total enthalpy profile should be related to the velocity profile by the Crocco integral, i.e.,

$$\frac{H}{H_e} = \frac{H_w}{H_e} + \frac{u}{u_e}\left(1 - \frac{H_w}{H_e}\right) \tag{96}$$

In all cases the current results satisfied the Crocco integral to within less than 1%.

Calculations were also made for a Mach number equal 2 flow over a flat plate with a wall to edge temperature ratio of 0.25. A Prandtl number of 0.75 and Sutherland's law for viscosity were used. Van Driest[29] accurately solved this problem, and the current results, in terms of skin friction, again agreed to about 1%.

In solving the above problems, as well as those to be described below, no attempt was made to obtain solutions accurate to four or more significant figures. Laminar solutions, being in a sense purely mathematical can be, if desired, compared on such a fine level. However, the empirical nature of the turbulence modeling does not warrant the effort or expense required to obtain (i.e., fine mesh and steps sizes and small convergence tolerances) solutions to four or more significant figures.

C. TURBULENT FLAT PLATE AND ACCELERATING FLOW

For the first check on the ability of the program to calculate turbulent flows, the flow over a flat plate was chosen since it is the simplest and most widely studied turbulent flow. Linear initial profiles were again used, however, a continuous variation in the x step was used. The x step size varied from 10^{-4} at the beginning to 2×10^{-2} at the end of the calculation. The first solution was obtained with n = 2 in the G function, $G'_{y=0} = 85$, and could not be continued past a local Reynolds number of somewhat less than 10^6. Additional solutions were carried out with n = 4 and n = 5 and were completely successful. It was determined that to compute turbulent flows with Reynolds numbers on the order of 10^7 to 10^8, the initial derivative at the wall, $G' = dy/d\tilde{y}|_{\tilde{y}=0}$ has to be on the order of 1000.

Figure 7a shows a comparison between the computed turbulent velocity profile and data, in law of the wall coordinates. The results shown are for a Reynolds number of 1×10^7 and it can be seen that excellent agreement was achieved. Figure 7b shows the local skin friction coefficient versus Reynolds number. The current results are compared to both data and results obtained by Cebici and Smith, Reference 1. The present results agree fairly well with the data but are a few percent too low. The present solutions were obtained using only about 100 points across the boundary layer while the results of Reference 1 were obtained with approximately 300 points. Also, the effective mesh stretching is somewhat different. Either one of these considerations could account for the small differences.

Incompressible flat plate turbulent boundary layer solutions were also obtained for some of the flows measured by Reynolds, Kays and Kline[31]. The plates were maintained at constant wall temperature and heat transfer data was obtained. The present Stanton number results agreed with the data to within a few percent in all cases.

During the past several years, Kays, Moffat and their co-workers at Stanford have carried out an extensive series of low speed turbulent boundary layer experiments (e.g., Refs. 10 and 32). As part of this series, Julien, Kays and Moffat[32] performed a series of tests which measured velocity profiles for a low speed flow with and without favorable pressure gradients and surface

mass transfer. Two of the flows measured by Julien, et al, have been calculated, one with, and one without, blowing at the wall. Figure 8 shows the experimental velocity distributions for both cases and the mass flux distribution for the case with blowing is shown in Figure 9. The acceleration parameter, $K = \nu(du_e/dx)/u_e^2$, for these cases is shown in Figure 10. The parameter is often used as a measure of the strength of the pressure gradient. Relaminarization is thought to occur for values of K greater than about 3×10^{-6}.

Using the present method excellent agreement with the data of Reference 32 was achieved. Some of the results obtained are shown in Figures 11-14. Figure 11 shows a comparison between the calculated and measured velocity profiles at the 45.67" station for the case with blowing. The profile is shown in "law of the wall" coordinates. Similar agreement with the measured profiles was obtained at all the locations compared. Figure 12 shows the calculated and measured values of momentum thickness, with, and without, blowing. A comparison with the measured shape factor is presented in Figure 13, while the measured and calculated local skin friction coefficients are shown in Figure 14. The skin friction data presented was not obtained by direct measurement, but was inferred from the measured velocity profiles. Several methods of inferring C_f were tried in Reference 32. The results reported herein were obtained from the velocity measurements made in the sublayer and have an estimated accuracy of $\pm$ .4 to .5.

The excellent agreement between the data and calculated results, for this more difficult case, lends credence to the turbulent transport models currently employed.

D. COMPRESSIBLE TURBULENT FLOW IN A NOZZLE

Back and Cuffel[33] made velocity and temperature profile and heat transfer measurements for a turbulent boundary layer flow in a cooled conical nozzle with 10° entrance and exit half angles. The geometry of the nozzle is shown in Figure 15. The locations of the 5 probe positions at which measurements were made are also shown. A turbulent boundary layer solution was obtained for this nozzle and the results compared to the data. The calculation was started at probe position 1 (x = 3.563") using the experimentally measured profiles. The pressure and wall temperature distributions used as boundary conditions are

are shown in Figures 16 and 17, respectively.

Comparisons of the measured and calculated velocity profiles, skin friction coefficient, momentum thickness, displacement thickness and heat transfer rate are shown in Figures 18-22. The velocity profiles shown in Figure 18 correspond to the fourth and fifth probe positions, as shown in Figure 15, and good agreement was obtained. The calculated and measured skin friction coefficient and momentum thickness (Figures 19 and 20) are also in good agreement. The calculated values at the end (probe position 5) are, however, somewhat higher than the data. The displacement thickness, Figure 21, and heat transfer rate, Figure 22, also agree quite well with the data in the convergent and throat regions of the nozzle, but are high in the divergent section.

The results obtained for this case are, in general, quite encouraging. It can be tentatively concluded that the current eddy viscosity model may be high in regions where strong wall cooling and significant compressibility effects occur simultaneously. Additional comparisons with other data should be made, however, before firm conclusions about the model are drawn.

A further comment about the behavior of the displacement thickness at the end of the nozzle is in order. Beginning about two inches past the throat, the calculated δ^* begins to rise and at the end of the nozzle is approximately .001 feet as opposed to the measured value of about - .001. The behavior of δ^* in this region is the only instance, of all the parameters compared, where the calculated trend did not match the trend of the data, and as such is somewhat of an enigma. While the exact reason or reasons for this result are not yet known it is speculated that one or all of the following are related to this problem. As previously noted the calculated eddy viscosity appears to be a little high in the divergent section; this accounts for at least part of the δ^* trend. In addition, when the displacement thickness is very small (+ or -) the contributions to the δ^* integral (equation 87) tend to be of opposite sign in the wall and edge regions of the boundary layer; i.e., ρu, tends to be less than $\rho_e u_e$ near the wall and greater than $\rho_e u_e$ near the edge. When two almost equal numbers of opposite sign are added together significant round off error can occur and relative error size increases. This effect tends to magnify the effect of errors in the calculated

velocity and density profiles. In addition, the stretching of the coordinate system currently employed (i.e., $\tilde{y}$ - y transformation) causes a large mesh size to be used near the edge of the boundary layer. This near edge loss in accuracy coupled with the magnification of the relative error, as discussed above, is probably also a factor in the false δ^* trend.

Other possible factors which could account for some of the difference between the calculated and measured δ^*, as well as the other parameters, are the neglect of curvature effects in the analysis, which are not necessarily insignificant in a small nozzle; and the fact that constant specific heat and Prandtl number were used in the analysis, while some real gas effects were present under the experimental conditions.

Additional solutions to the nozzle flow described previously have also been obtained. These solutions tested, to a limited degree, the effect of step size, mesh spacing, coordinate stretching, laminar and turbulent Prandtl number and initial profiles. The first solution described previously used a total of 230 finite difference steps, 120 mesh points, initial profiles based on the experimental data, stretching parameters n = 4 and $d\tilde{y}/dy|_{y=0} = 1000$ (see Eq. (67)), a laminar Prandtl number of .7 and the turbulent Prandtl number formulation given by equation (16). Decreasing the step size by a factor of 2 gave essentially identical results, while the calculation with double the original step size could not integrate past the throat. Changing the stretching parameters to n = 5 and $d\tilde{y}/dy|_{y=0} = 3000$, increasing the number of mesh points to 160 and changing the laminar Prandtl number to .75 all had essentially no effect upon the solution (i.e., the parameters of interest varied by less than 1%).

When the turbulent Prandtl number formulation given by equation (16), or a similar formula, is not used, most investigators have used a constant value of $Pr_T = .9$. A solution was obtained with all input identical to the original solution, but with equation (16) replaced by $Pr_T = .9$. A comparison of the resulting heat transfer rate with the original solution, and the data, is shown in Figure 22. Up to 10% differences between the two solutions are noted with the $Pr_T = .9$ solution always closer to the data. One comparison with a single set of data is certainly not conclusive, however, based on these results, the

relative merit of using a variable turbulent Prandtl number formulation like equation (16) for compressible cool wall flows is certainly open to question.

Solutions were also obtained using linear and 1/7th power law initial profiles of the experimentally measured thickness. As demonstrated by the heat transfer results shown in Figure 22, the 1/7th power law solution, while different in the initial portion of the flow, became approximately equal to the original solution after about 2". The solution with linear initial profiles was poor. Six inches downstream of the starting point the heat transfer was still only half of the solution started from the experimental profiles. These calculations illustrate the fact that if nozzle solutions are initiated when the boundary layer has appreciable thickness (as opposed to near the origin of the flow) a fairly accurate specification of the initial profiles is required. This is due to the constantly accelerating nature of the flow in rocket nozzles. The flow acceleration keeps the boundary layer from growing appreciably, and in some regions the boundary layer actually shrinks. Thus, the errors contained in the initial profiles are not "diluted" by rapid boundary layer growth as they are if the boundary layer is initiated near the origin of the flow.

E. HYDROGEN-OXYGEN BOUNDARY LAYERS IN CHEMICAL EQUILIBRIUM

1. Preliminary Results

In order to check out the mathematical accuracy of the solution for equilibrium hydrogen oxygen flows, solutions were obtained for flat plate flows with the Prandtl number (laminar and turbulent) set equal to unity. Under these conditions the "Crocco Integral" solutions relating the total enthalpy and element concentrations to the velocity profile are valid, and may be used to verify the accuracy of the numerical solutions. The enthalpy integral is given by equation (96), while the relation between the element mass fractions and the velocity profile may be expressed as

$$\alpha = \alpha_w + (\alpha_e - \alpha_w) \frac{u}{u_e} \tag{97}$$

The test cases considered both laminar and turbulent flows and had a wall temperature of 1800°R, an edge temperature of 5700°R, and O/F at the wall of 2.333* and 10.17 at the edge. Starting from linear initial profiles, all of the solutions agreed very well with the exact integrals given above after 60 stations had been computed. The solutions usually satisfied the integrals to four significant figures.

2. A Regeneratively Cooled Rocket Engine

An equilibrium boundary layer solution for the flow in the two dimensional-planar nozzle depicted in Figure 23 was obtained. The configuration, together with heat transfer data, was supplied by B. Waldman of Rocketdyne[34]. Since the TDK program does not contain a planar option we had to be satisfied with a one-dimensional pressure distribution obtained using ODE. The pressure distribution obtained is shown in Figure 24. The wall temperature distribution for the engine is shown in Figure 25. The solution was started at the injector face (x = - 4"); although physically, a boundary layer flow in the usual sense is not established until some distance downstream of the injector. The calculated momentum thickness and local skin friction coefficients are shown in Figures 26 and 27, respectively, while the experimentally measured and calculated heat transfer rates are shown in Figure 28. The agreement with the data is quite good (within the accuracy of the data, $\pm$ 20%) despite the somewhat unrealistic use of the ODE pressure distribution. The ODE solution assumed complete combustion at the injector face and, hence, a Mach number of approximately 1/10 (velocity of about 500 ft/sec) and an initial temperature of about 6400°R were computed. Both these figures are unrealistically high and account for the initial overprediction of heat transfer. It can also be noticed that the calculated heat transfer rate peaks somewhat past the experimentally measured peak. This again is probably attributable to the 1-D pressure distribution. In one dimension the sonic line is at the throat plane while physically, it is known that at the nozzle wall the sonic point is reached somewhat upstream of the throat. Thus, it is felt that the good agreement between the experimental and measured heat

*For these solutions the boundary condition on α_w was temporarily changed to $\alpha_w(x)$ = constant.

transfer could be even further enhanced if a more appropriate and accurate pressure distribution were used.

It should be mentioned that the laminar transport property subroutine was not yet available when the solution was obtained. Thus, in order to run the case the Prandtl number was set to 0.58 (a good approximation for the range of given conditions) and the viscosity was obtained by curve fitting the results of Svehla[19]. One hundred and eighty finite difference steps were taken in the solution and 120 mesh points were taken initially. The computation time was about 12 minutes (UNIVAC 1108).

3. A Transpiration Cooled Rocket Engine

An equilibrium hydrogen-oxygen boundary layer solution was also obtained for a rocket engine configuration which utilized transpiration cooling from the injector face to a point somewhat downstream of the throat. The solution is based on an engine configuration supplied by T. Mayes of Pratt and Whitney[35], however, some of the boundary conditions (wall temperature and transpiration coolant flow rate) were modified from those given in Reference 35. No boundary layer data corresponding to the solution obtained exist. The solution was obtained for the purpose of demonstrating that the current method could provide reasonable boundary layer solutions for difficult engine geometries with boundary conditions at least qualitatively similar to those encountered in practice (i.e., rapidly varying and/or discontinuous wall temperature and coolant flow rate distributions).

The engine geometry which was considered is shown in Figures 29 and 30. The engine had a throat radius of 3.6603 inches, a convergent section area ratio of 2.968 and an exit area ratio of 60. The chamber pressure was 3097 psia and the O/F was 6.29. The TDK program[13] was used to obtain a pressure distribution for the engine and in doing so the sharp corner expansion at the throat was replaced, for numerical reasons, by an arc which had a radius of curvature ratio (to the throat radius) of .05. The resulting pressure distribution is given in tabular form in Volume II of this report, as part of the sample case input data. The wall temperature and coolant (hydrogen) flow rate distributions are shown in Figures 31 and 32, respectively. A second solution, with twice the coolant flow rate, was also obtained (up to a point just before the throat)

for comparison.

Although boundary layer data for this case was not available the results appear to be reasonable and the complexity and trends of the results can all be traced back to the nature of the boundary conditions and their mutual interactions. The heat transfer rate results that were obtained are shown in Figure 33. The complexity of the results is self evident. Except for the initial steep decline in $\dot{q}_w$, which is due to the smoothing out of the approximate initial profiles, the gyrations in the heat transfer rate can all be qualitatively traced back to boundary condition variations. Note the large reduction in heat transfer rate resulting from the doubling of the coolant flow rate. The great effectiveness of hydrogen as a transpiration coolant can be traced to its low molecular weight and large heat capacity. Figure 34 shows the calculated species mass fraction profiles at a point .05 throat radii upstream of the throat. The dominant species are hydrogen (H_2) and water. Note that at this station the solutions show that the mass fraction of hydrogen at the wall for the higher coolant flow rate is almost double that of the original solution (94% to 50%). This result, to a large degree, is responsible for the large gain in cooling effectiveness.

Figure 33 also shows that negative heat transfer results were calculated for some regions. This situation is related to the nature of the boundary conditions which were imposed. Physically, it means that in those regions the specified coolant flow rate was excessive, from the standpoint of maintaining the specified wall temperature. A negative heat transfer rate means that the wall is transferring energy into the boundary layer. As one would expect this energy addition is partially converted into momentum, and overshoot* is found to occur in the velocity profiles. Figure 35 shows the calculated velocity profiles, for the two mass addition rates, at the same location as the mass fraction profiles. It can be seen that the greater energy addition (more negative $\dot{q}_w$) associated with the larger mass addition rate results in a corresponding increase in velocity profile overshoot.

*Overshoot being defined as velocities greater than the boundary edge velocity.

The tight throat geometry coupled with the rapidly varying, and sometimes discontinuous, behavior of the boundary conditions for this case, places strict limitations on the size of finite difference steps which can be successfully employed. In the complete solution discussed previously, a total of over 500 finite difference steps were taken and the total computation time was about 25 minutes (equilibrium calculations were performed at every eighth mesh point). At the present time, it is not known how much, if any, improvement in operating efficiency could have been realized by a more optimal selection of step and mesh size.

F. FILM COOLING

The different types of rocket engines (fuels, geometries, operating pressure, thrust level, etc.) all have typical cooling problems. For some of the high performance engines currently under consideration, especially H_2/O_2 engines, film cooling appears to offer an attractive alternative as a candidate cooling technique. Figure 36 shows an idealized picture of a film cooling geometry. In actual operating systems, the slot injection parameters such as: slot width and height; injection angle, velocity and pressure; and slot wall (lip) thickness may vary over a considerable range. In addition, multiple slots may be employed to increase the cooling effectiveness and/or the effective length which can be cooled. The actual coolant can be either in a liquid or gaseous state upon injection, however, in its present form the present analysis would not be applicable or easily extendible to liquid cooling problems.

Over the years a relatively large body of literature and data on film cooling has been generated. References 36 and 37 contain enough references to serve as preliminary bibliographies on the subject. Until the last several years the analytical capability to predict film cooling effectiveness consisted mainly of semi-empirical correlations which usually were developed for specific configurations and had limited general applicability. In recent years, however, the finite difference method of Reference 2 has been applied to the calculation of film cooling problems[38,39] and good agreement with low speed data was obtained (except in the near slot exit region). Recently Bushnell and Beckwith[37] published an extension of their finite difference method[5] to flows with

tangential slot injection. By modifying the mixing length formulation in their eddy viscosity model they were able to obtain good agreement with supersonic slot injection data, even in the region near the slot exit. It is also pointed out in Reference 37 that many of the correlational techniques previously employed underestimate the cooling effectiveness of tangential slot jets.

Unlike the finite difference solutions based on the methods of References 2 and 5, the current method is not restricted to nonreacting flows and, hence, could in principal, be used to calculate film cooling effectiveness in rocket engines under actual hot firing conditions*.

Based on the results of References 37 to 39, and other investigations, it appears, however, that the current turbulent transport models, which were developed strictly for boundary layer flows, will probably have to be modified before realistic solutions can be achieved. Modifications to the mixing laws will definitely be required in the near slot exit region and most likely a transition region in which the mixing rates relax back to normal boundary layer values will be in order (in a manner similar to that of Reference 37). The effects of chemical reactions and the large transport property and density variations which are associated with the use of a coolant like hydrogen must also be assessed.

For the usual boundary layer equations to be strictly valid for a film cooling configuration, the static pressure of the jet and boundary layer flow should be matched, the lip to slot thickness ratio should be small and the injection angle should be very small or zero. Many practical systems violate one or all of these constraints, however, the results of Reference 37 encourage one to believe that unless the constraints are seriously violated the usual boundary layer equations will be adequate, since a certain amount of nonideal behavior can be empirically accounted for by modifications to the mixing model.

In order to demonstrate that the current analysis and computer program are applicable to film cooling analysis in H_2-O_2 engines, a sample, somewhat idealized, problem was considered. The initial conditions at the slot exit were

*Currently only H_2-O_2 engines can be considered.

chosen so as to approximate a representative chamber film cooling configuration for Space Shuttle APS class engines. The boundary layer edge conditions were as follows: $T_e = 5870^{\circ}R$; $P_e = 24$ atmospheres; $u_e = 700$ ft/sec; $O/F_e = 5.19$. The wall temperature was assumed to be $680^{\circ}R$. The coolant slot exit height was taken to be .0035 feet, which is approximately the same as the initial assumed boundary layer thickness. The initial velocity profile of the coolant hydrogen was approximated by a pipe flow type profile and had a peak velocity ratio of 1.2. The initial temperature of the coolant was assumed to be constant and equal to the wall temperature. The initial boundary layer profiles were obtained by calculating the boundary layer development up to the midway point of a sample combustion chamber. The initial O/F profile is given by a step function, since the injected flow was all hydrogen and the initial boundary layer was all at an O/F of 5.19.

The initial conditions described previously are somewhat arbitrary and idealized. They ignore the effect of the slot exit lip thickness and the temperature gradients which almost certainly exist in the injected coolant. The initial conditions are, however, sufficiently reasonable for illustrative purposes.

The initial conditions are input in tabular form and the initial boundary layer profiles are then set up by interpolation in the tables. The calculations for the previously described sample case were continued a distance of 2.8 inches (about 67 slot heights). Figures 37 and 38 show the initial velocity and O/F profiles, respectively, and their development at two downstream stations (.42 and 2.8 inches). Qualitatively the results obtained from this sample case are reasonable. In order to get good quantitative results the current eddy viscosity model will most likely have to be extended. The characteristics of the stretching function presently used to transform the normal coordinate are also not particularly well suited to film cooling analysis. The current normal coordinate transformation yields physical step sizes which monatonically increase from the wall to the edge. During the early development of the mixing layer between the injected coolant and the initial boundary layer, significant gradients are present well away from the wall. The need for transformations which allow better step size control for such cases should be investigated.

IV. CONCLUSIONS AND RECOMMENDATIONS

A Crank-Nicolson finite difference solution of the turbulent boundary layer equations has been developed, and evaluated, by comparison with data and other solutions, for a series of laminar and turbulent test cases. These comparisons showed that the current program is quite accurate and yields satisfactory results for a wide range of boundary layer flow problems.

Preliminary conclusions based on the limited number of solutions obtained to date indicate that while, in general, the current eddy transport model yields excellent results further refinement may be needed to obtain completely satisfactory results in cool wall divergent nozzle sections and in the near exit region of a film cooled configuration.

While the program was developed on a Univac 1108 computer an IBM 360/65 version is also available. In its current form the computer program requires the following approximate computation times (Univac 1108) for the type of turbulent boundary layer problem indicated:

1.	Incompressible flow	25-40 sec.
2.	Compressible flow	1.5-2.5 minutes
3.	Equilibrium H_2-O_2 rocket engines	10-20 minutes

Further development of the program, either to broaden its range of applicability, or to optimize and refine its present capabilities, is certainly feasible. Efforts to improve the current capability, especially as applied to H_2-O_2 rocket engines, would be greatly aided by the availability of good experimental data. Before embarking upon further development it is suggested that it be established whether a data base sufficient to fully evaluate the program exists for:

1. Regeneratively cooled engines
2. Transpiration cooled engines
3. Film cooled engines

If the data exists, an effort to fully evaluate the program would be in order. If a data base only partially exists, the feasability of acquiring additional data should be investigated.

With additional experience and effort the efficiency of the program could be increased and the input and output functions could be "human engineered" to provide greater flexibility and control. The scope of the program can also, if deemed desirable, be widened to include equilibrium chemical systems other than H_2-O_2, or nonequilibrium effects. More efficient methods of performing the required equilibrium state calculations could be developed.

V. REFERENCES

1. Smith, A.M.O., and Cebeci, T., "Numerical Solution of the Turbulent Boundary Layer Equations", Douglas Aircraft Company Report Number DAC33735, May 29, 1967 (also see, "Calculation of Compressible Adiabatic Turbulent Boundary Layers", presented at the AIAA 2nd Fluid and Plasma Dynamics Conference, June 1969).

2. Pantankar, S. V. and Spalding, D. B., "Heat and Mass Transfer in Boundary Layers", C.R.C. Press, Cleveland, Ohio, 1968.

3. Herring, H. J. and Mellor, G. L., "A Method of Calculating Compressible Turbulent Boundary Layers", NASA CR-1144, September 1968.

4. Carr, L. W. and Fox, H., "Numerical Solution of the Turbulent Boundary Layer," Aerospace Research Labs, Rept. No. ARL 68-0215, Dec. 1968.

5. Beckwith, I. E., and Bushnell, D. M., "Detailed Description and Results of A Method for Computing Mean and Fluctuating Quantities in Turbulent Boundary Layers", NASA TN D-4815, 1968.

6. Fish, R. W. and McDonald, A., "Practical Calculations of Transitional Boundary Layers", United Aircraft Co., Rept. No. UARH 48, March 1969.

7. Bushnell, D. M. and Beckwith, I. E., "Calculation of Nonequilibrium Hypersonic Turbulent Boundary Layers and Comparisons with Experimental Data", AIAA Reprint No. 69-684, 1969.

8. Cebeci, T., "Calculation of Compressible Turbulent Boundary Layers with Heat and Mass Transfer", AIAA Reprint No. 70-741, 1970.

9. Simpson, R. L., Whitten, D. G., and Moffat, R. J., "An Experimental Study of the Turbulent Prandtl Number of Air with Injection and Suction", International Journal of Heat and Mass Transfer, Vol. 13, pp. 125-143, 1970.

10. Thielbahr, W. H., Et Al, "The Turbulent Boundary Layer: Experimental Heat Transfer With Blowing, Suction, and Favorable Pressure Gradient", NASA-CR-104141, April 1969.

11. Jenkins, R., "Variation of the Eddy Conductivity With Prandtl Modulus and Its Use in Prediction of Turbulent Heat Transfer Coefficients", Institute of Heat Transfer and Fluid Mechanics, pp. 147-158, 1951.

12. Peters, C. E., Chriss, D. E., and Paulk, R. A., "Turbulent Transport Properties in Subsonic Coaxial Free Mixing Systems", AIAA Reprint No. 69-681, June 1969.

13. Frey, H. M. and Nickerson, G. R., "Two Dimensional Kinetic Nozzle Analysis Reference Computer Program", Dynamic Science Report No. CS-12-70-1, December, 1970.

14. Zeleznik, F. J., and Gordon, S., "A General IBM 704 or 7090 Computer Program for Computation of Chemical Equilibrium Compositions, Rocket Performance, and Chapman Jouget Detonations", NASA TN D-1454, Oct. 1962.

15. Anon., JANAF Thermochemical Tables. Contract No. AF33(616)-6149, Thermal Lab., Dorv Chemical Co., PB 168 370 (also see Addenda PB 168 370-1,-2,-3).

16. Svehla, R. A., "Estimated Viscosities and Thermal Conductivities of Gases at High Temperatures", NASA TR-132, 1962.

17. Bird, R. B., Stewart, U. E., and Lightfoot, E. N., Transport Phenomena, John Wiley & Sons, 1960.

18. Mason, E. A., and Saxena, S. C., Physics of Fluids, Vol. 1, no. 5, pp. 361-369, 1958.

19. Svehla, R., "Thermodynamic and Transport Properties for the Hydrogen-Oxygen System", NASA SP-3011, 1964.

20. Bartlett, E. P., Kendall, R. M., Rindal, R. A., "An Analysis of the Coupled Chemically Reacting Boundary Layer and Charring Ablator", Part IV, A Unified Approximation for Mixture Transport Properties for Multicomponent Boundary Layer Applications", NASA CR-1063, June 1968.

21. Crank, J. and Nicolson, P., "A Practical Method for Numerical Evaluation of Solutions of Partial Differential Equations of the Heat Conduction Type", Proc. Camb. Phil. Soc., Vol. 43, 1947, p. 50.

22. Blottner, F. G., "Nonequilibrium Laminar Boundary Layer Flow of a Binary Gas", General Electric Co. Report no. TIS R63SD17, June 1963.

23. Levine, J. N., "Finite Difference Solution of the Laminar Boundary Layer Equations Including the Effects of Transverse Curvature, Vorticity and Displacement Thickness", General Electric Co., Report no. TIS 66SD349, 1966.

24. Richtmyer, R. D., Difference Methods for Initial Value Problems, Interscience Publishers, Inc., New York, 1957.

25. Weingold, H. D., and Zupnik. T. F., "Turbulent Boundary Layer Nozzle Analysis Computer Program - TBL", Prepared for the ICRPG Performance Standardization Working Group, July 1969, AD 841202.

26. Clausing, O. M., "Finite Difference Solutions of the Boundary Layer Equations", NASA CR-108909, Feb. 1970.

27. Schlicting, H., Boundary Layer Theory, McGraw Hill, 1955.

28. Howarth, L., "On the Solution of the Laminar Boundary Layer Equations," Proc. Royal Society, Vol. 164, P. 547 (1938).

29. Van Driest, E. R., "Investigation of Laminar Boundary Layer in Compressible Fluids Using the Crocco Method," NACA TN 2597, January 1952.

30. Coles, D., "Measurements in the Boundary Layer on a Smooth Flat Plate in Supersonic Flow," JPL Report No. 20-69, June 1, 1953.

31. Reynolds, W. C., Kays, W. M., and Kline, S. J., "Heat Transfer in the Turbulent Incompressible Boundary Layer. I - Constant Wall Temperature," NASA Memo 12-1-58W, December 1958.

32. Julien, H. L., Kays, W. M., and Moffat, R. J., "The Turbulent Boundary Layer on a Porous Plate: Experimental Study of the Effects of a Favorable Pressure Gradient," Stanford University Report No. HMT-4, April 1969.

33. To be published. ASME Journal of Heat Transfer about August, 1971.

34. Private comm.

35. Private Comm.

36. Terry, J. E. and Caras, G. J., "Transpiration and Film Cooling of Rocket Engines," Redstone Scientific Information Center Report No. RSIC 535, March, 1966.

37. Beckwith, I. E. and Bushnell, D. M., "Calculation by a Finite-Difference Method of Supersonic Turbulent Boundary Layers with Tangetial Slot Injection," NASA TN D-6221, April 1971.

38. Pai, B. R. and Whitelaw, J. H., "The Influence of Density Gradients on the Effectiveness of Film Cooling", C. P. No. 1013, British A.R.C., 1968.

39. Kacker, S. C., Pai, B. R., and Whitelaw, J. H., "The Prediction of Wall Jet Flows with Particular Reference to Film Cooling," Vol. 2 of Progress in Heat and Mass Transfer, Thomas F. Irvine, Jr. Et Al, eds., Pergamon Press, Inc., 1969, pp. 163-186.

40. JANNAF Manual and Procedures Revision Subcommittee, T. Tyson, Chairman, "JANNAF Interim Performance Calculation Methodology for Use in the SSME Proposal Response," Addendum No. 1 to CPIA Publication No. 178, Jan. 1971.

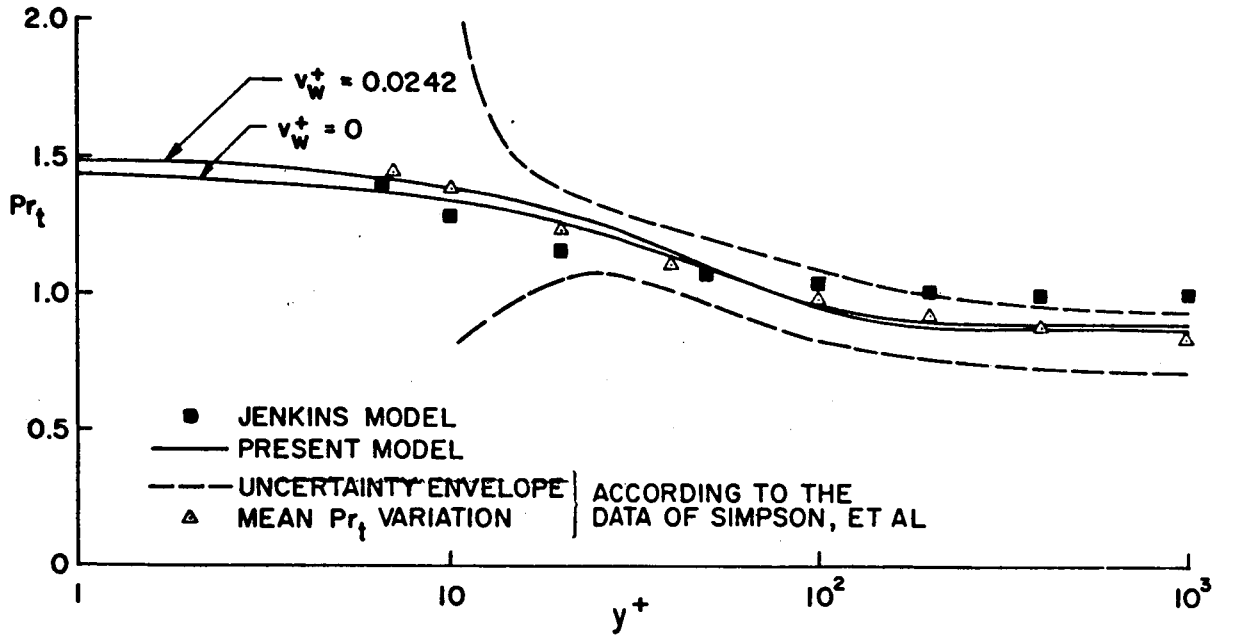

Figure 1. Comparison of Calculated Turbulent Prandtl Numbers with Experimental Data and with Jenkins Model

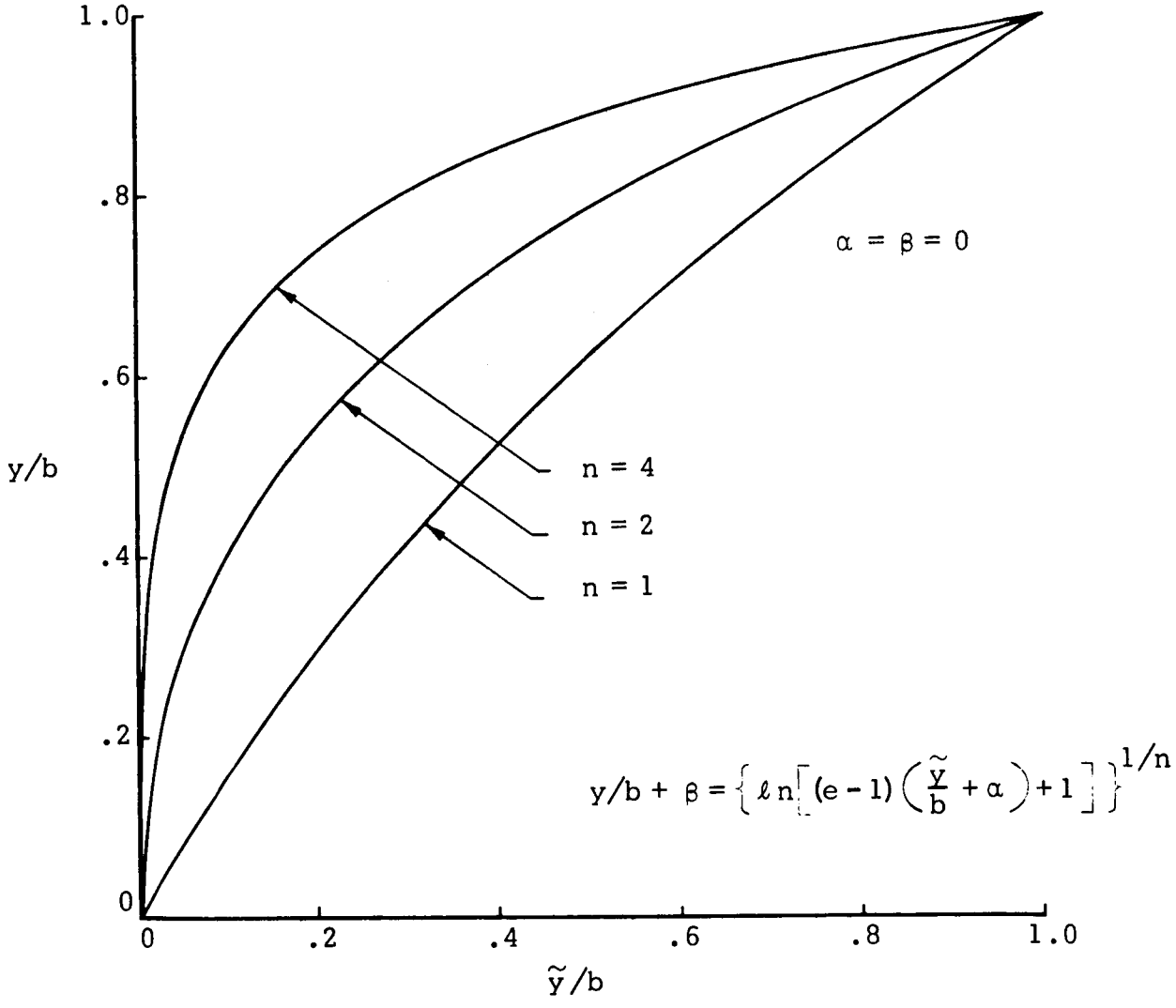

Figure 2. The "G" Function Used to Transform the Normal Coordinate

$$\text{at } x_{m_i} : \quad F'_i = \frac{F_{i+1} - F_i}{x_{i+1} - x_i} \qquad i = 1 \ldots n$$

$$F'(x) = F'_i + (F'_{i+1} - F'_i) \frac{(x - x_{m_i})}{(x_{m_{i+1}} - x_{m_i})} \qquad x_{m_i} \leq x \leq x_{m_{i+1}}$$

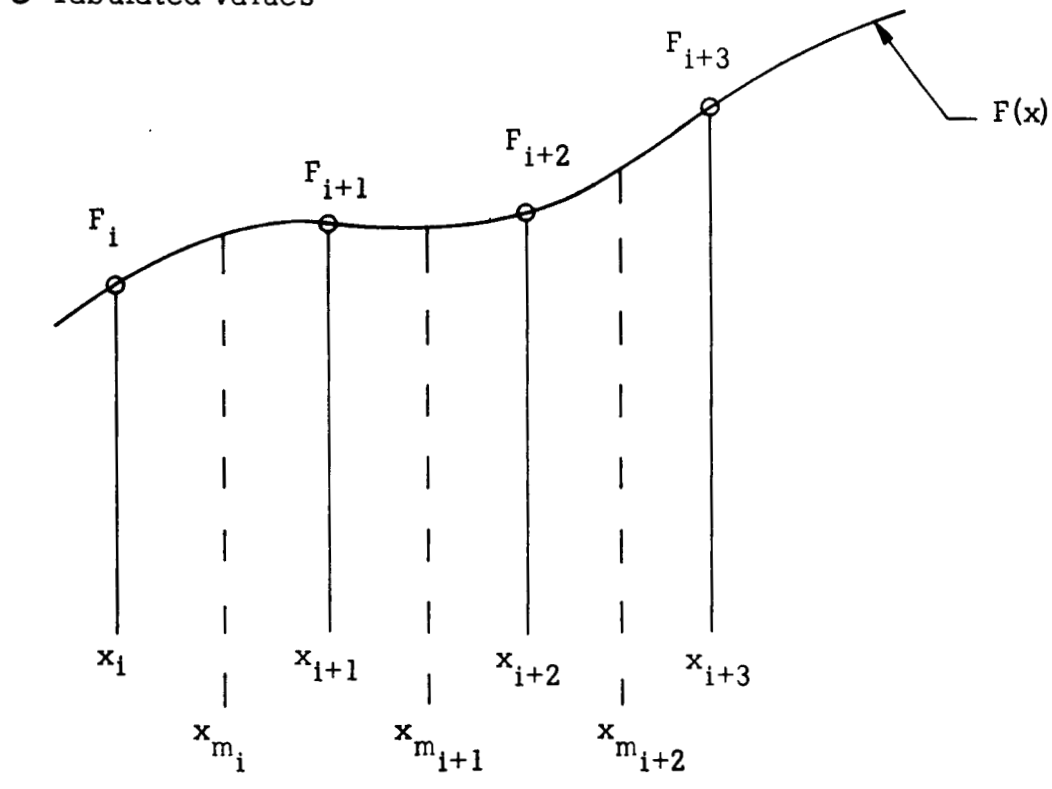

Figure 3. Illustration of the "Linear Averaged Derivative" Method for Numerically Differentiating A Graphically or Table Defined Function

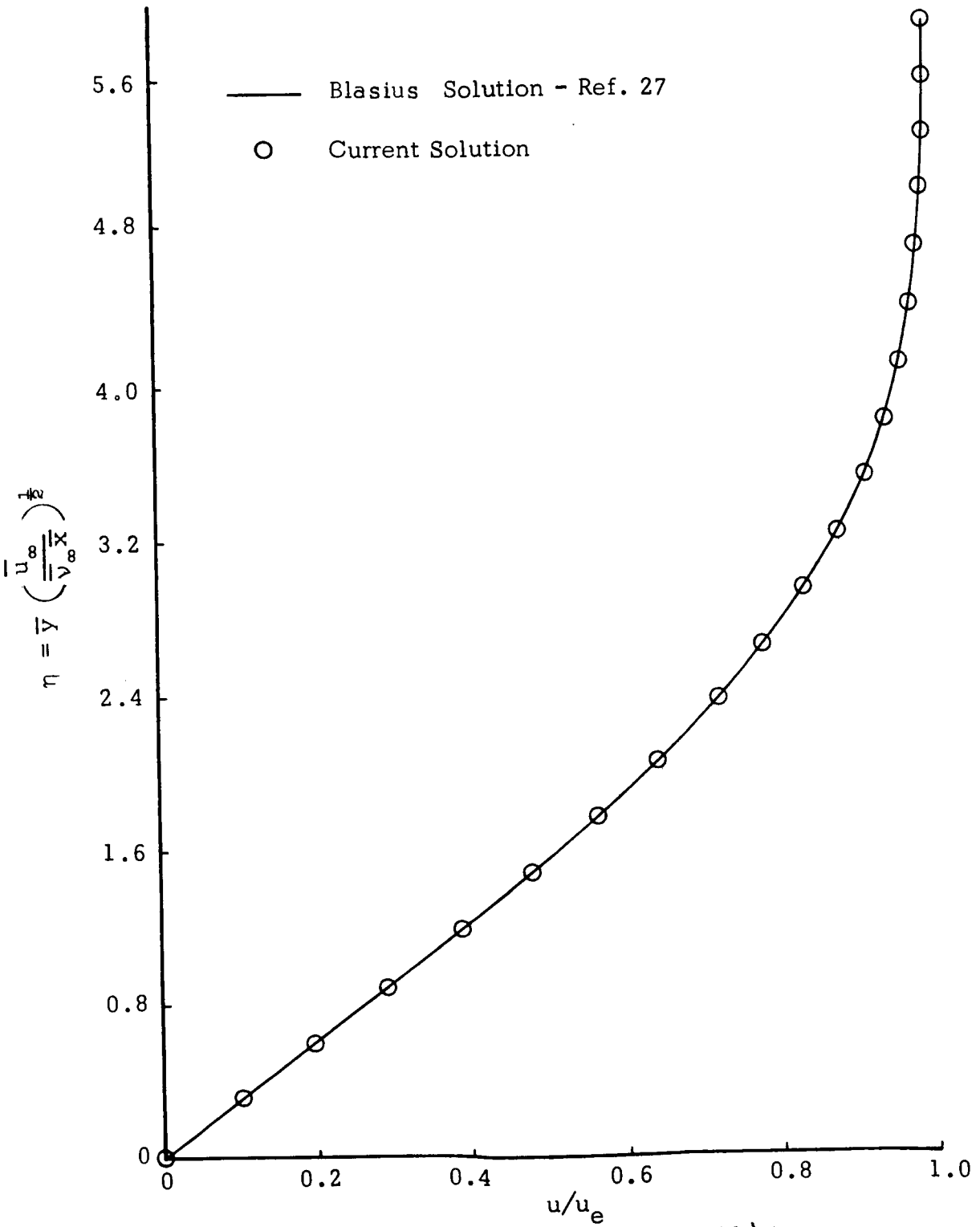

Figure 4. Blasius Velocity Profile Comparison

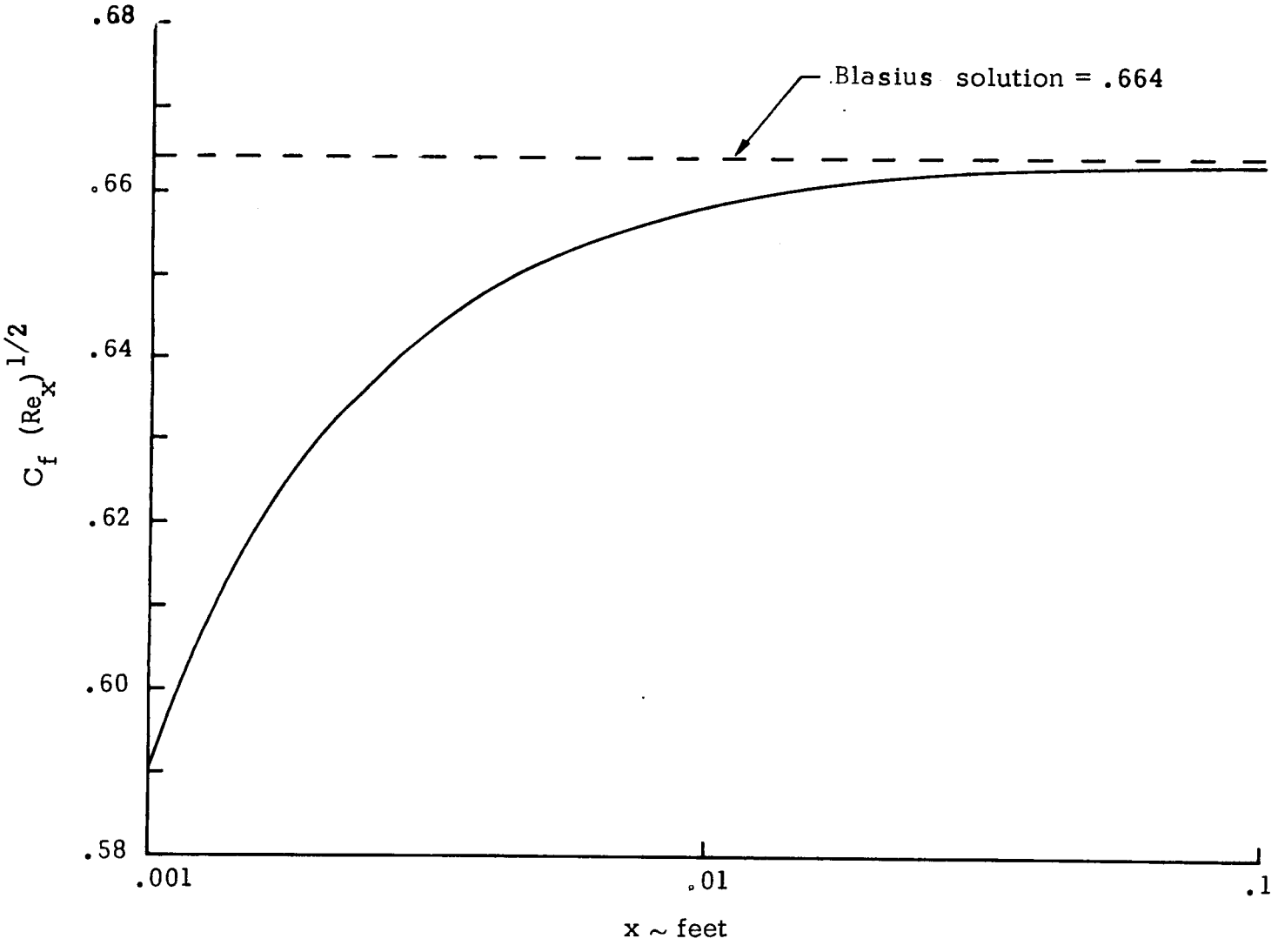

Figure 5. Relaxation to Correct Blasius Solution Starting from Linear Initial Profiles

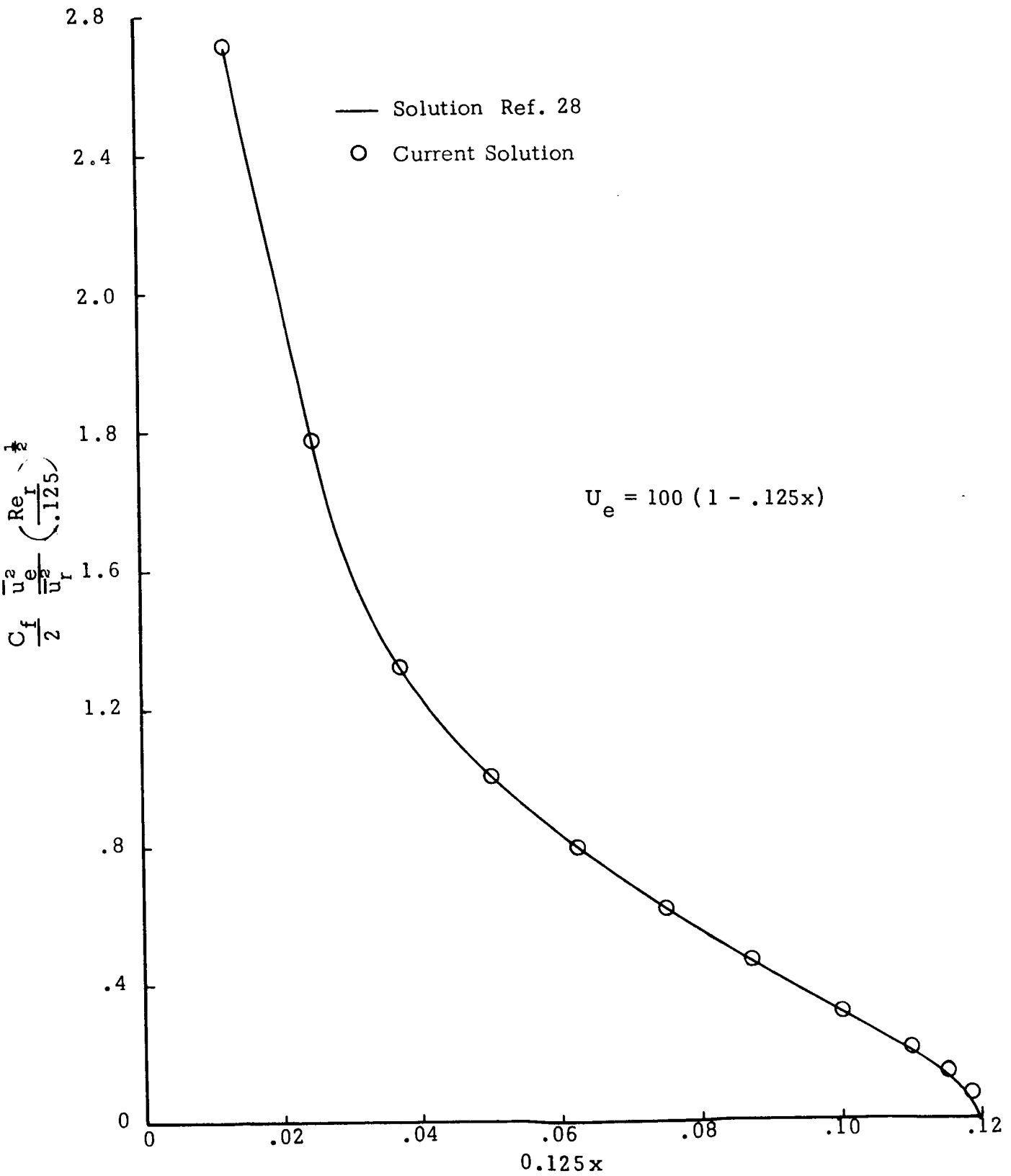

Figure 6. Shear Stress Coefficient Versus Distance for Howarth Retarded Flow

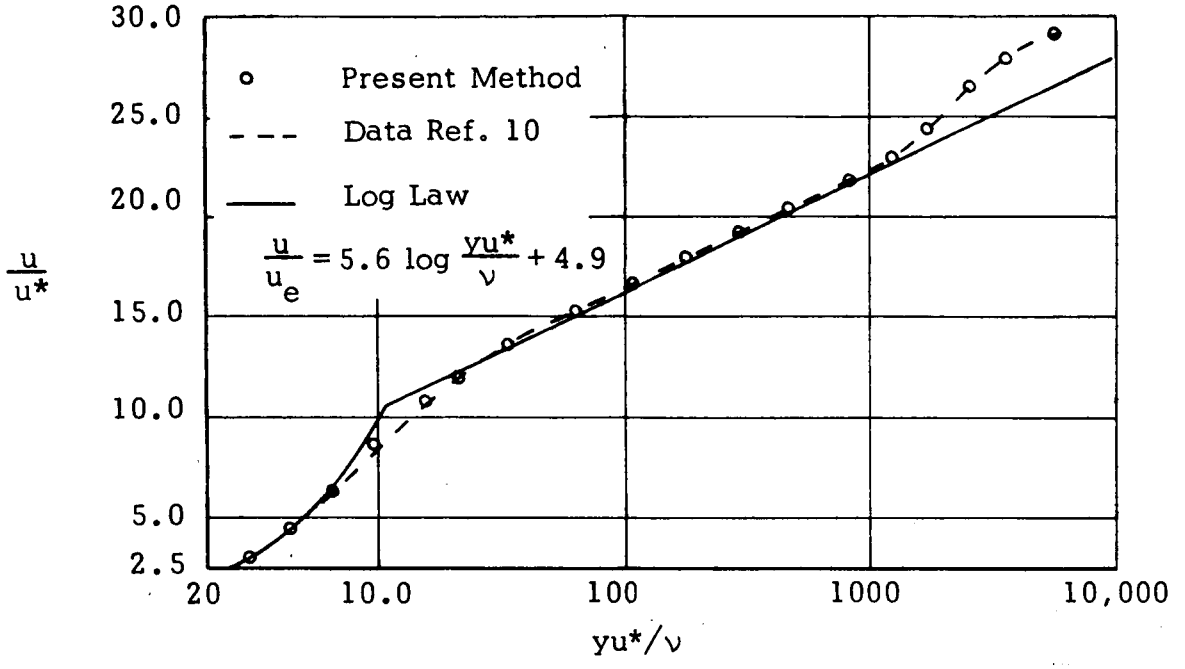

Figure 7a. Comparison of Calculated and Experimental "Law of the Wall" Profiles, $Re_x = 1.0 \times 10^7$

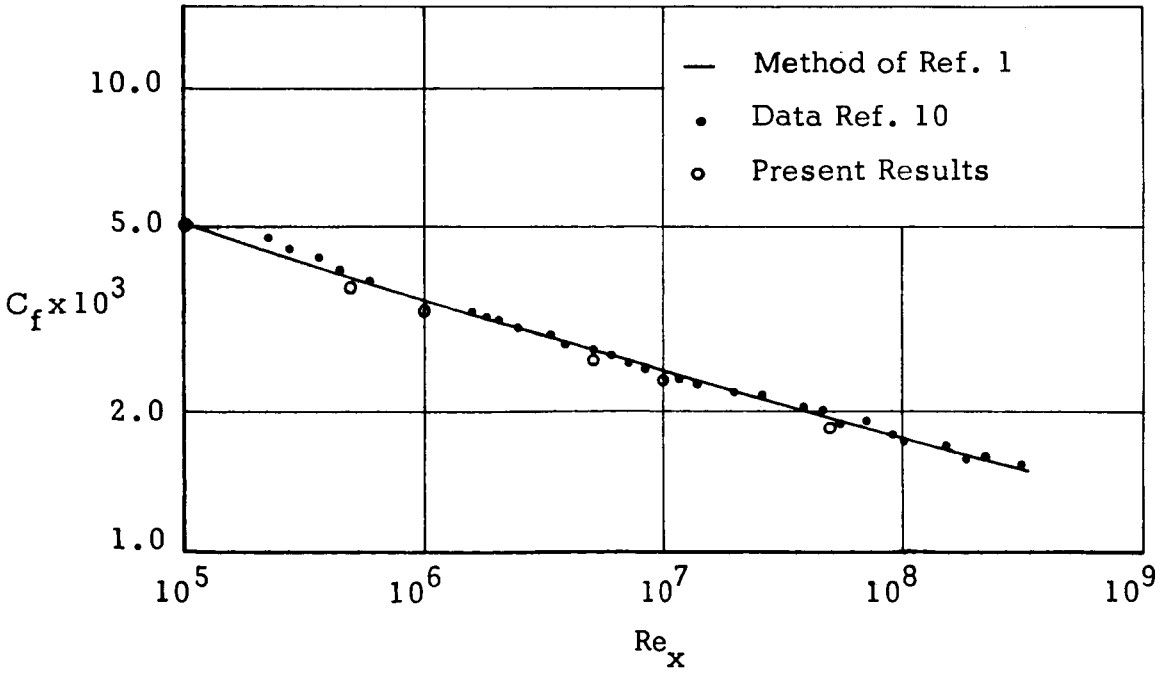

Figure 7b. Local Turbulent Shear Stress Coefficient on a Flat Plate

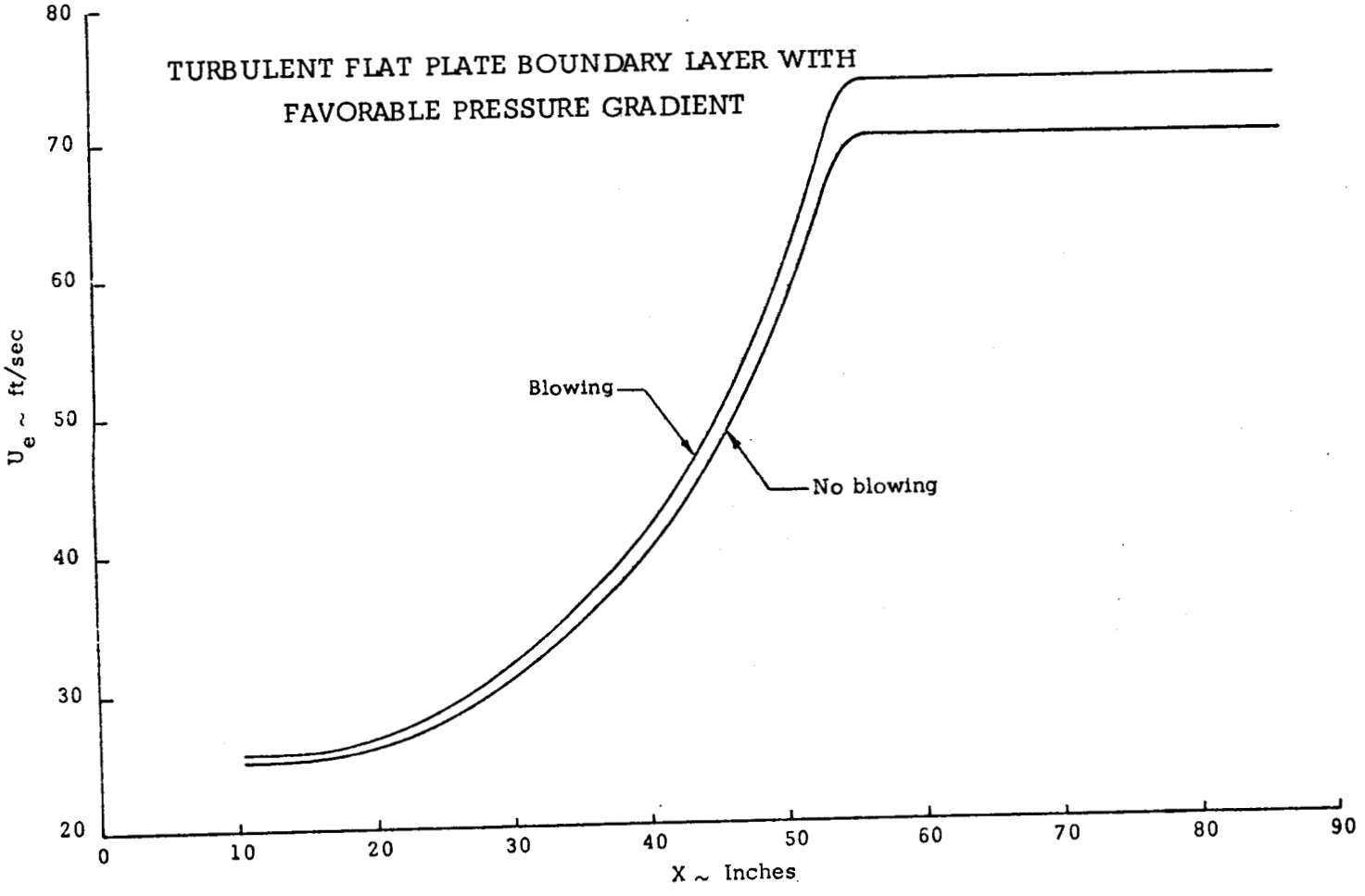

Figure 8. Boundary Layer Edge Velocity versus Distance

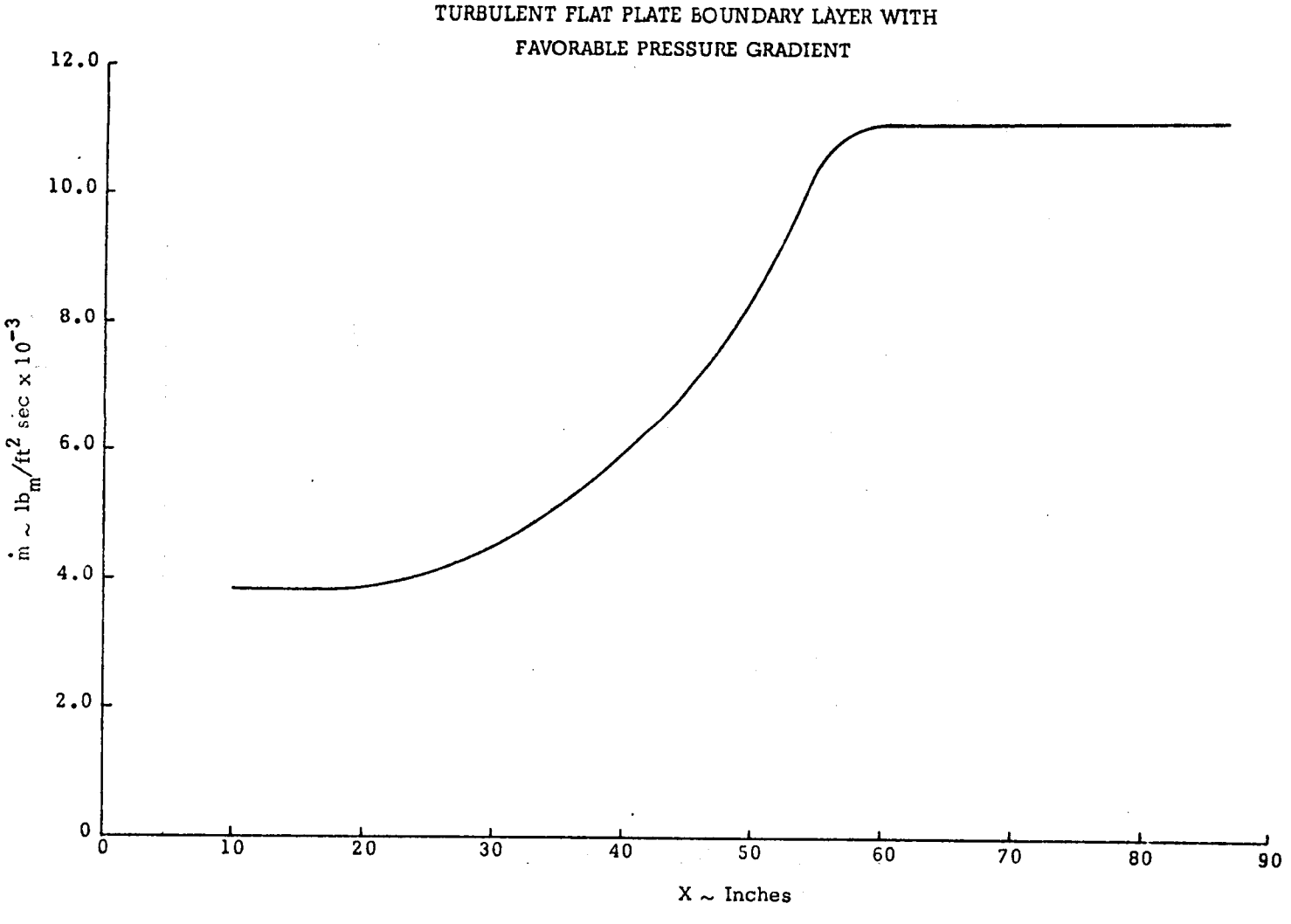

Figure 9. Wall Mass Transfer Rate versus Distance

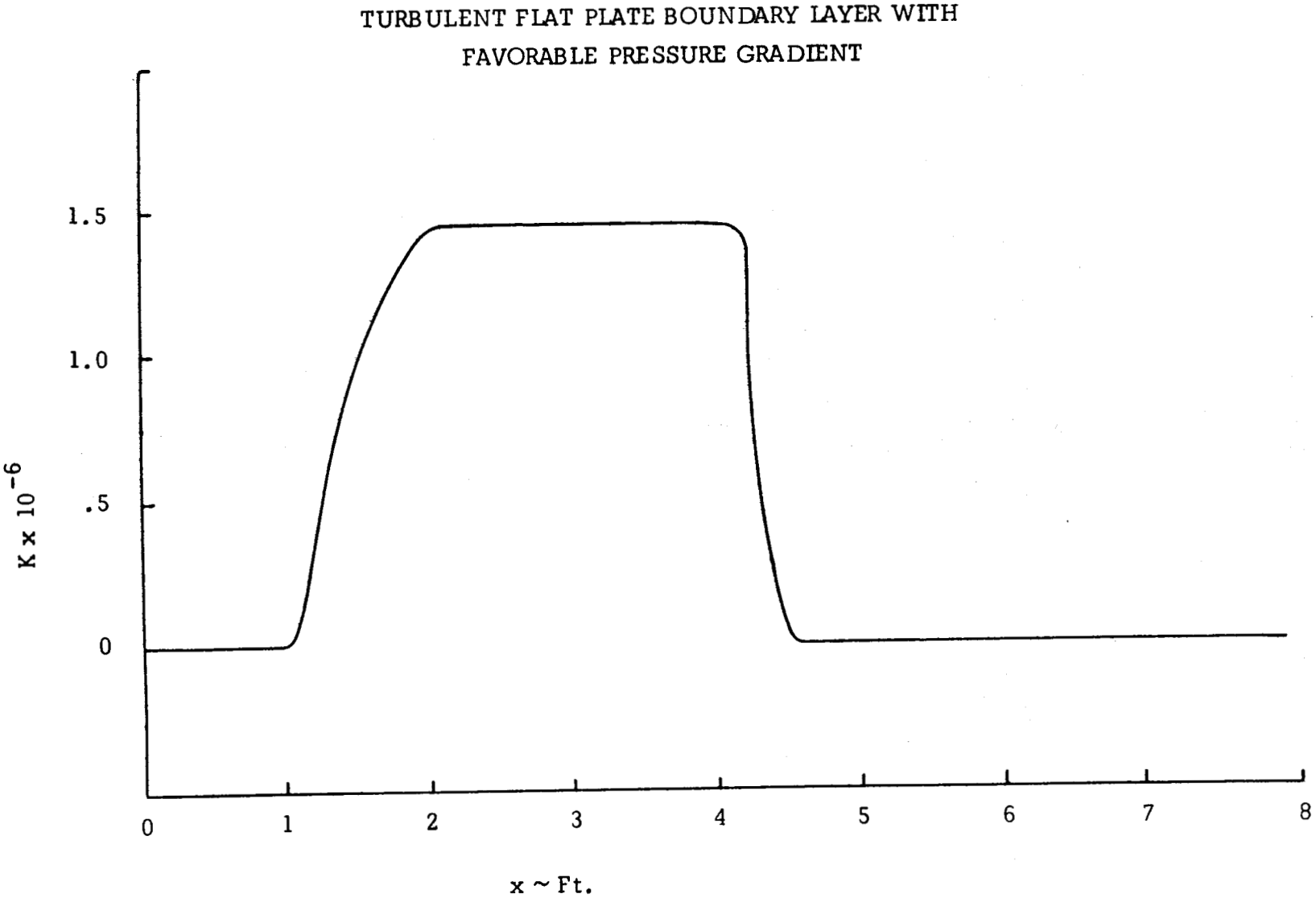

Figure 10. Acceleration Parameter versus Distance

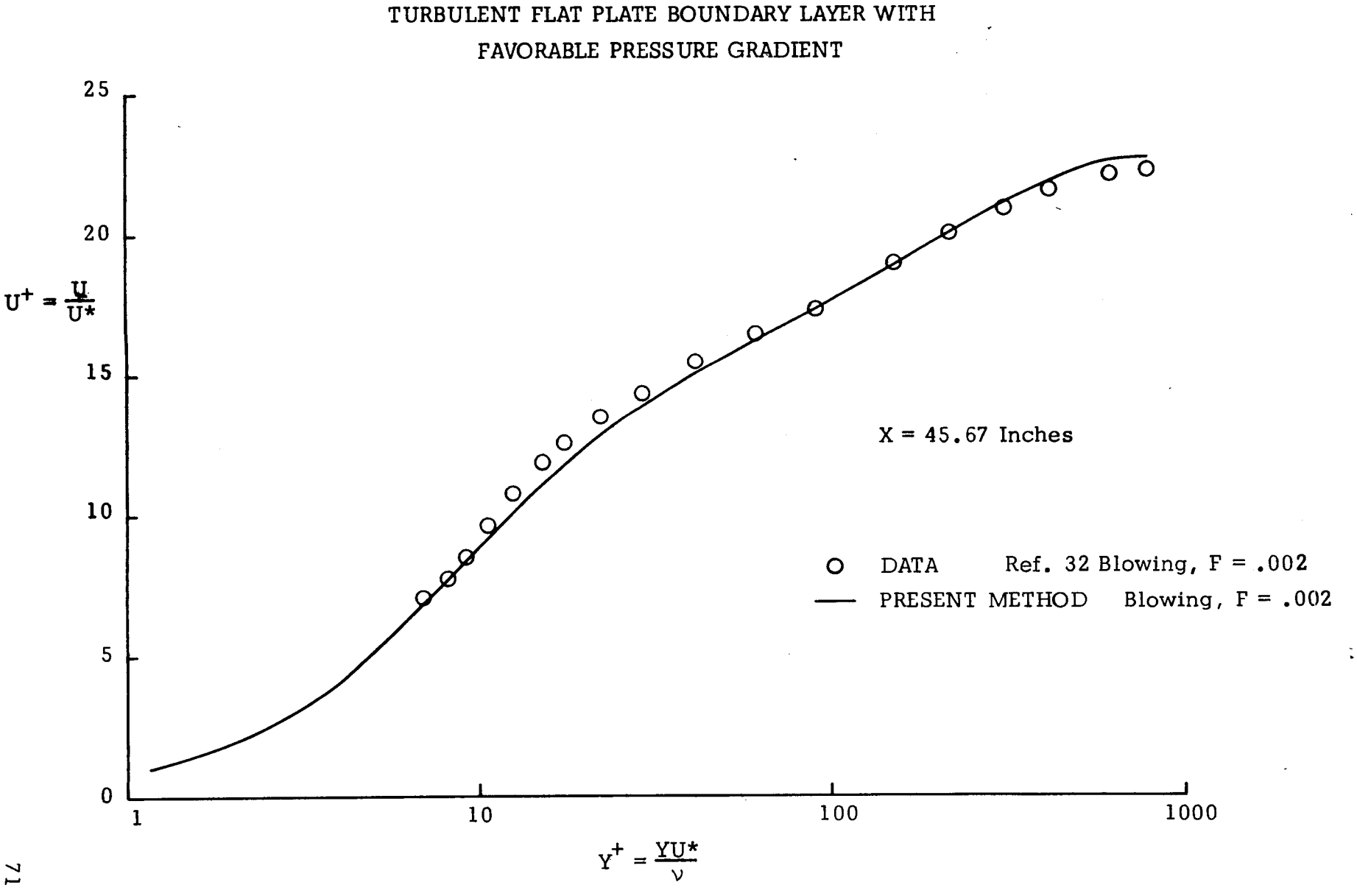

Figure 11. Velocity Profile Comparison with Blowing in Law of the Wall Coordinates

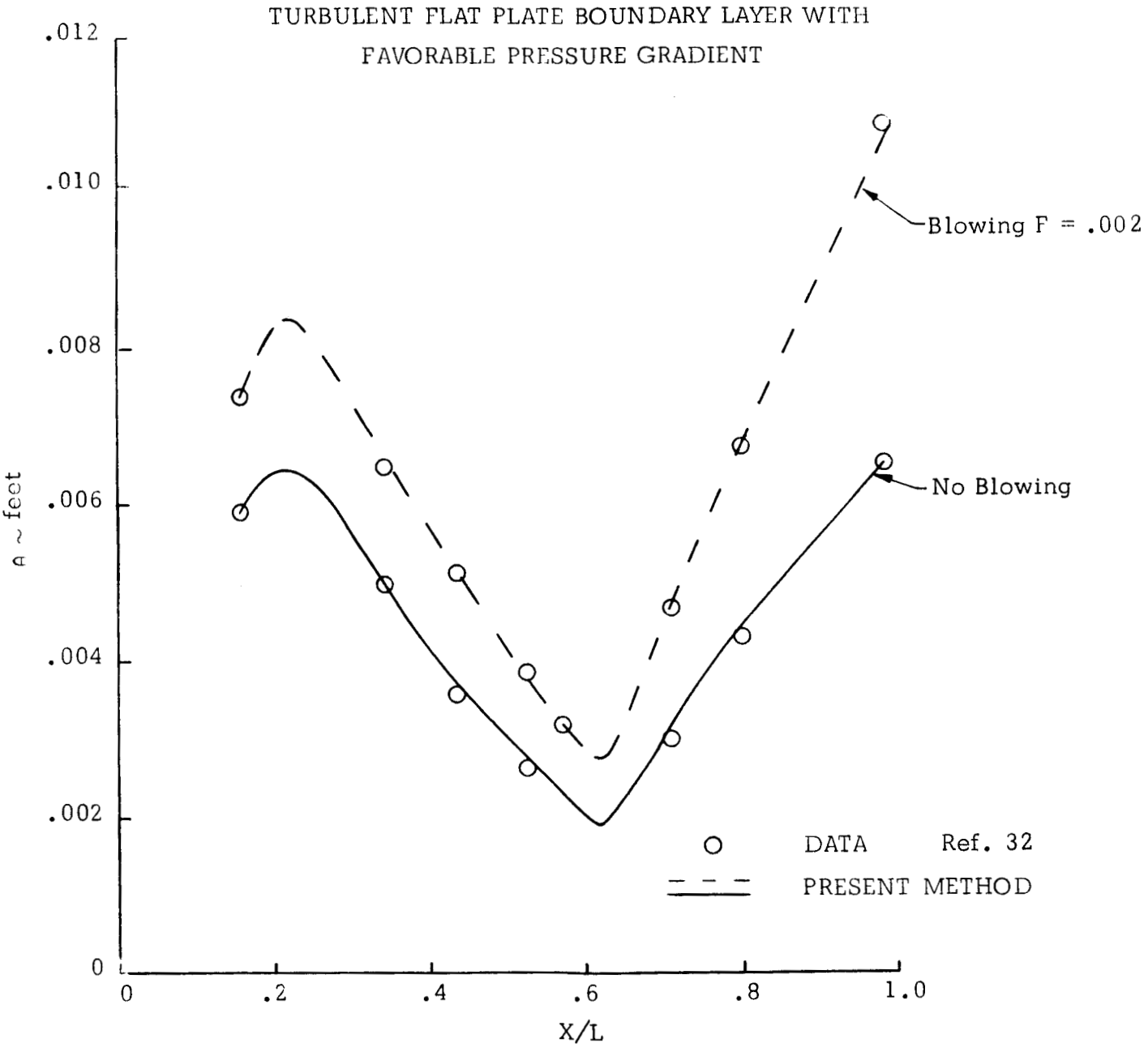

Figure 12. Comparison of Calculated and Measured Momentum Thickness with and without Blowing

TURBULENT FLAT PLATE BOUNDARY LAYER WITH
FAVORABLE PRESSURE GRADIENT

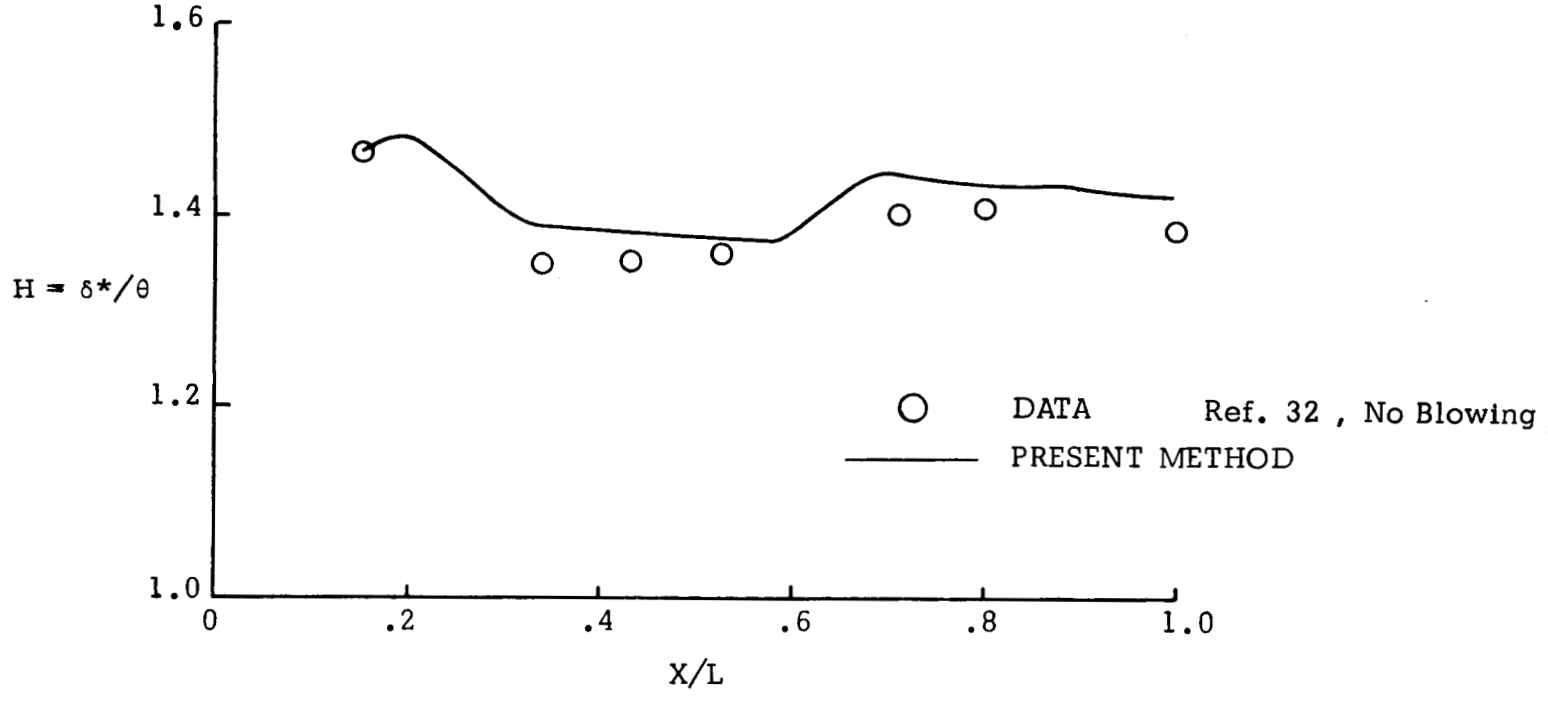

Figure 13. Comparison of Calculated and Measured Shape Factor

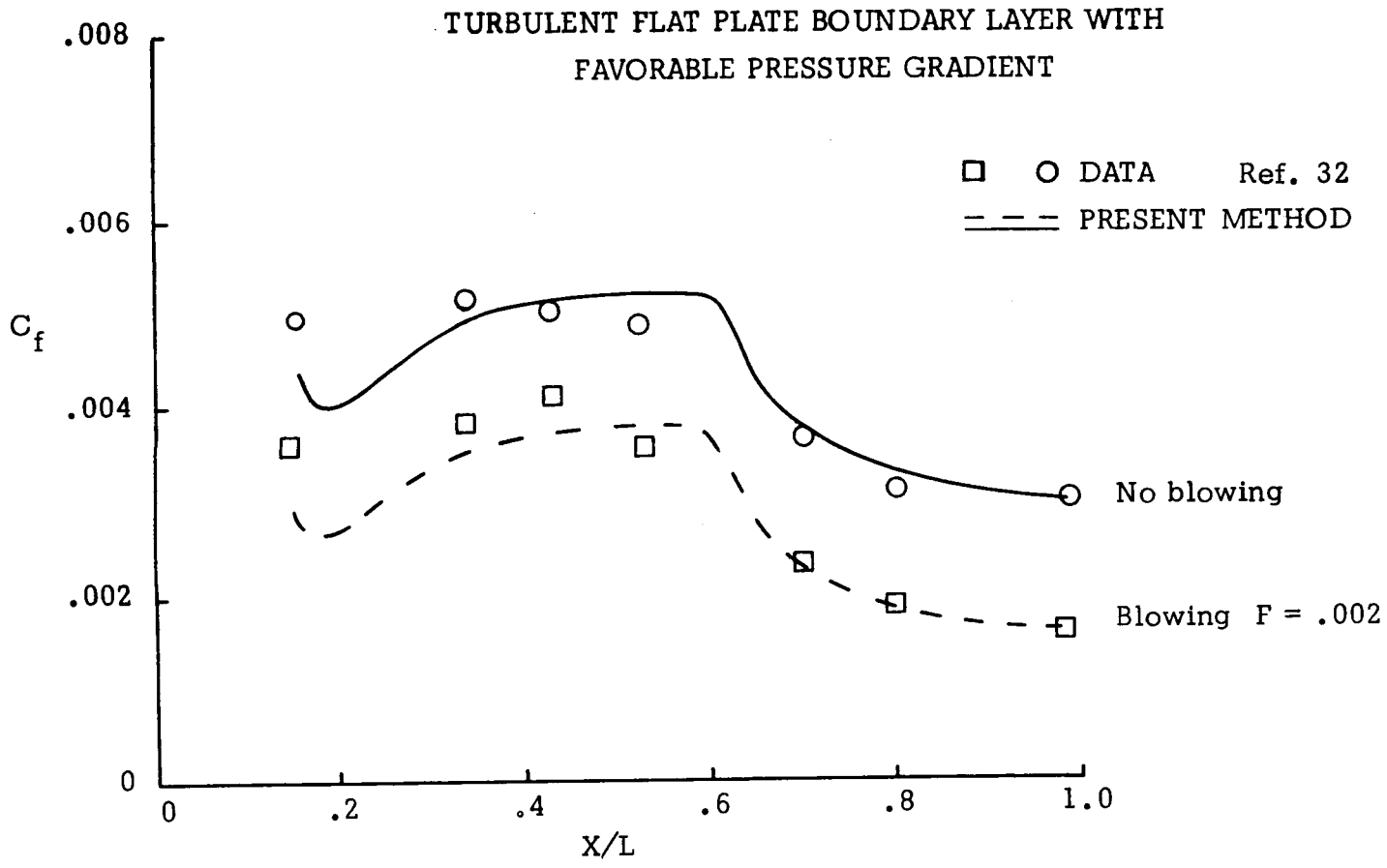

Figure 14. Comparison of Calculated and Measured Skin Friction Coefficient

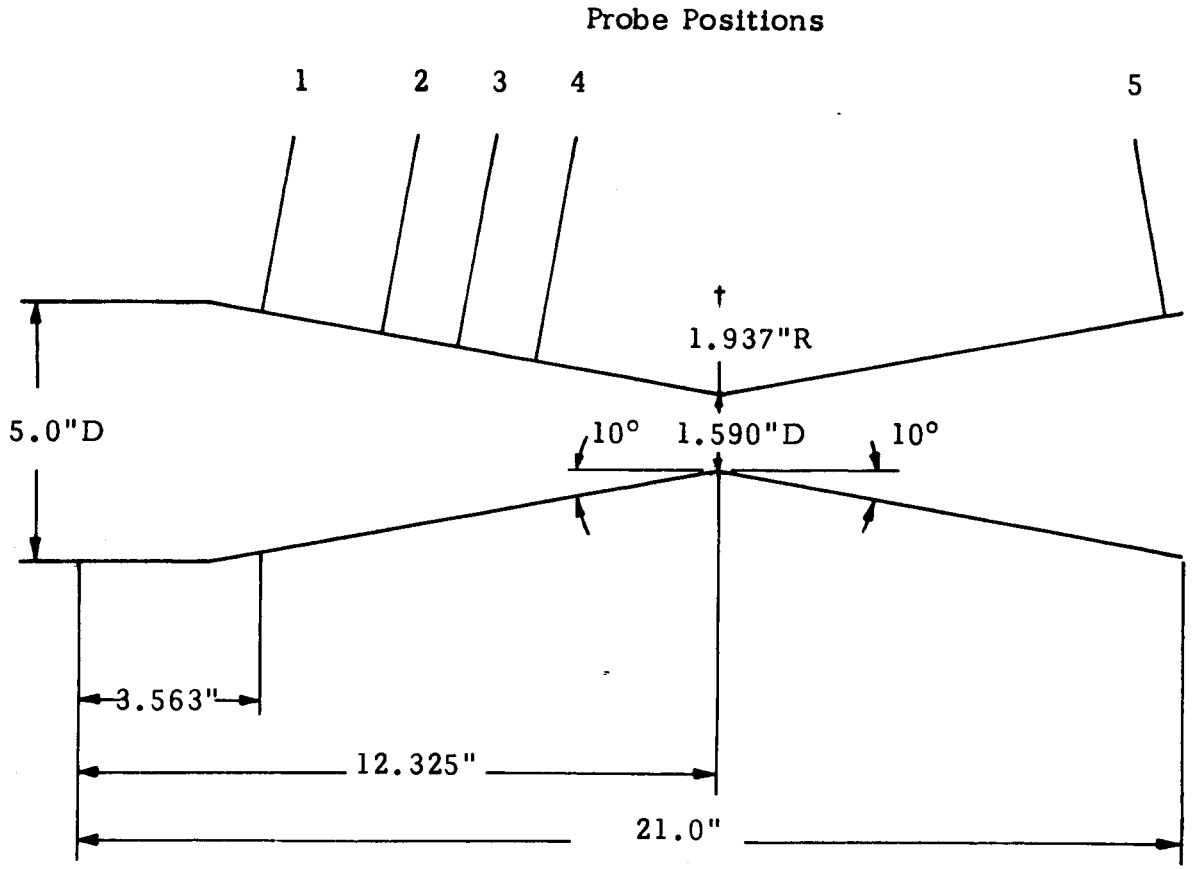

Figure 15. Nozzle Geometry from Reference 33

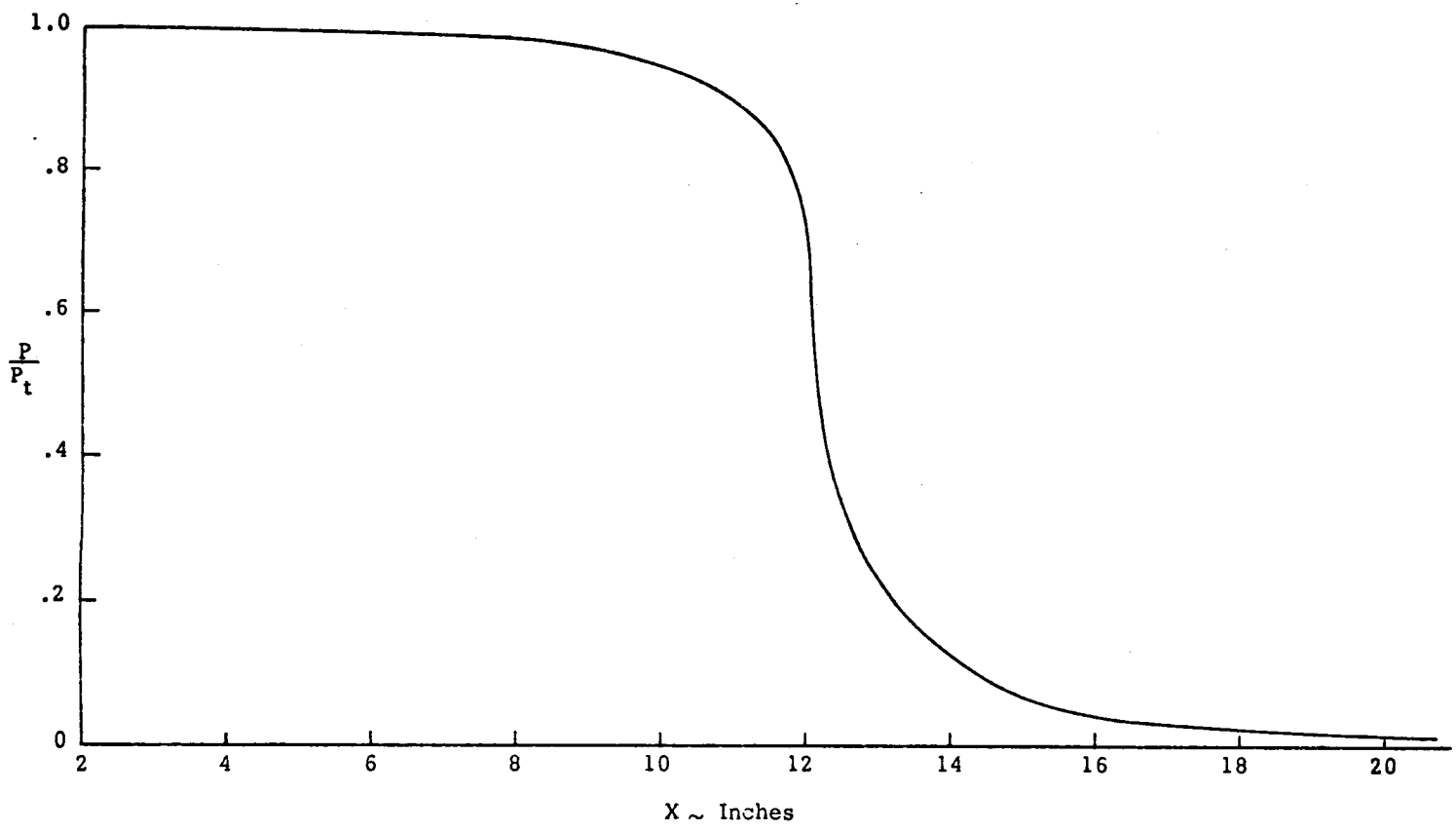

Figure 16. Experimental Pressure Distribution from Ref. 33 (slightly smoothed)

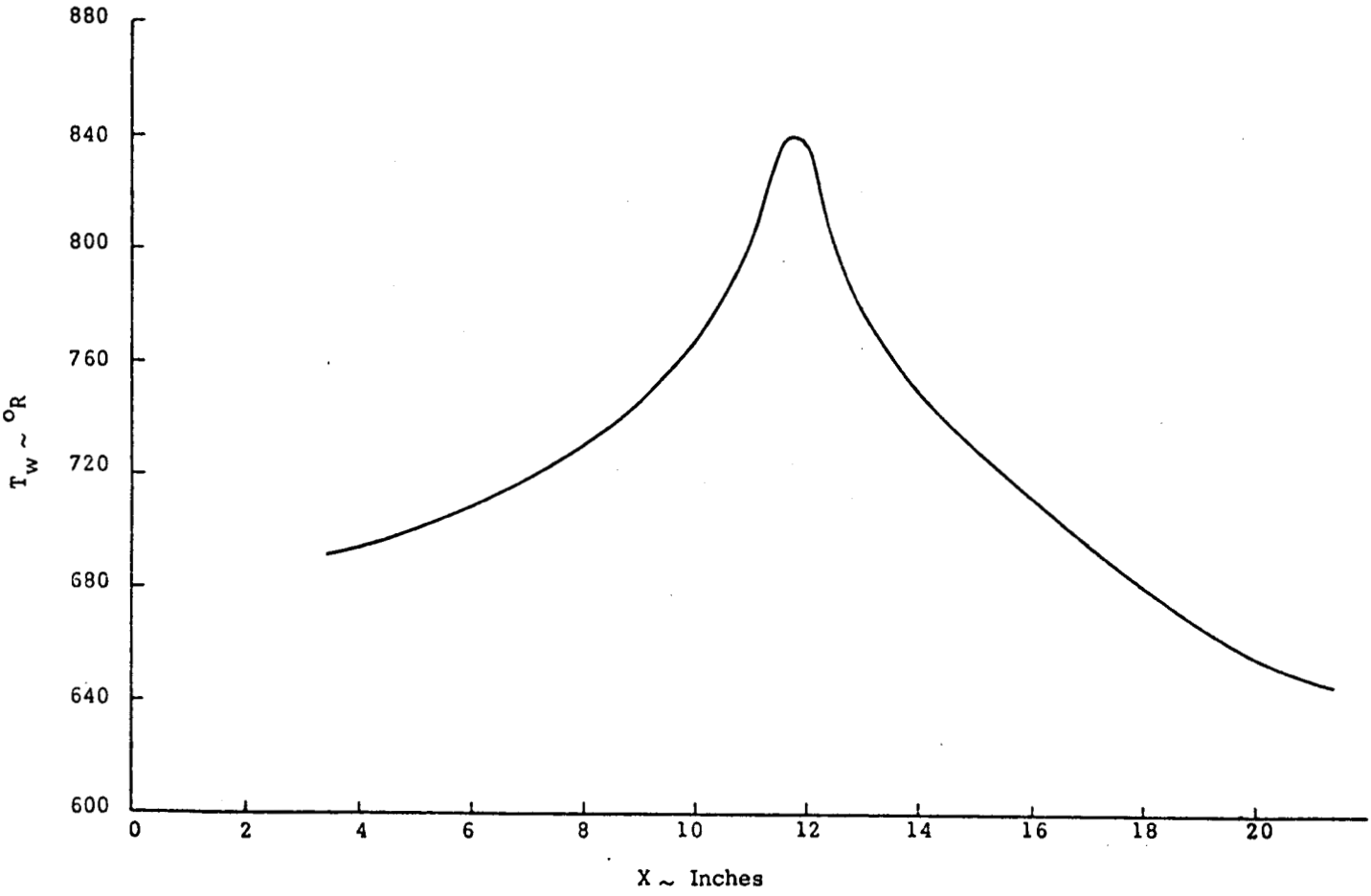

Figure 17. Experimental Wall Temperature Distribution From Ref. 33 (slightly smoothed)

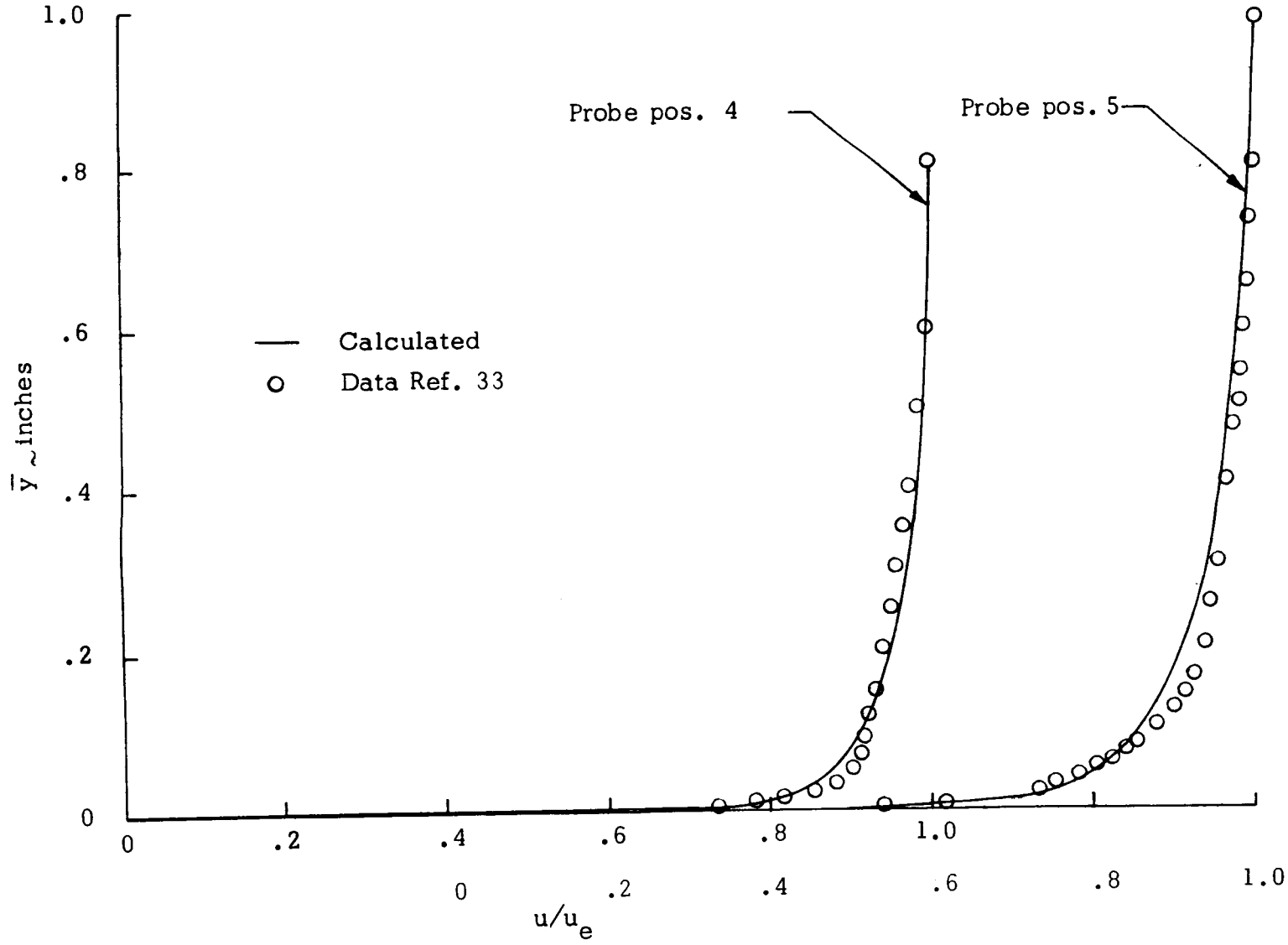

Figure 18. Comparison of Calculated Velocity Profiles with Data of Ref. 33

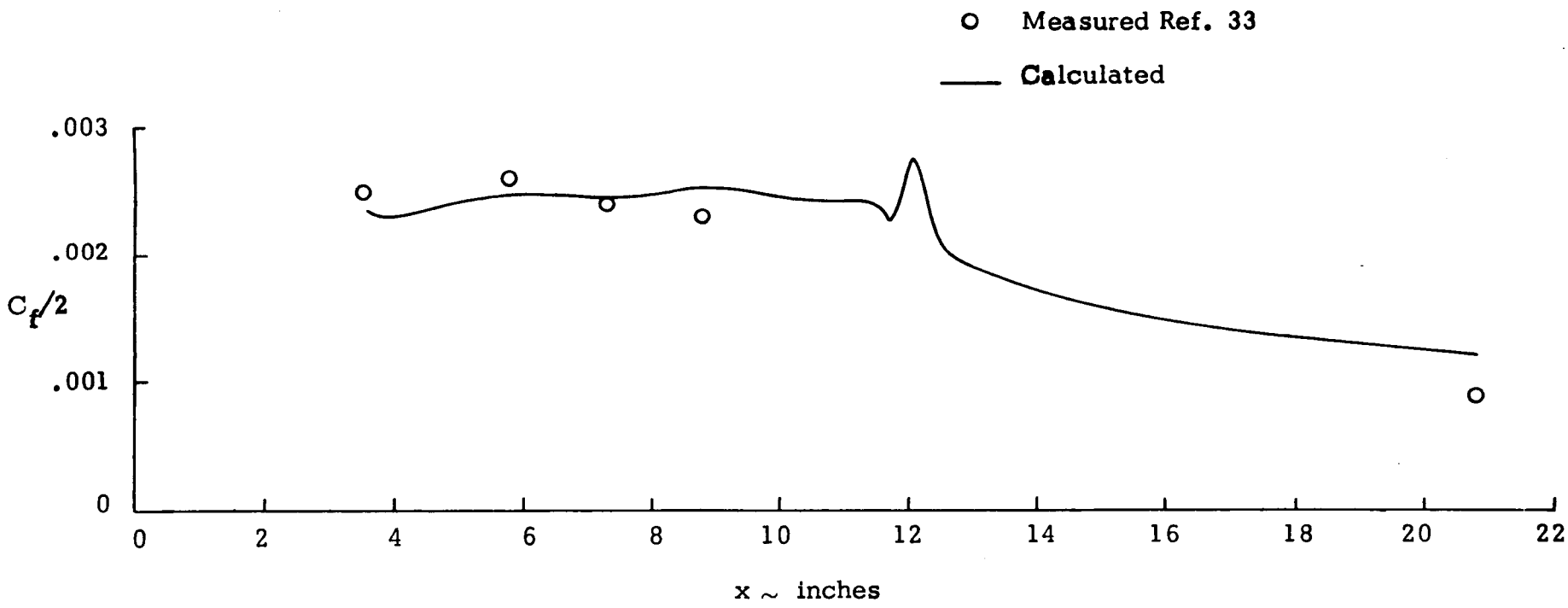

Figure 19. Comparison of Calculated Skin Friction Coefficient with Data of Ref. 33

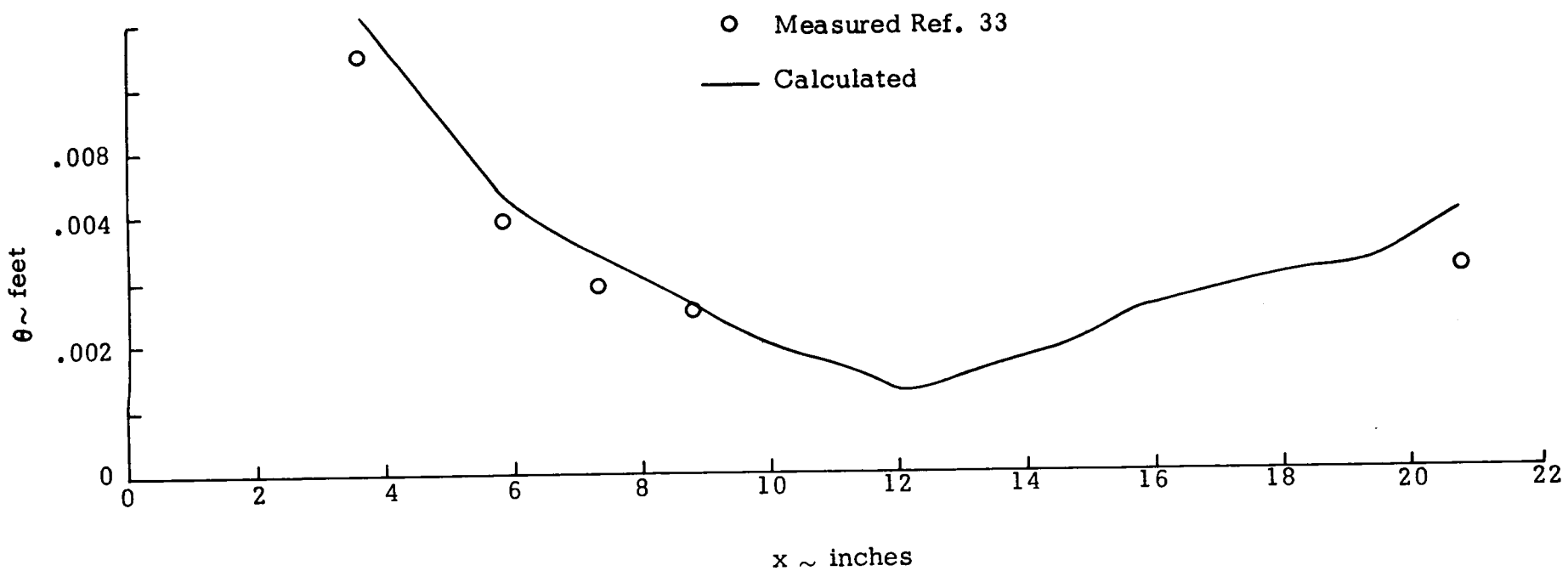

Figure 20. Comparison of Calculated Momentum Thickness with Data of Ref. 33

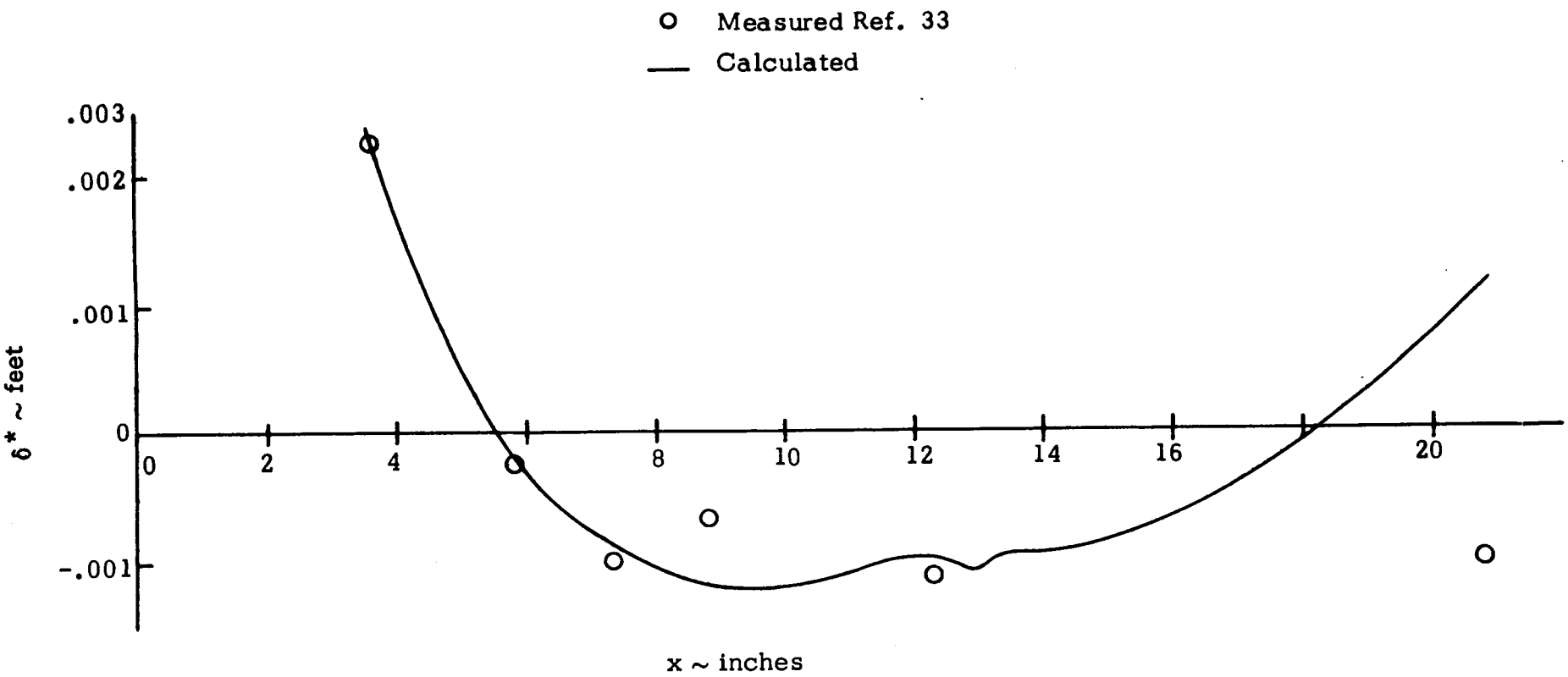

Figure 21. Comparison of Calculated Displacement Thickness with Data of Ref. 33

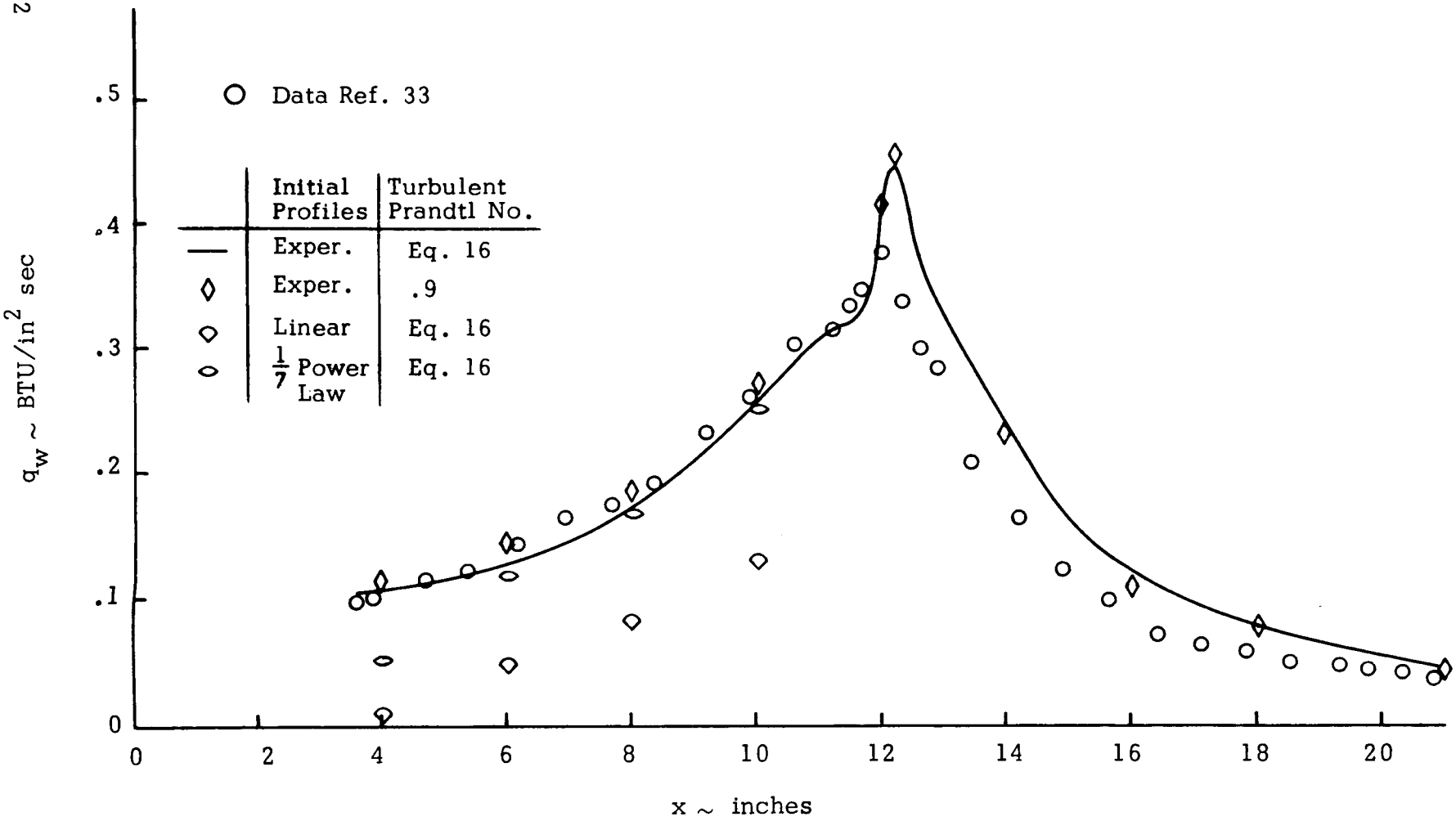

Figure 22. Comparison of Heat Transfer Rate With Data of Reference 33

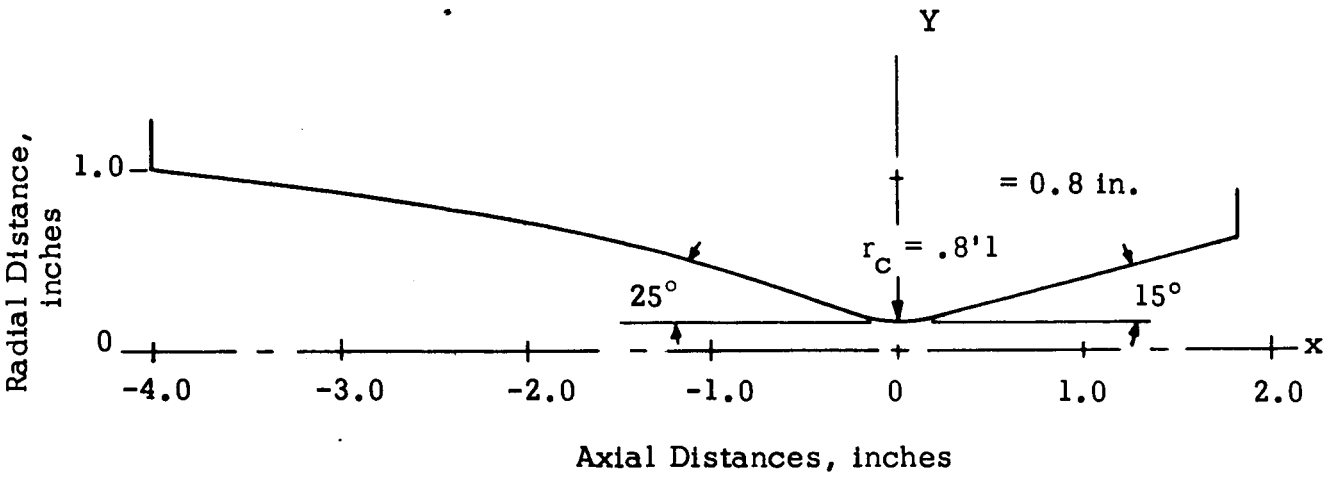

Throat Gap	=	0.310 inches
Injector Height	=	1.015 inches
Contraction Ratio	=	6.55
Nozzle Area Ratio	=	4.0

Figure 23. Rocketdyne Planar Nozzle Configuration

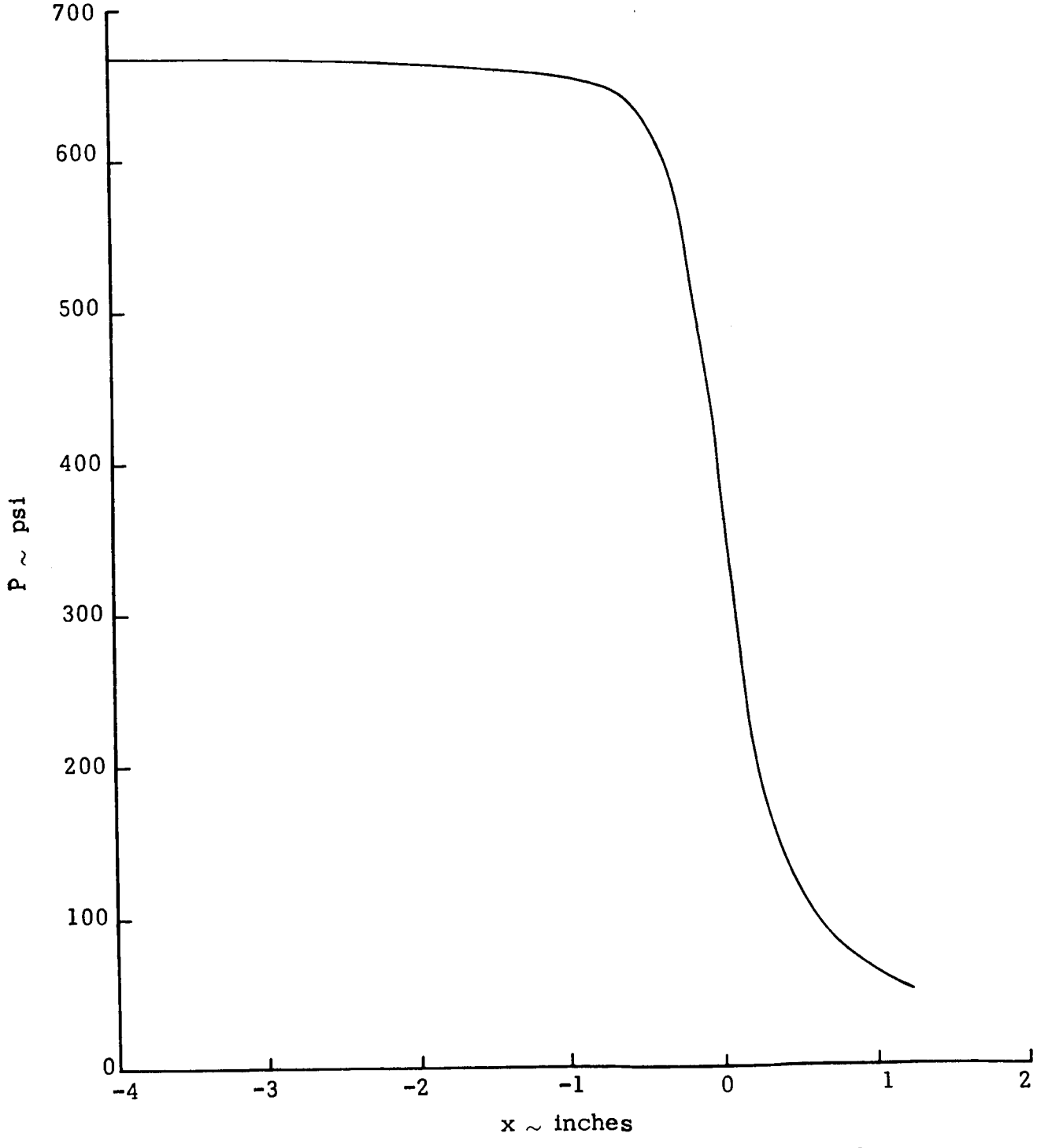

Figure 24. ODE Pressure Distribution for Rocketdyne Planar Nozzle

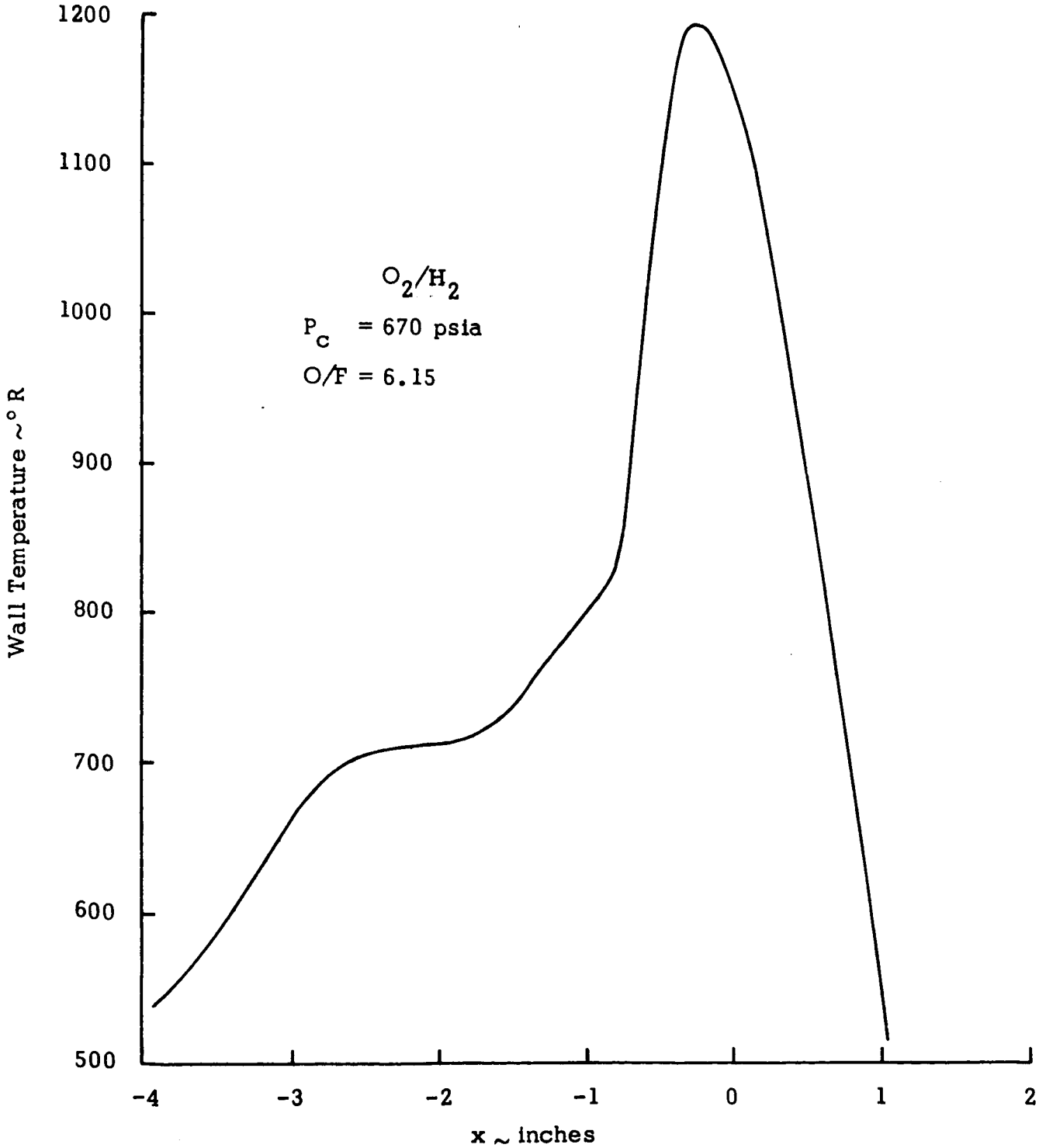

Figure 25. Wall Temperature Distribution for Rocketdyne Planar Nozzle

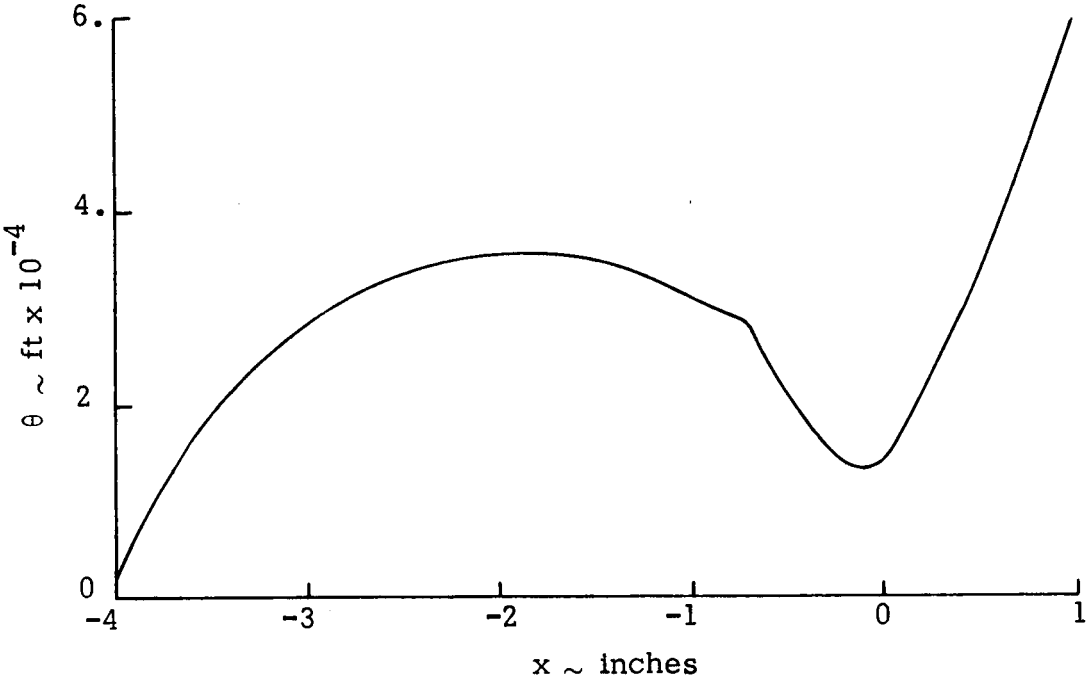

Figure 26. Momentum Thickness for Rocketdyne Planar Nozzle

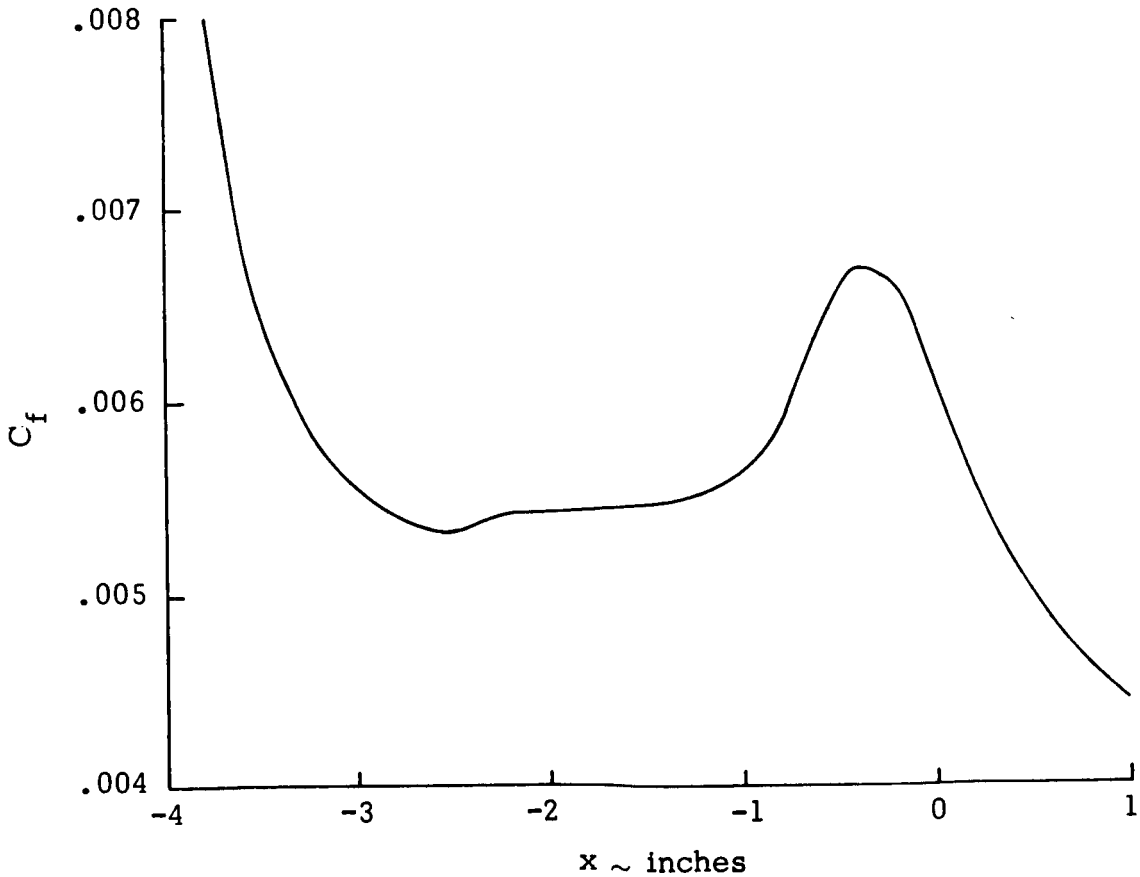

Figure 27. Local Skin Friction Coefficient for Rocketdyne Planar Nozzle

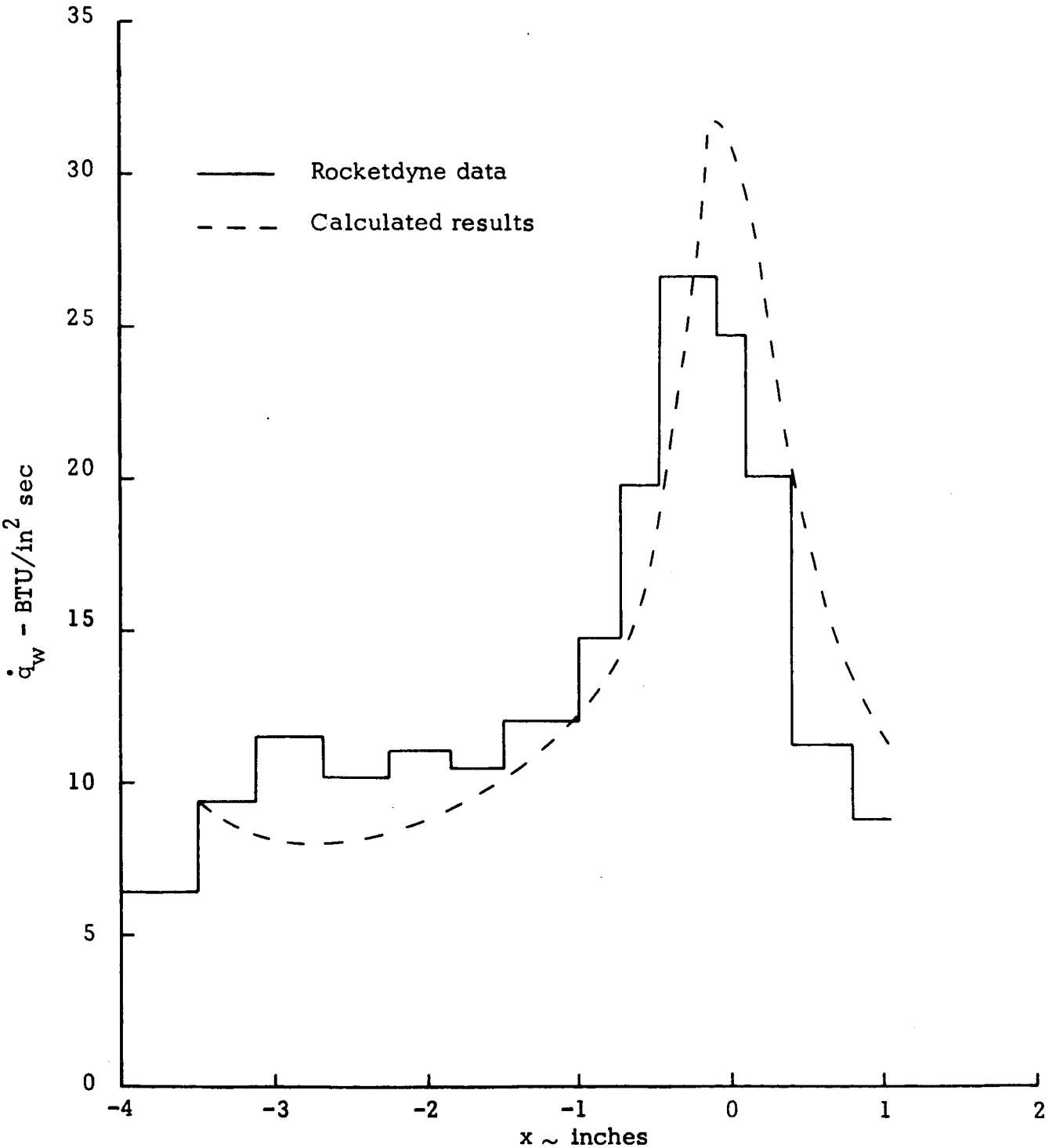

Figure 28. Heat Transfer Rate for Rocketdyne Planar Nozzle

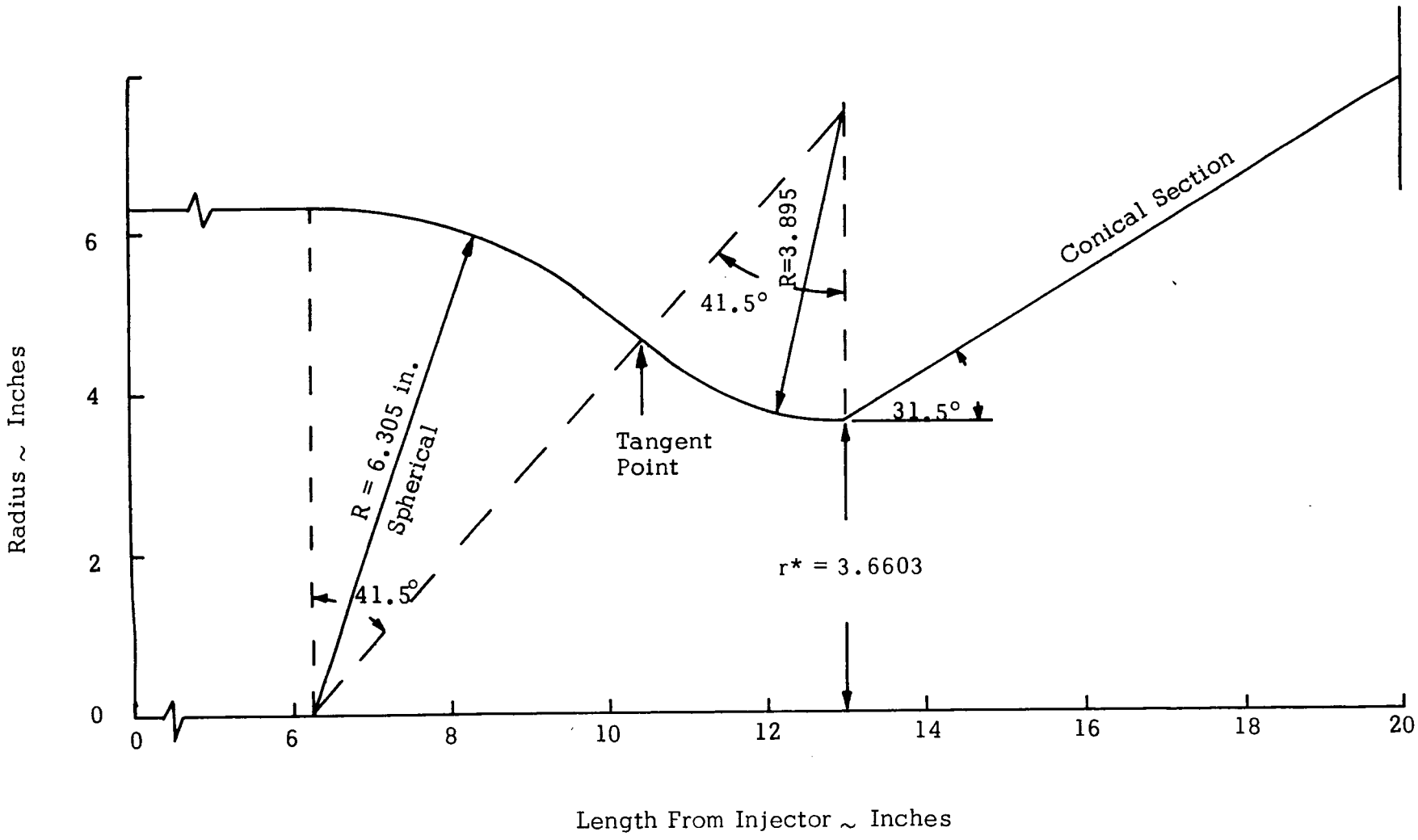

Figure 29. Chamber, Throat and Conical Divergent Section Geometry of the Transpiration Cooled Engine

Figure 30. Contoured Divergent Section Geometry of the Transpiration Cooled Geometry

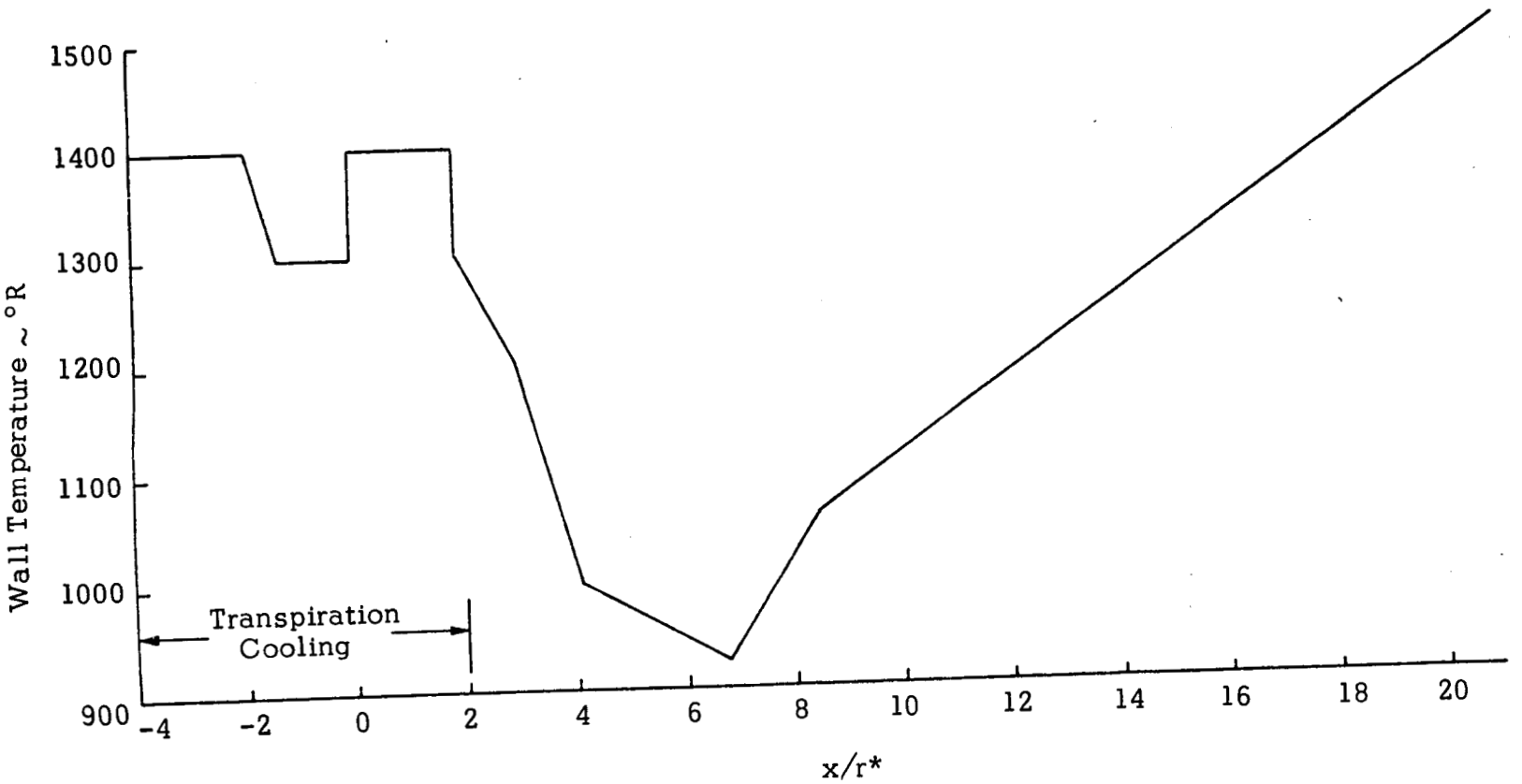

Figure 31. Wall Temperature Distribution for Transpiration Cooled Engine

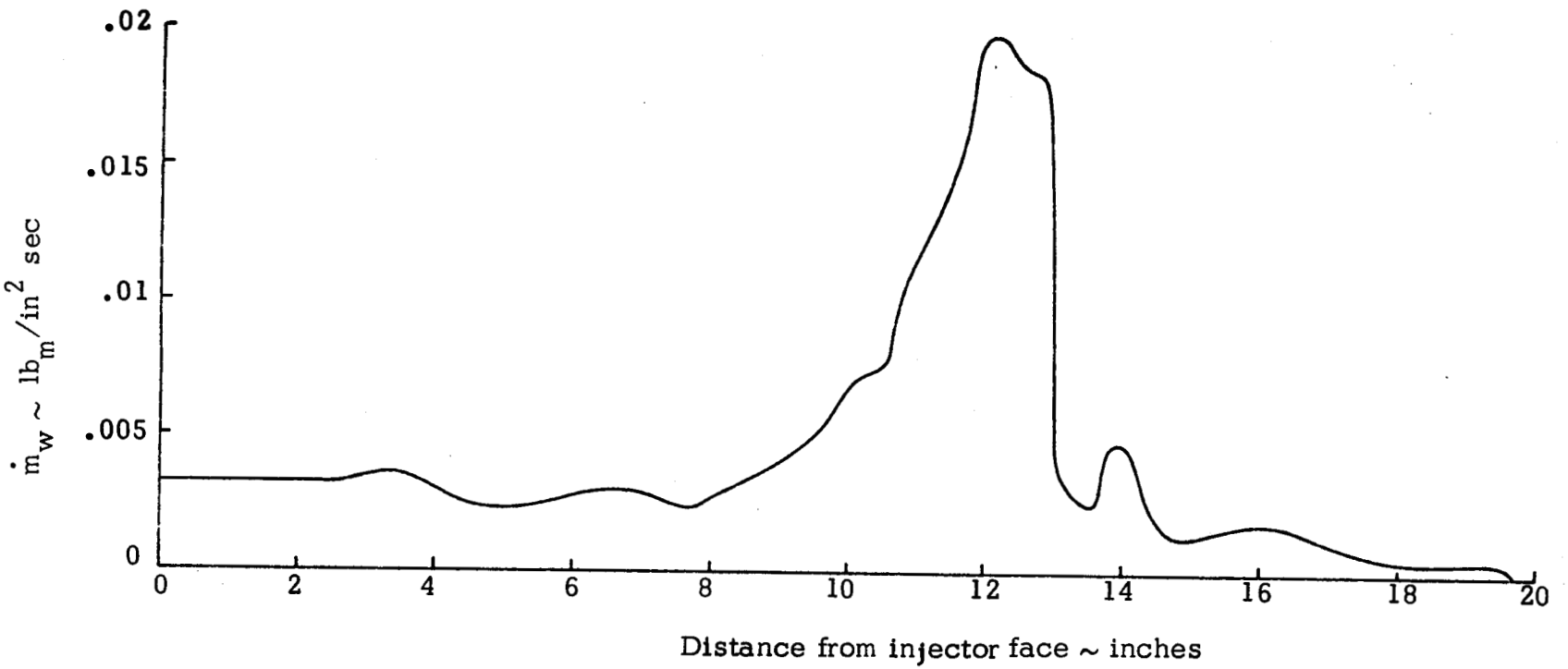

Figure 32. Coolant Flow Rate Distribution for Transpiration Cooled Engine

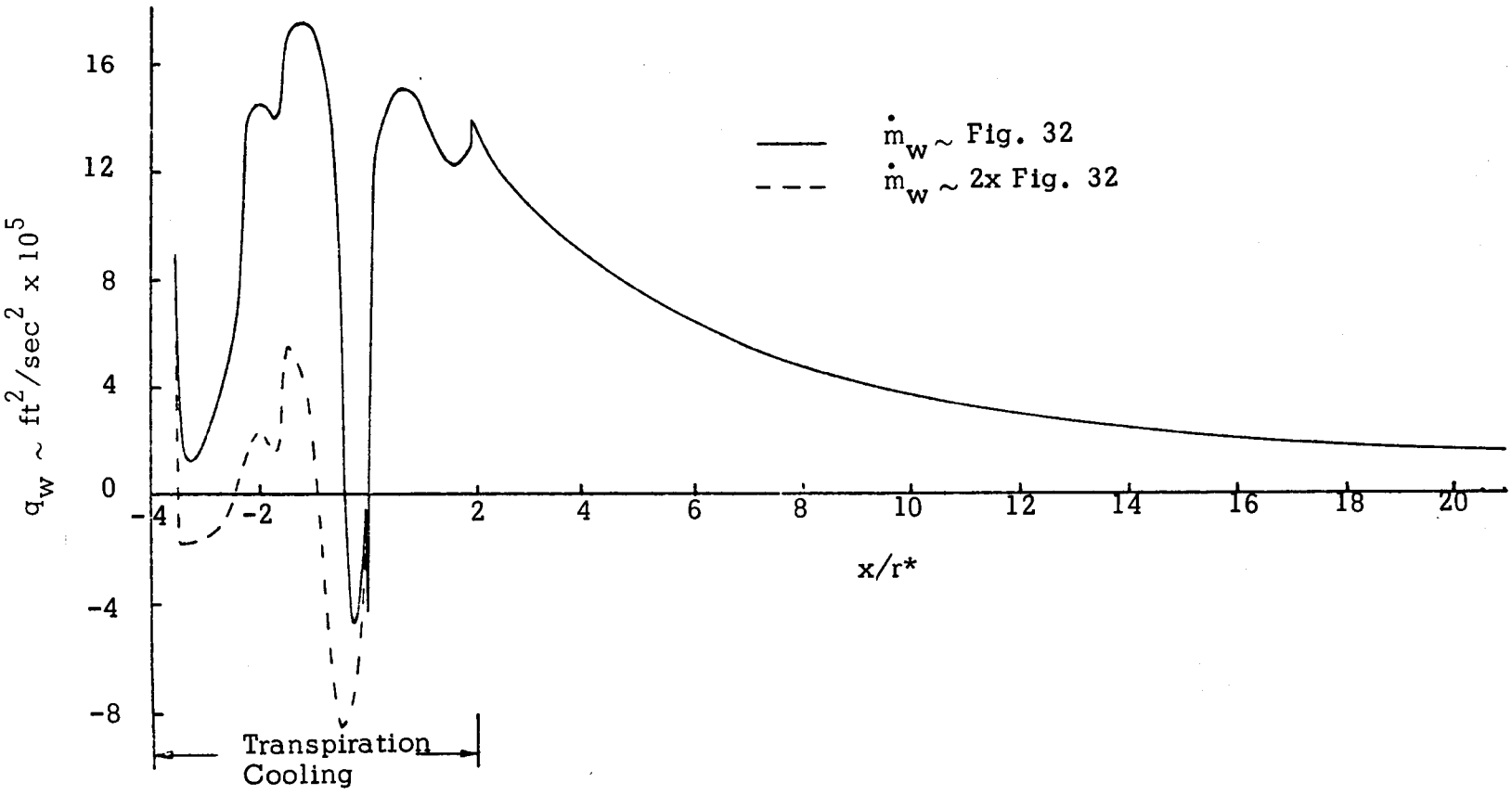

Figure 33. Calculated Heat Transfer Rate for Transpiration Cooled Engine

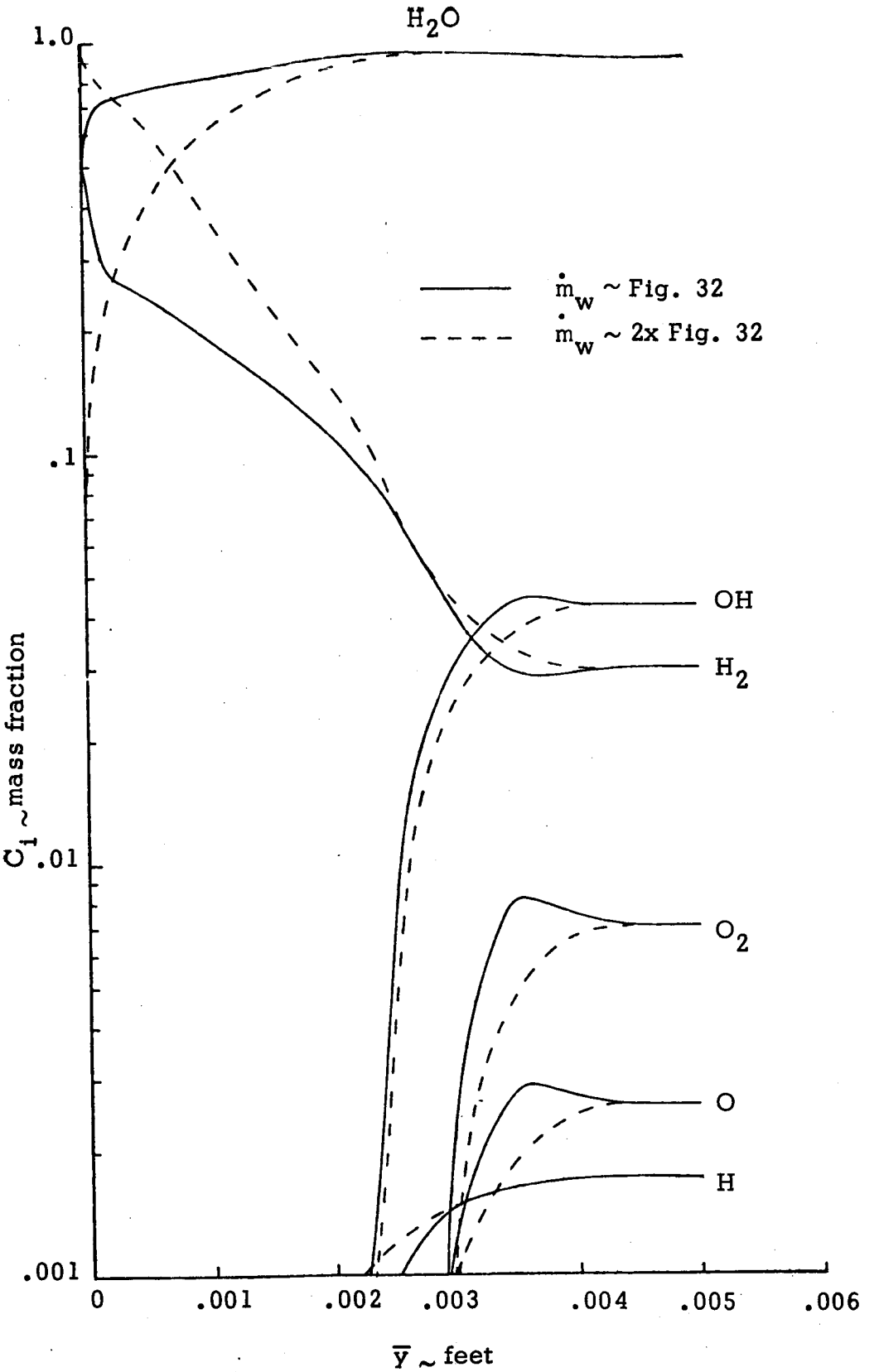

Figure 34. Mass Fraction Profiles for Transpiration Cooled Engine

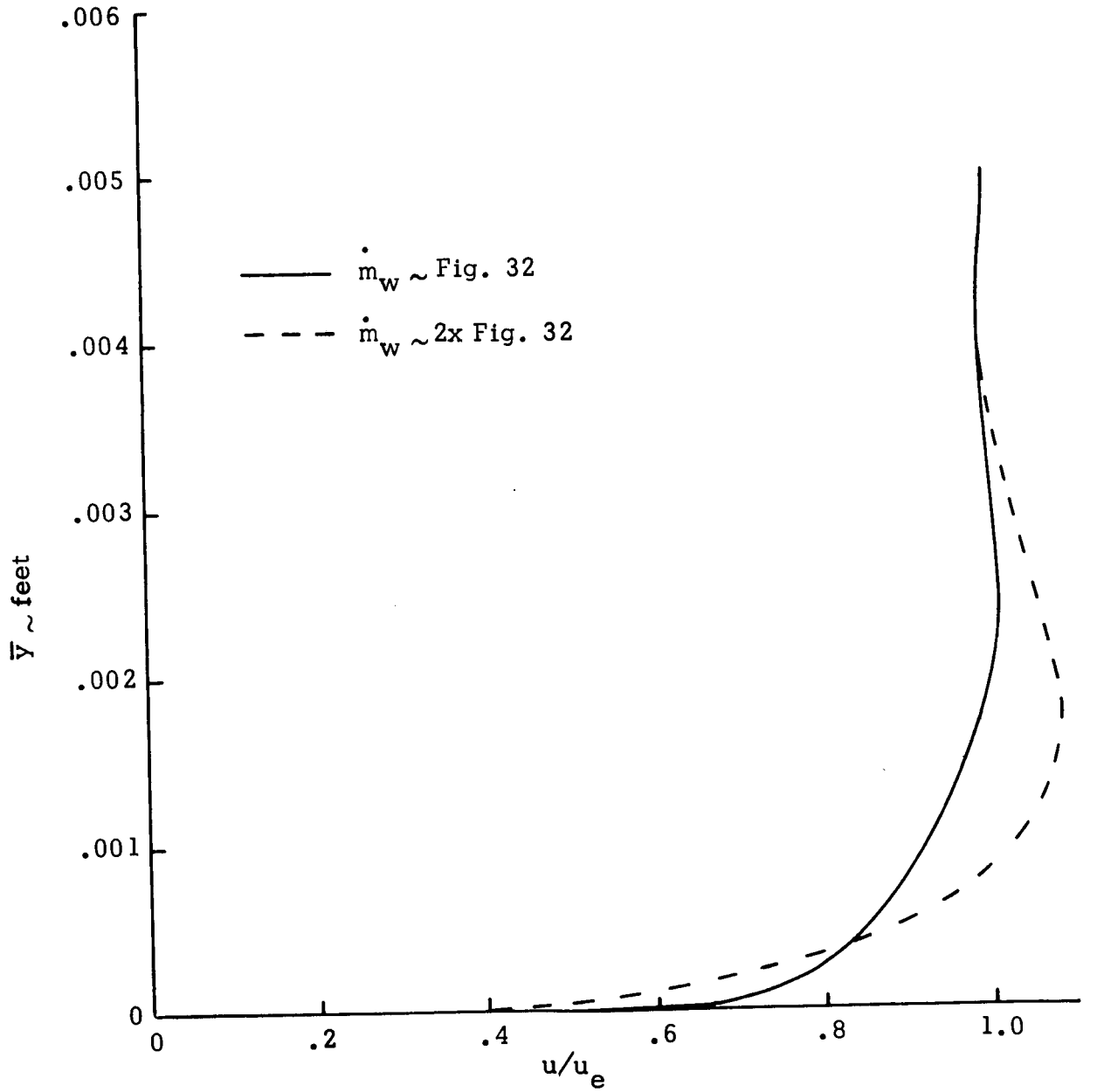

Figure 35. Velocity Profiles for Transpiration Cooled Engine

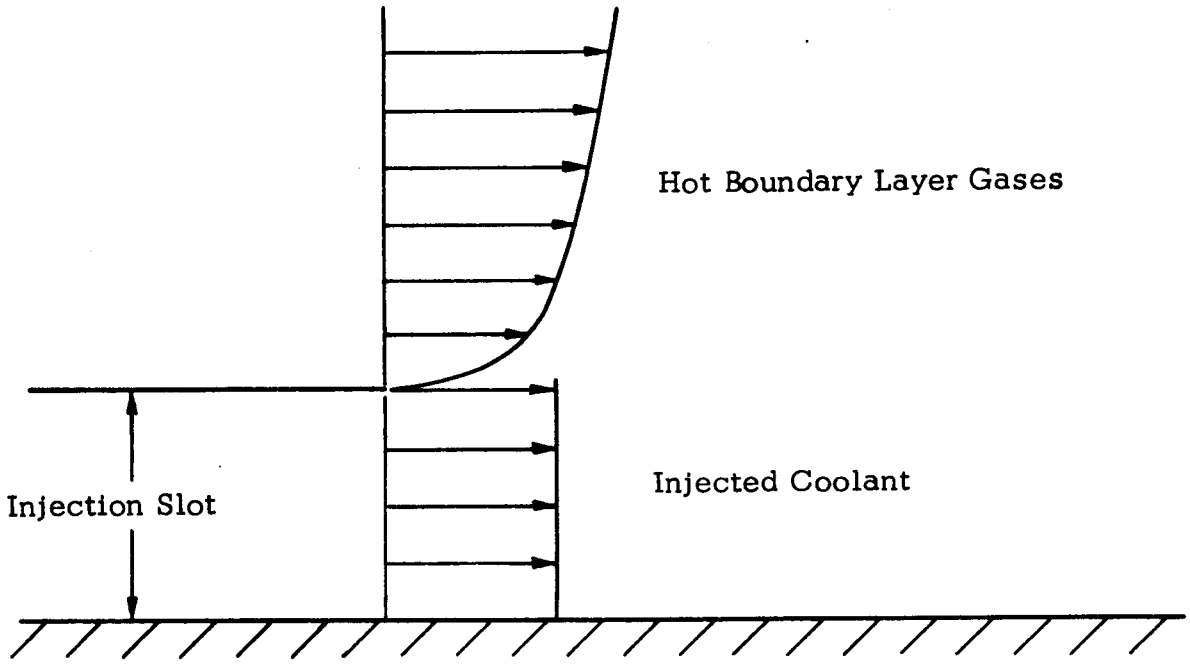

Figure 36. Film Cooling Geometry

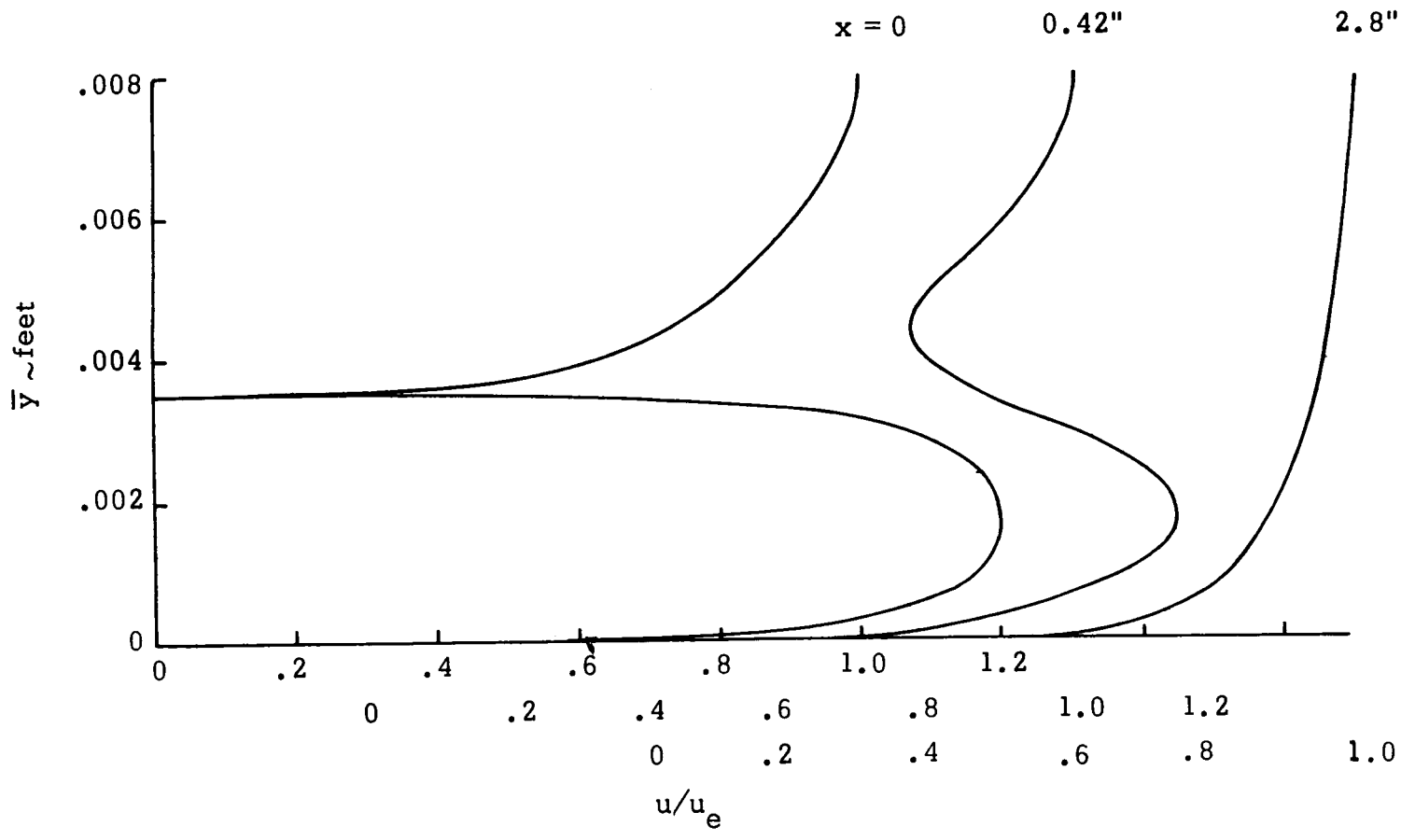

Figure 37. Sample Film Cooling Problem - Development of the Velocity Profile

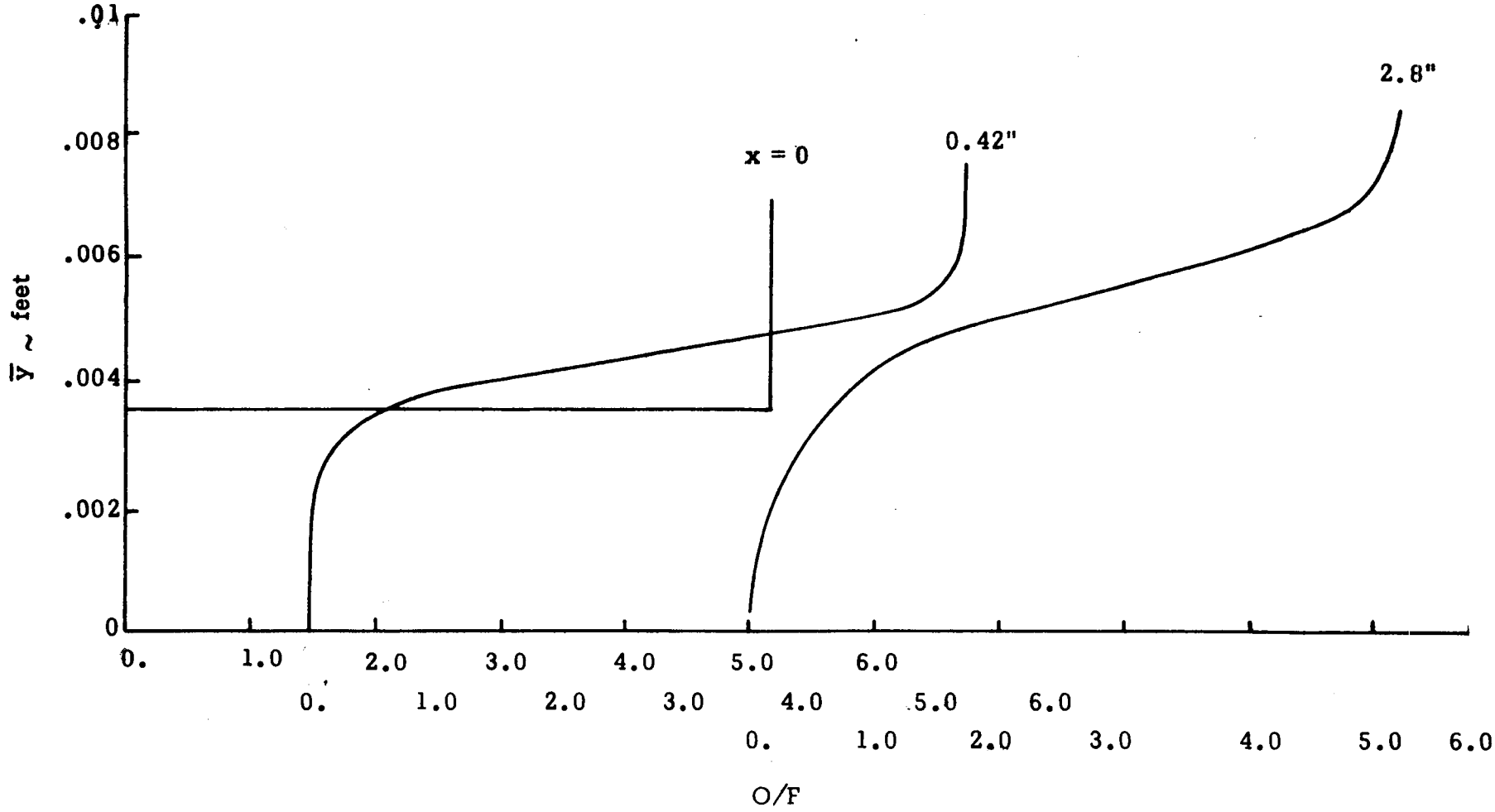

Figure 38. Sample Film Cooling Probelm - Development of the O/F Profile

APPENDIX A
DISTRIBUTION LIST

DISTRIBUTION LIST FOR FINAL REPORT, VOL. I

CONTRACT NAS7-791

NASA Headquarters
Washington, D.C . 20546
Attn: Contracting Officer

NASA Headquarters
Washington, D. C. 20546
Attn: Patent Office

NASA Lewis Research Center
21000 Brookpark Road
Cleveland, Ohio 44135
Attn: Office of Technical Information

NASA Manned Spacecraft Center
Houston, Texas 77058
Attn: Office of Technical Information

NASA Marshall Space Flight Center
Huntsville, Alabama 35812
Attn: Office of Technical Information,
MS-IP

NASA Marshall Space Flight Center
Huntsville, Alabama 35812
Attn: Technical Library

NASA Marshall Space Flight Center
Huntsville, Alabama 35812
Attn: Dale Burrows S+E-ASTN-PJ

NASA Ames Research Center
Moffet Field, Calif. 94035
Attn: Patents and Contracts Management

Jet Propulsion Laboratory
4800 Oak Grove Drive
Pasadena, California 91103
Attn: W. B. Powell

Manager, Liquid Rocket Propulsion
Tech., Code RPL
Office of Advanced Res. and Tech.
NASA Headquarters
Washington, D. C. 20546

Director, Technology Utilization Division
Office of Technology Utilization
NASA Headquarters
Washington, D. C. 20546

NASA Scientific and Technical Information
Facility
P. O. Box 33
College Park, Maryland 20740

Director, Launch Vehicles and Propulsion, SV
Office of Space Science and Applications
NASA Headquarters
Washington, D. C. 20546

Director, Advanced Manned Missions, MT
Office of Manned Space Flight
NASA Headquarters
Washington, D. C. 20546

Mission Analysis Division
NASA Ames Research Center
Moffett Field, Calif. 94035

Ames Research Center
Moffett Field, Calif. 94035
Attn: Technical Librarian

Goddard Space Flight Center
Greenbelt, Maryland 20771
Attn: Technical Librarian

Jet Propulsion Laboratory
California Institute of Technology
4800 Oak Grove Drive
Pasadena, California 91103
Attn: Technical Librarian

John F. Kennedy Space Center, NASA
Cocoa Beach, Florida 32931
Attn: Technical Librarian

Langley Research Center
Langley Station
Hampton, Virginia 23365
Attn: Technical Librarian

Lewis Research Center
21000 Brookpark Road
Cleveland, Ohio 44135
Attn: Technical Librarian

Marshall Space Flight Center
Huntsville, Alabama 35812
Attn: Technical Librarian

Manned Spacecraft Center
Houston, Texas 77058
Attn: Technical Librarian

Headquarters, U.S. Air Force
Washington 25, D. C. 20546
Attn: Technical Librarian

Arnold Engineering Development Center
Arnold Air Force Station
Tullahoma, Tennessee 37388
Attn: Technical Librarian

Air Force Rocket Propulsion Lab.
Research and Technology Div.
Air Force Systems Command
Edwards, California 93523
Attn: Technical Librarian

Air Force Missile Test Center
Holloman Air Force Base
New Mexico 45433
Attn: Technical Librarian

Air Force Missile Test Center
Patrick Air Force Base, Florida
Attn: Technical Librarian

Aeronautical Systems Division
Air Force Systems Command
Wright-Patterson Air Force Base
Dayton, Ohio 45433
Attn: Technical Librarian

Space and Missile Systems Organization
Air Force Unit Post Office
Los Angeles 45, California 90045
Attn: Technical Librarian

Bureau of Naval Weapons
Department of the Navy
Washington, D. C. 20546
Attn: Technical Librarian

U.S. Naval Ordnance Test Station
China Lake
California 93527
Attn: Technical Librarian

Picatinny Arsenal
Dover, New Jersey 07801
Attn: Technical Librarian

U.S. Army Missile Command
Redstone Arsenal
Alabama 35809
Attn: Technical Librarian

Chemical Propulsion Information Agency
Applied Physics Laboratory
8621 Georgia Avenue
Silver Spring, Maryland 20910
Attn: Technical Librarian

Aerojet-General Corporation
P. O. Box 296
Azusa, California 91703
Attn: Technical Librarian

Aerojet Liquid Rocket Company
P. O. Box 13222
Technical Library, Bldg. 2015, Dept. 2410
Sacramento, California 95813

Aerojet-General Corporation
Space Division
9200 East Flair Drive
El Monte, California 91734
Attn: Technical Librarian

Aerospace Corporation
2400 East El Segundo Boulevard
P. O. Box 95085
Los Angeles, California 90045
Attn: Technical Librarian

Defense Documentation Center Headquarters
Cameron Station, Building 5
5010 Duke Street
Alexandria, Virginia 22314
Attn: TISIA

Avco Systems Division
Wilmington, Massachusetts
Attn: Technical Librarian

Beech Aircraft Corporation
Boulder Division
Box 631
Boulder, Colorado
Attn: Technical Librarian

Bell Aerosystems Company
P. O. Box 1
Buffalo, New York 14240
Attn: Technical Librarian

Bellcomm
955 L-Enfant Plaza, S.W.
Washington, D. C.
Attn: Technical Librarian

Bendix Systems Division
Bendix Corporation
3300 Plymouth Road
Ann Arbor, Michigan 48105
Attn: Technical Librarian

Boeing Company
P. O. Box 3999
Seattle, Washington 98124
Attn: Technical Librarian

Boeing Company
1625 K Street, N.W.
Washington, D. C. 20006
Attn: Technical Librarian

Boeing Company
P. O. Box 1680
Huntsville, Alabama 35801
Attn: Technical Librarian

Missile Division
Chrysler Corporation
P. O. Box 2628
Detroit, Michigan 48231
Attn: Technical Librarian

Wright Aeronautical Division
Curtiss-Wright Corporation
Wood-Ridge, New Jersey 07075
Attn: Technical Librarian

Research Center
Fairchild Hiller Corporation
Germantown, Maryland
Attn: Technical Librarian

Republic Aviation Corporation
Fairchild Hiller Corporation
Farmingdale, Long Island, New York
Attn: Technical Librarian

General Dynamics, Convair Division
P. O. Box 1128
San Diego, California
Attn: Technical Librarian

Missile and Space Systems Center
General Electric Company
Valley Forge Space Technology Center
P. O. Box 8555
Philadelphia, Pa.
Attn: Technical Librarian

Grumman Aircraft Engineering Corp.
Bethpage, Long Island
New York 11714
Attn: Technical Librarian

Honeywell, Inc.
Aerospace Division
2600 Ridgway Road
Minneapolis, Minnesota
Attn: Technical Librarian

Hughes Aircraft Company
Aerospace Group
Centinela and Teale Streets
Culver City, California 90230
Attn: Technical Librarian

Walter Kidde and Company, Inc.
Aerospace Operations
567 Main Street
Belleville, New Jersey
Attn: Technical Librarian

Ling-Temco-Vought Corporation
P. O. Box 5907
Dallas, Texas 75222
Attn: Technical Librarian

Arthur D. Little, Inc.
20 Acorn Park
Cambridge, Massachusetts 02140
Attn: Technical Librarian

Lockheed Missiles and Space Co.
Attn: Technical Information Center
P. O. Box 504
Sunnyvale, California 94088

Lockheed Propulsion Company
P. O. Box 111
Redlands, California 92374
Attn: Technical Librarian

The Marquardt Corporation
16555 Saticoy Streey
Van Nuys, California 91409
Attn: Technical Librarian

Baltimore Division
Martin Marietta Corporation
Baltimore, Maryland 21203
Attn: Technical Librarian

Denver Division
Martin Marietta Corporation
P. O. Box 179
Denver, Colorado 80201
Attn: Technical Librarian

Orlando Division
Martin Marietta Corp.
Box 5837
Orlando, Florida
Attn: Technical Librarian

McDonnell-Douglas Astronautics Co.
5301 Bolsa Avenue
Huntington Beach, California 92647
Attn: Technical Librarian

McDonnell-Douglas Corp.
P. O. Box 516
Municipal Airport
St. Louis, Missouri 63166
Attn: Technical Librarian

Space & Info. Systems Division
North American Rockwell
12214 Lakewood Boulevard
Downey, California 90241
Attn: Technical Librarian

Rocketdyne (Library 586-306)
6633 Canoga Avenue
Canoga Park, California 91304
Attn: Technical Librarian

Northrop Space Laboratories
3401 West Broadway
Hawthorne, California 90250
Attn: Technical Librarian

Aeroneutronic Corporation
Philco Corporation
Ford Road
Newport Beach, California 92663
Attn: Technical Librarian

Astro-Electronics Division
Radio Corporation of America
Princeton, New Jersey 08540
Attn: Technical Librarian

Rocket Research
York Center
Redmond, Washington 98052
Attn: Technical Librarian

Scientific Service Bureau, Inc.
P. O. Box 375
Morrisplains, New Jersey 07950
Attn: Technical Librarian

Stanford Research Institute
333 Ravenswood Avenue
Menlo Park, California 94025
Attn: Technical Librarian

Sunstrand Aviation
4747 Harrison Avenue
Rockford, Illinois 61101
Attn: Technical Librarian

TRW Systems Group
TRW Incorporated
One Space Park
Redondo Beach, Calif. 90278
Attn: Technical Librarian

Tapco Division
TRW, Incorporated
23555 Euclid Avenue
Cleveland, Ohio 44117
Attn: Technical Librarian

Thiokol Chemical Corp.
Aerospace Services
Elkton Division
Bristol, Penna.
Attn: Technical Librarian

Thiokol Chemical Corp.
Huntsville Division
Huntsville, Alabama 35807
Attn: Technical Librarian

Research Laboratories
United Aircraft Corp.
400 Main Street
East Haraford, Conn. 06108
Attn: Technical Librarian

Hamilton Standard Division
United Aircraft Corp.
Windsor Locks, Conn. 06096
Attn: Technical Librarian

United Technology Center
587 Methilda Avenue
P. O. Box 358
Sunnyvale, California 94088
Attn: Technical Librarian

Florida Research and Development
Pratt and Whitney Aircraft
United Aircraft Corporation
P. O. Box 2691
West Palm Beach, Florida 33402
Attn: Technical Librarian

Vickers, Inc.
Box 302
Troy, Michigan
Attn: Technical Librarian

Air Force Rocket Propulsion Laboratory
Research and Technology Division
Air Force Systems Command
Edwards, California 93523
Attn: T. J. Fanciullo

Lewis Research Center
21000 Brookpark Road
Cleveland, Ohio 44135
Attn: H. Neumann

Lewis Research Center
21000 Brookpark Road
Cleveland, Ohio 44135
Attn: T. Fortini

Lewis Research Center
21000 Brookpark Road
Cleveland, Ohio 44135
Attn: L. Gordon

Lewis Research Center
21000 Brookpark Road
Cleveland, Ohio 44135
Attn: D. Nored

Manned Spacecraft Center
Houston, Texas 77058
Attn: R. Kahl

Marshall Space Flight Center
Huntsville, Alabama 35812
Attn: K. Gross

Marshall Space Flight Center
Huntsville, Alabama 35812
Attn: T. Greenwood

Jet Propulsion Laboratory
4800 Oak Grove Drive
Pasadena, California 91103
Attn: Lloyd Back

Aerospace Corporation
2400 East El Segundo Boulevard
P. O. Box 95085
Los Angeles, California 90045
Attn: W. Roessler

Florida Research and Development
Pratt & Whitney Aircraft
United Aircraft Corporation
P. O. Box 2691
West Palm Beach, Florida 33402
Attn: G. Zimmerman

Florida Research and Development
Pratt & Whitney Aircraft
United Aircraft Corporation
P. O. Box 2691
West Palm Beach, Florida 33402
Attn: T. Mayes

United Aircraft Research Laboratories
Pratt and Whitney Engineering Group
400 Main Street
East Hartford, Connecticut 06108
Attn: W. G. Burwell

Aerojet Liquid Rocket Company
P. O. Box 13222
Sacramento, California 95813
Attn: D. Kors

Aerojet Liquid Rocket Company
P. O. Box 13222
Sacramento, California 95813
Attn: D. Calhoun

Rocketdyne
6633 Canoga Avenue
Canoga Park, California 91304
Attn: W. Wagner

General Applied Science Laboratory
Stewart and Merrill Avenues
Westbury
Long Island, New York 11590
Attn: R. Edelman

Aerotherm Corporation
485 Clyde Avenue
Mountain View, California 94040
Attn: R. M. Kendall

Grumman Aircraft Engineering Corp.
Bethpage, Long Island
New York 11714
Attn: B. Piper

Lockheed Aircraft Corp.
P. O. Box 1103
Huntsville, Alabama 35807
Attn: R. J. Prozan

LTV Aerospace Corp.
3221 N. Armistead Avenue
Hampton, Virginia 23366
Attn: G. S. Bahn

The Marquardt Corporation
16555 Saticoy Street
Van Nuys, Calif. 91409
Attn: C. R. Halbach

McDonnell-Douglas Aircraft Co., Inc.
5301 Bolsa Avenue
Huntington Beach, Calif. 92647
Attn: W. A. Gaubatz, M.S. 9 BBFO

Langley Research Center
Langley Station
Hampton, Virginia 23365
Attn: D. Bushnell

Langley Research Center
Langley Station
Hampton, Virginia 23365
Attn: R. S. Levine

TRW Systems Group
TRW, Incorporated
One Space Park
Redondo Beach, Calif. 90278
Attn: Steve Cherry

Bell Aerosystems Company
P. O. Box 1
Buffalo, New York 14240
Attn: A. H. Blessing

United Aircraft Corp.
United Technology Center
P. O. Box 358
Sunnyvale, Calif. 94088
Attn: T. D. Myers

Texas A & M University
College Station, Texas 77843
Attn: David J. Norton, Aerospace Eng. Dept.

Purdue University
West Lafayette, Indiana
Attn: Warren Brecheisen
Mechanical Eng. (JPC)

Martin Marietta Corporation
P. O. Box 709
Denver, Colorado 80201
Attn: W. R. Scott
Mail Zone 0431

ORIGINAL DISTRIBUTION OF MABL PROGRAM
CONTRACT NAS7-791

Rocketdyne
P & W - Connecticut
P & W - Florida
Aerojet LRC
TRW Systems
NASA-Houston
NASA-Huntsville
JPL